CENTRAL RESEARCH LIBRARY
DOCUMENT COLLECTION

2

OAK RIDGE NATIONAL LABORATORY
operated by
UNION CARBIDE CORPORATION
NUCLEAR DIVISION
for the
U.S. ATOMIC ENERGY COMMISSION

UNION CARBIDE

OAK RIDGE NATIONAL LABORATORY LIBRARY
3 4456 0023712 5

ORNL-TM-2014

NUMERICAL METHODS FOR SINTERING BY VOLUME DIFFUSION

(Thesis)

Roy Thomas King

OAK RIDGE NATIONAL LABORATORY
CENTRAL RESEARCH LIBRARY
DOCUMENT COLLECTION
LIBRARY LOAN COPY
DO NOT TRANSFER TO ANOTHER PERSON
If you wish someone else to see this document, send in name with document and the library will arrange a loan.
UCN-7969
(3 3-67)

Submitted to Carnegie-Mellon University in partial fulfillment of the requirements for the Doctor of Philosophy degree in Metallurgy and Materials Science.

LEGAL NOTICE

This report was prepared as an account of Government sponsored work. Neither the United States, nor the Commission, nor any person acting on behalf of the Commission:

A. Makes any warranty or representation, expressed or implied, with respect to the accuracy, completeness, or usefulness of the information contained in this report, or that the use of any information, apparatus, method, or process disclosed in this report may not infringe privately owned rights; or

B. Assumes any liabilities with respect to the use of, or for damages resulting from the use of any information, apparatus, method, or process disclosed in this report.

As used in the above, "person acting on behalf of the Commission" includes any employee or contractor of the Commission, or employee of such contractor, to the extent that such employee or contractor of the Commission, or employee of such contractor prepares, disseminates, or provides access to, any information pursuant to his employment or contract with the Commission, or his employment with such contractor.

ORNL-TM-2014

Contract No. W-7405-eng-26

METALS AND CERAMICS DIVISION

NUMERICAL METHODS FOR SINTERING BY VOLUME DIFFUSION

Roy Thomas King

JANUARY 1968

Submitted to Carnegie-Mellon University in partial fulfillment of the requirements for the Doctor of Philosophy degree in Metallurgy and Materials Science

OAK RIDGE NATIONAL LABORATORY
Oak Ridge, Tennessee
operated by
UNION CARBIDE CORPORATION
for the
U.S. ATOMIC ENERGY COMMISSION

OAK RIDGE NATIONAL LABORATORY LIBRARY
3 4456 0023712 5

ACKNOWLEDGMENTS

The author is extremely grateful to his adviser, Dr. W. W. Mullins, for his patient guidance during the course of this work. Appreciation is also expressed to Dr. P. G. Shewmon, Dr. F. Nichols, and Dr. R. Trevedi for discussions which contributed significantly to the author's understanding of the subject matter, and to Dr. D. I. Dunthorn for many fruitful discussions of numerical and computer techniques. The cooperation of the Mathematics and Computation Departments of the Carnegie-Mellon University and the Mathematics Division of the Oak Ridge National Laboratory are acknowledged. The author is deeply indebted to J. R. Weir for his support and encouragement during the later stages of this work, and to Dr. G. R. Love for editing this manuscript. The illustration work of D. Gates and the typing efforts of Mrs. Jane Morrison are gratefully acknowledged. The author wishes to thank Mrs. Bette Thomas of the Metals and Ceramics Division Reports Office for the final typing and preparation of this manuscript.

Above all, the author wishes to thank his wife for her patience and understanding.

Portions of this work were sponsored by the United States Department of Army Research, Durham, North Carolina and the Oak Ridge National Laboratory, operated for the U. S. Atomic Energy Commission by Union Carbide Corporation.

TABLE OF CONTENTS

PAGE

Introduction 1

Nondiffusional Mechanisms 2

Diffusional Mechamisms 4

Theory 4

Experimental Observations 9

Relaxation of Kuczynski's "Small Neck Assumptions" 12

Numerical Method for Solution of Sintering Volume Diffusion in Two Dimensions 25

Physical Assumptions 25

Method of Solving for the Concentration Gradient of Vacancies Normal to an Arbitrary Interface 27

Cauchy Principal Value for the Singular Kernel 32

Replacing the Integral Equation with a System of Linear Equations 33

Solving the Set of Linear Equations 38

Tests of the Methods Used 40

Decay of an Ellipse by Volume Diffusion 40

Planar Analog of Sintering Using a Nonclosed Contour 45

Initial Profile Migration Behavior in Rod-to-Rod Sintering 47

The Nonclosed Contour 47

Errors Arising from the Nonclosed Contour and Finite Arc Spacing 52

PAGE

Correcting the Solution for the Nonclosed Contour and Reflected Neck 58

Defining the Migrating Boundary on Successive Time Steps 63

Solution to the Rod-to-Rod Sintering Problem and Errors in the Final Solutions 67

Errors Due to Finite Arc Spacing 67

Errors Due to Finite Time Steps 71

Solution to the Rod-to-Rod Sintering Problem 71

Dimensionless Parameters and Treatment of Experimental Data 77

Conservation of Volume 78

The Rod-to-Plane Sintering Problem 80

Discussion of Results 87

Numerical Methods and Errors 87

Comparison with Earlier Analyses 88

Calculations of Diffusion Coefficients from Experimental Data 89

Applicability of Numerical Techniques to Other Problems 94

Summary and Conclusions 94

References 97

Appendix 1: Numerical Solution of Sintering Problems Using Kuczynski-Type Geometrical Relations 100

Appendix 2: Quadrature Weighting Factors 109

PAGE

Closed Contour 109

Nonsingular Contour Integral 109

Nonclosed Contours 111

Nonsingular Nonclosed Contour Integral 111

Singular Nonclosed Contour Integral 113

Singular Closed Contour Integral 114

The Reflected Neck 115

Appendix 3: Two-Dimensional Crystal Growth 116

Introduction and Circle Test Case 116

Method of Numerical Solution for Noncircular S_1 119

Trial Applications of the Methods Developed 121

LIST OF TABLES

TABLE PAGE

1. Nichols Reciprocal Slopes from Numerical Results on Surface Diffusion Controlled Sintering 10
2. Tabulated Values of $\dot{\delta}/(D_v\delta)$ for Decay of Ellipse by Volume Diffusion 43
3. Comparison of Calculated D′ with D from Tracer-Diffusion Experiments 92

LIST OF FIGURES

FIGURE PAGE

1. Geometrical Relationships for Rod-to-Rod and Sphere-to-Sphere Sintering. (a) Cross section through two sintering rods or spheres. (b) Kuczynski's geometrical approximations for spheres. (c) Geometrical approximations similar to Kuczynski's for rods 5
2. Plot of x/a versus τ_V for Rod-to-Rod and Sphere-to-Sphere Sintering by Volume Diffusion 14
3. Plot of x/a versus τ_S for Rod-to-Rod and Sphere-to-Sphere Sintering by Surface Diffusion 15
4. Plot of x/a versus τ_V for Rod-to-Plane and Sphere-to-Sphere Sintering by Volume Diffusion 16
5. Plot of x/a versus τ_S for Rod-to-Plane and Sphere-to-Plane Sintering by Surface Diffusion 17
6. Plot of 1/n versus x/a for Rod-to-Rod Sintering by Volume Diffusion 18
7. Plot of 1/n versus x/a for Sphere-to-Sphere Sintering by Volume Diffusion 19
8. Plot of 1/n versus x/a for Rod-to-Rod and Sphere-to-Sphere Sintering by Surface Diffusion 20
9. Plot of 1/n versus x/a for Rod-to-Plane and Sphere-to-Plane Sintering by Volume Diffusion 21
10. Plot of 1/n versus x/a for Rod-to-Plane and Sphere-to-Plane Sintering by Surface Diffusion 22

FIGURE PAGE

11. Construction for Cauchy Integral Equation 23

12. Construction Used to Define (a) Real and Imaginary Parts of $ds/(s-z)$ and (b) the Angle $(r\upsilon)$ 31

13. Partitioning of the Continuous Contour S 34

14. Construction Used in Defining Kernels Numerically 37

15. Ellipse Geometry of Test Case 41

16. Plot of $\dot{\delta}/(D_v\delta)$ for the Decay of an Ellipse by Volume Diffusion versus $1/(\text{number of points on contour})^2$ 44

17. The Planar Analog of Rod-to-Rod Sintering 46

18. Schematic Plots of $C_I(s)$ and $\partial C_I(s)/\partial s$ for the Planar Analog Problem 48

19. Schematic Plot of Anticipated $C_I(s)$ and $\partial C_I(s)/\partial s$ for Rod-to-Rod Sintering. Discontinuous behavior dotted, numerical solution full lines. Cyclic boundary conditions shown fully. Shaded regions are neck regions 51

20. Initial Morphology Assumed for Rod-to-Rod Sintering. $P_{n'r}$ is the reflection of $P_{n'}$. S_q is the contour distance from $P_{n'}$ to P_q 53

21. Plot of $Q(k,m)$ versus $(\Delta s)^2$ for Rod-to-Rod Sintering, $x/a|_o = 0.10$ 55

22. Plot of $Q(k,m)$ versus $(1/k)$ for Rod-to-Rod Sintering, $x/a|_o = 0.10$ 56

23. Plot of $\Phi_I(s)$ versus s for $x/a|_o = 0.10$ 59

24. Migration of $P_i(x_i,y_i)$ on Curve S to $P_i'(x_i',y_i')$ on Curve SS 64

FIGURE PAGE

25. Plot of $D_v t$ versus x/a for Rod-to-Rod Sintering 69

26. Extrapolation of $D_v t$ versus $1/m^2$ to Estimate Error in Solution of Rod-to-Rod Sintering Problem 70

27. Plot of $D_v t$ versus x/a for Various Values of $\Delta N_{n'} = d \cdot \Delta s$ 72

28. Contours Generated During Early Stages of Rod-to-Rod Sintering 73

29. Contours Generated During Later Stages of Rod-to-Rod Sintering 74

30. Log-Log Plot of x/a versus $D_v t$ for Rod-to-Rod Sintering . . . 75

31. Plot of 1/n versus x/a for Rod-to-Rod Sintering 76

32. Plot of Q(k,m) versus $(\Delta s)^2$ for Rod-to-Plane Sintering $x/a|_o = 0.10$ 81

33. Plot of Q(k,m) versus 1/k for Rod-to-Plane Sintering $x/a|_o = 0.10$ 82

34. Log-Log Plot of x/a versus $D_v t$ for Rod-to-Plane Sintering 84

35. Plot of 1/n versus x/a for Rod-to-Plane Sintering 85

36. Profiles Generated During the Sintering of a Rod to a Plane 86

1-1. Geometry Common to Rod-to-Rod and Sphere-to-Sphere Sintering 102

1-2. Geometry Common to Rod-to-Plane and Sphere-to-Plane Sintering 103

FIGURE PAGE

2-1. General Closed Contour 110

2-2. Nonclosed Contour for Rod-to-Rod Sintering 112

3-1. Two-Dimensional Crystal Growth System 117

ABSTRACT

Given a two-dimensional region on which the concentration of a diffusing species satisfies Laplace's equation, and on whose boundary the concentration is specified, the Cauchy integral equation is used as a basis for determining the concentration gradient normal to the boundary at all points on the boundary.

Numerical methods based on this principle have been developed for treating volume diffusion controlled migration of arbitrarily shaped boundaries. These techniques are described, tested, and applied to the sintering of a rod to a rod and a rod to a plane.

Calculations of the volume diffusion coefficient for copper and silver systems to which the results are applicable indicate that neck growth in these systems proceeds one to two orders of magnitude too slowly to be accounted for by these results. However, the volume diffusion coefficient calculated from nickel sintering experiments agrees with that obtained from tracer diffusion experiments.

INTRODUCTION

The two features of sintering processes of greatest experimental and theoretical interest are the driving force and the dominant mechanism of material transport. A great deal of effort has been devoted to understanding these aspects of sintering in the past, but no unambiguous understanding of the process has yet emerged. It is reasonable to believe that different mechanisms are dominant in the sintering of different types of materials, and at different stages of the sintering of any one material. A short history of the evolution of the field provides supporting evidence for these statements.

Sintering is the process by which two or more bodies in contact form increasingly larger contact areas by material transport to the growing contact, or neck, area (1). This discussion will be primarily limited to sintering processes in which no external forces, including gravity, play a significant role as driving forces for the sintering reaction.

Attractive forces between particles (2), the transformation from the amorphous to solid state or changes in crystal structure (3), and recrystallization in the neck region (4) have all been proposed as driving forces for sintering. However, it is generally conceded today that surface tension is the most important driving force for sintering of bodies under no external forces (5).

Numerous material transport mechanisms have been cited for sintering in various systems. However, with the single exception of the surface diffusion mechanism, rigorous mathematical solutions for the rate at which sintering should occur by any mechanism have not been developed; there is considerable controversy over the role played by any mechanism

in the sintering of various materials. Plastic deformation, evaporation and condensation, surface diffusion, grain-boundary diffusion, and volume diffusion have all been proposed (6). Each deserves some attention.

Nondiffusional Mechanisms

The plastic deformation mechanism was first suggested by Frenkel (7) who attempted to relate the self-diffusion coefficient to viscosity and to treat the growth of a neck between spherical particles as a viscous flow problem. He derived the relationship that the neck radius, x, should be proportional to the square root of the sintering time, t. Kuczynski (8) sintered 0.05-in. diam. glass spheres to glass blocks and obtained a linear relationship between x and $t^{1/2}$ as well as reasonable values for the viscosity of glass in the temperature range studied. Although caution must be exercised in the application of time laws to determine a mechanism for sintering and will be discussed further below, it is felt that this experiment offers good evidence that viscous flow may be an operative sintering mechanism in materials of low viscosity. The $t^{1/2}$ law has never been reported for metals (6). Alexander and Baluffi (9) have discussed attempts to measure viscosities of metals and to apply Frenkel's mechanism to metal sintering systems and have concluded that a diffusion process is responsible for sintering in metal systems.

In a more recent attempt to demonstrate that plastic deformation may contribute the sintering of metals, Early *et al.* (10) sintered pure copper and internally oxidized Cu-Al compacts at high temperatures under externally applied loads. The rate of shrinkage was shown to depend upon the maximum calculated shear stress in the particles in agreement with

the dislocation climb creep models of Weertman (11,12) and Ansell and Weertman (13). The activation energy for the process was very close to that for self diffusion in pure copper; this observation supports either a diffusion or a plastic flow model. Salkind et al. (1) investigated the rate of change of electrical resistivity of loose beds of silver powder at 300°C and found that the activation energy for the process decreased as the externally applied stress increased. The activation energy for creep of silver wires behaved similarly. A dislocation mechanism was proposed as dominating the sintering process.

The experiments of Salkind and Early are difficult to evaluate, since the state of stress in their experimental systems is not known. While it is conceivable that plastic deformation may contribute to the early stages of neck growth, Wilson and Shewmon (6) question that dislocation multiplication can occur if the neck radius is greater than a tenth of the body radius. Further evidence that plastic deformation does not contribute to sintering in metal is provided by the experiments of Brett and Seigle (14). They observe that inert markers in sintering rods do not migrate into the neck region during the sintering of nickel, and conclude that a diffusion process is the dominant mass transport mechanism. However, marker material in glass and cellulose acetate fibers did migrate into the neck region, as would be expected if plastic deformation were the dominant transport mechanism.

Evaporation and condensation has never been seriously considered as a transport mechanism in the sintering of metals because metals have very low vapor pressures. In any event, the predicted relationship for neck growth (15), $x \propto t^{1/3}$, has never been observed.

Diffusional Mechanisms

Theory

Two diffusional mechanisms of transport, volume diffusion and surface diffusion, have been treated by Kuczynski in his classic work (15). Since most of the current literature is concerned with determining whether volume diffusion or surface diffusion is dominant for a particular set of experimental conditions, it is worthwhile to examine Kuczynski's treatments in some detail, and then to discuss Nichols' numerical solution of the surface diffusion problem.

Kuczynski assumed the surface tension, the volume diffusion coefficient, and the surface diffusion coefficient to be isotropic. These assumptions will be retained throughout this work. In order to facilitate further discussion, the remainder of Kuczynski's assumptions will be broken into two sets, which will be called geometrical assumptions and small neck assumptions. The geometrical assumptions are illustrated in Fig. 1(a). (1) Two spheres of radius "a" and separation of centers "2a" retain that radius and separation throughout the sintering process: this implies that material is constantly being added to the system. (2) The neck root is of constant curvature, smoothly joined to the sintering bodies.

The small neck assumptions include the following approximations [see Fig. 1(b)]: (1) the differential increments of volume for a neck growing between two spheres may be approximated by a right circular cylinder; (2) the area through which the flux is defined in the case of volume diffusion is the cylinder side; and (3) the length of the flux path for surface diffusion is approximately the neck radius of curvature, ρ.

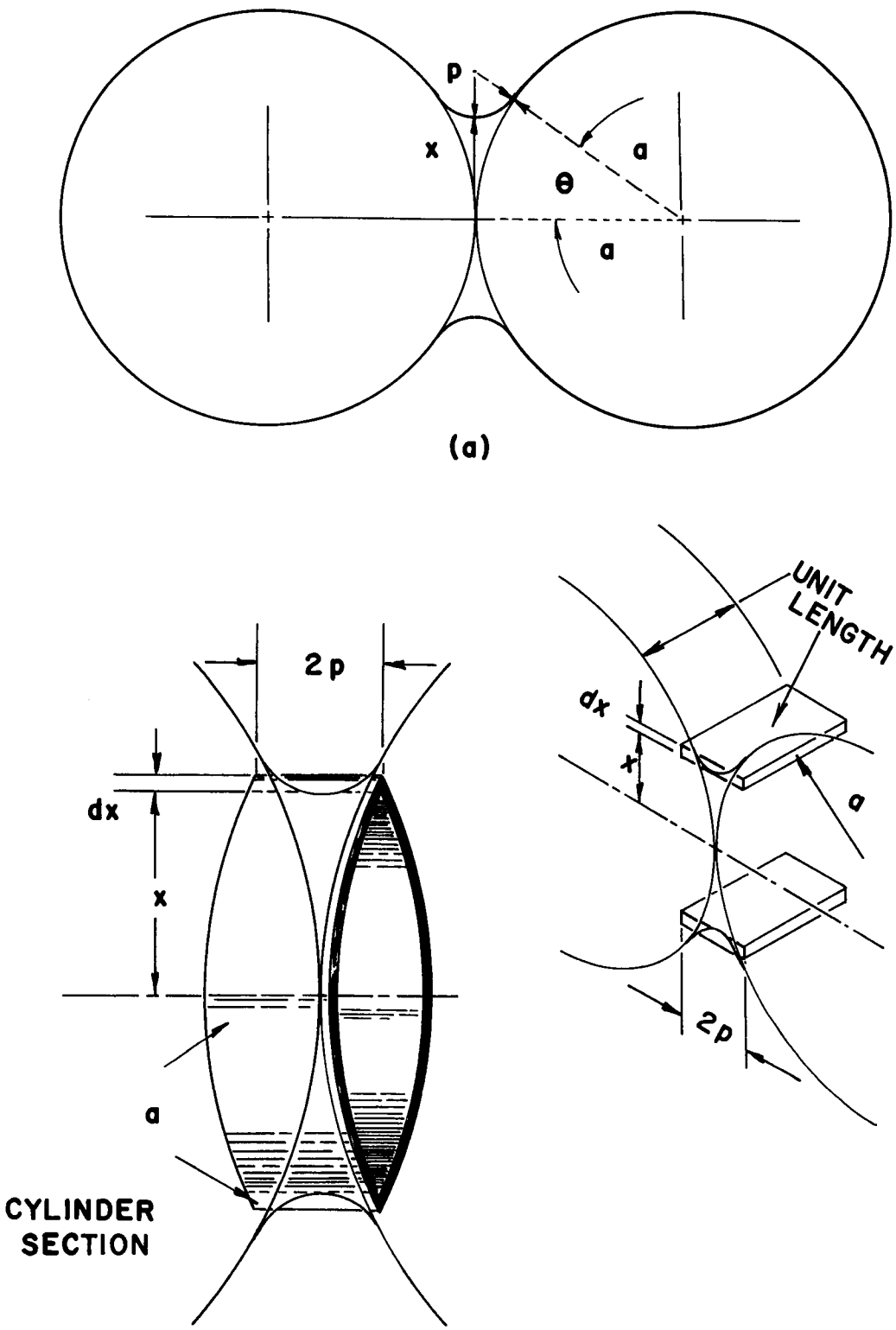

Fig. 1. Geometrical Relationships for Rod-to-Rod and Sphere-to-Sphere Sintering. (a) Cross section through two sintering rods or spheres. (b) Kuczynski's geometrical approximations for spheres. (c) Geometrical approximations similar to Kuczynski's for rods.

For our future use, small neck assumptions of the same nature are shown for the sintering of two rods in Fig. 1(c), where the differential element of volume is a slab, and the flat face of the slab is the area across which flux occurs by volume diffusion.

The relationship between the neck curvature and neck width, x, for sphere-to-sphere and rod-to-rod sintering is obtained from the Pythagorean theoreom; the equality on the left is exact while the approximation on the right is valid only if $x \ll a$. The latter is a "small neck assumption."

$$\rho = \frac{x^2}{2a - 2x} \cong \frac{x^2}{2a} \; . \tag{1}$$

The Gibbs-Thompson equation (5) is used to define ΔC_v^K, the difference between the equilibrium concentration of vacancies beneath a surface of local curvature K, C_v^K, and C_v°, the equilibrium concentration of vacancies under a flat surface:

$$\Delta C_v^K = C_v^K - C_v^\circ = -\frac{\gamma\Omega C_v^\circ}{kT} K \tag{2}$$

where γ is surface tension, Ω atomic volume, and k is Boltzmann's constant. If it is assumed that the vacancy concentration at a distance ρ from the neck interface equals that just under the main sphere surface, then the concentration gradient normal to the surface at the neck of sintering spheres is

$$\frac{\Delta C_v^s}{\rho} = -\frac{\gamma\Omega C_v^\circ}{kT\rho}\left(\frac{2}{a} + \frac{1}{\rho} - \frac{1}{x}\right) \cong -\frac{\gamma\Omega C_v^\circ}{kT\rho^2} \tag{3}$$

where the right approximation is a "small neck assumption" for $x \ll a$. The analogous concentration gradient expression for the sintering of rods is

$$\frac{\Delta C_v^r}{\rho} = -\frac{\gamma\Omega C_v^\circ}{kT\rho}\left(\frac{1}{a} + \frac{1}{\rho}\right) \cong \frac{\gamma\Omega C_v^\circ}{kT\rho^2} . \tag{4}$$

Conservation of material in either system, setting $x = 0$ at $t = 0$, requires that transport of material volume, V, across area, A, satisfy

$$\int_0^t dt = -\int_0^V \frac{dV}{\left(A_v \cdot D_v \frac{\partial c}{\partial n}\right)} \tag{5}$$

where D_v is the vacancy diffusion coefficient and n is taken normal to A. Making appropriate substitutions for V and A from Fig. 1 and integrating, one obtains the following relationship between neck radius and time for two spheres sintering by volume diffusion:

$$\frac{x^5}{a^2} = 20\,\frac{D_v\gamma\Omega C_v^\circ}{kT} \cdot t . \tag{6}$$

The analogous result for two sintering rods is given by:

$$\frac{x^5}{a^2} = 10\,\frac{D_v\gamma\Omega C_v^\circ}{kT} \cdot t . \tag{7}$$

Solutions for the rate of neck growth by surface diffusion are based on an expression given by Nichols (16) for the surface current of atoms, J_S, due to a surface gradient of curvature $\partial K/\partial s$ (υ is the surface density of atoms, D_s the surface-diffusion coefficient):

$$J_s = -\frac{D_s \gamma \upsilon \Omega^2}{kT} \frac{\partial K}{\partial s} . \tag{8}$$

The surface gradient of curvature is approximated as the difference between that of the sintering body and that of the neck root, which for sphere-to-sphere sintering is given by

$$\frac{\Delta K}{\Delta S_{Sphere}} = \frac{1}{\rho\left(\frac{\pi}{2} - \theta\right)} \left(\frac{2}{a} + \frac{1}{\rho} - \frac{1}{x}\right) \cong \frac{1}{\rho^2} , \tag{9}$$

while the corresponding approximations for rod-to-rod sintering are

$$\frac{\Delta K}{\Delta S_{rod}} = \frac{1}{\rho\left(\frac{\pi}{2} - \theta\right)} \left(\frac{1}{a} + \frac{1}{\rho}\right) \cong \frac{1}{\rho^2} . \tag{10}$$

If the surface current occurs over an area of $4\ \pi x \Omega^{2/3}$ for the sintering of spheres, or $4\ \Omega^{2/3}$ for the sintering of rods, then the same relationship is obtained for sphere-to-sphere and rod-to-rod neck growth by surface diffusion, that

$$\frac{x^7}{a^3} = 56\ \frac{D_s \gamma \upsilon \Omega^2}{kT} \cdot t . \tag{11}$$

However, Nichols (16) recently obtained a numerical solution for the sintering of a line of spheres and a sphere to a plane by surface diffusion in which both the geometrical and small neck assumptions were relaxed. The initially spherical surface was allowed to evolve into whatever shape naturally developed. Consequently, the neck root grew at the expense of material from just beyond the neck-sphere junction and the radius of

curvature at the neck root was larger than that assumed in Kuczynski's geometrical model. No simple time law such as Eq. (6), (7), or (11) fits the results; however, Nichols fit an equation of the form $x/a = At^{1/n}$ to the results for small ranges of x/a and obtained the values of n given in Table 1. At x/a = 0.1, the smallest n was 5.7, while at x/a = 0.3, the smallest n was 6.3. Nichols concludes, on the basis of a comparison of his numerical solution with Kuczynski's approximate solution, that for real metal bodies of 100 μ in diameter or smaller, volume diffusion does not dominate when $x/a \lesssim 0.6$. He further demonstrates that reasonable values for the surface diffusion coefficient of copper may be obtained by applying his results to the experimental data for the sintering of copper, and regards any volume self-diffusion coefficients obtained by applying Kuczynski's analysis to real data (17), however reasonable, as being fortuitous.

Experimental Observations

Wilson and Shewmon (6) have sintered lines of copper spheres of 100 to 300 μ in diameter in perhaps the most carefully executed of all sintering experiments to date. Their conclusion, that surface diffusion was the dominant transport mechanism for $T > 950°C$ and for $0.2 \leq x/a \leq 0.4$ was based on two types of analyses: (1) comparison of the rates of neck growth by volume and surface diffusion using solutions similar to Eqs. (6), (7), and (11); (2) application of Herring's scaling laws (5). The application of Herring's scaling laws, which relate reaction kinetics to the initial particle dimensions, indicate that surface diffusion transported a large fraction of the material deposited in the neck up to

Table 1. Nichols Reciprocal Slopes from Numerical Results on Surface Diffusion Controlled Sintering

x/a	Values of n from $x/a = At^{1/n}$	
	Sphere-to-Sphere	Sphere-to-Plane
0.05	5.7	5.6
0.1	5.9	5.7
0.3	6.3	6.5
0.5	6.8	7.3
0.7	6.9	7.9

$x/a = 0.28$, but they do not provide a clearcut indication of whether surface diffusion ever ceases to dominate the process.

The most recent evidence available for evaluating the contribution to neck growth between sintering spheres of diffusion along grain boundaries was obtained by Wilson and Shewmon. They measured the shrinkage which occurred during the sintering of lines of spheres, and concluded that less than 5% of the total material transported to the neck region during their experiments was due to grain-boundary diffusion.

Until Nichols' analysis was presented, much emphasis was placed upon the value of the slope of log-log plots of x/a versus t, since a slope of 1/5 would indicate volume diffusion dominance according to Eqs. (6) and (7), while Eq. (11) indicates that a slope of 1/7 should be obtained if surface diffusion were dominant. Kuczynski (15,17), Kingery and Berg (18), Alexander and Baluffi (9), Wilson and Shewmon (6), and numerous other experimenters have obtained data yielding slopes ranging between 1/5 and 1/5.5, and until recently this was a powerful argument favoring volume diffusion as the dominant material transport mechanism in systems of particles of diameter greater than 20 to 50 μ. However, Nichols' analysis indicates that such experimental observations also nearly agree with the slope predicted for a surface diffusion mechanism for some values of x/a. To further confuse the issue, Wilson has demonstrated that if $\rho \sim x^{5/3}$, assuming that the shapes evolved by volume diffusion are similar to those evolved by surface diffusion, that a slope of 1/5.8 is obtained for sintering by volume diffusion if shrinkage is accounted for.

Relaxation of Kuczynski's "Small Neck Assumptions"

It is of some interest to determine what portion of the difference between Nichols' numerical results and Kuczynski's analysis can be accounted for by what have been previously termed "geometrical assumptions," and what portion arises from the "small neck assumptions." This will be accomplished by relaxing the "small neck assumptions." The results will also provide an indication of the validity of Kuczynski's statement that his time laws are only valid for $x/a < 0.3$.

The details of the analysis for both volume diffusion and surface diffusion controlled sintering in rod-to-rod, sphere-to-sphere, rod-to-plane, and sphere-to-plane configurations are provided in Appendix 1. The variable $U = x/a$ is introduced, and the constants τ_V, τ_D, and $f(U)$ are evaluated exactly for the geometrical constraints prescribed by Kuczynski. Thus eight equations of the form

$$\frac{dU}{dt} = \tau_V \cdot f(U) \tag{12a}$$

$$\frac{dU}{dt} = \tau_s \cdot f(U) \tag{12b}$$

are derived for the eight sintering cases, the former form being used for the volume diffusion mechanism and the latter for a surface diffusion mechanism.

The solution of the differential Eq. (12) was performed numerically by the familiar "Modified Euler Method" (19), in which the errors are $O(\tau\Delta t)^3$. The technique involves determining an intermediate approximation to U in the $(i + 1)^{th}$ time step, $\bar{U}_{i+1}$. The system of equations to be solved is

$$U = U_o, \; t' = t_o, \; \frac{dU}{dt} = \tau \cdot f(U)$$

$$\overline{U}_{i+1} = U_i + \tau \cdot \Delta t' \cdot f(U_i)$$

$$U_{i+1} = U_i + \frac{\tau \Delta t}{2} [f(U_i) + f(\overline{U}_{i+1})] \; . \tag{13}$$

Because solutions were required over some ten orders of magnitude of t' to sinter from $U = 0.001$ to $U = 0.5$, a constant value of $A\Delta t'$ was not used on successive time steps; rather, the time steps were determined so that on successive time steps $\overline{U}_{i+1} = MU_i$. A number of trial solutions were computed for values of M ranging from 1.1 to 1.001. The values of At' required to achieve any particular value U converged rapidly for decreasing M. The results for $M = 1.005$ differed by less than 0.01% from those computed for $M = 1.001$. The numerical results presented in Figs. 2 through 5 were all obtained using $M = 1.001$.

In Figs. 2 and 4, the results are plotted for rod-to-rod, sphere-to-sphere, rod-to-plane, and sphere-to-plane sintering by volume diffusion. Figures 3 and 5 are plots of the results for the same geometries, for a surface diffusion mechanism.

The slope of $\ln(x/a)$ versus $(\tau_s t)$ or $(\tau_v t)$ was also determined numerically for each time step by differencing. This slope, which is comparable to $1/n$ in Kuczynski's results, is plotted as a function of x/a for each of the eight cases. (See Figs. 5 through 11.) It should be noted that significant deviation from the 1/5 and 1/7 slopes commences for $x/a \leq 0.1$. Further, the deviations in all cases except the sphere-to-sphere case tend toward increasing n with increasing x/a.

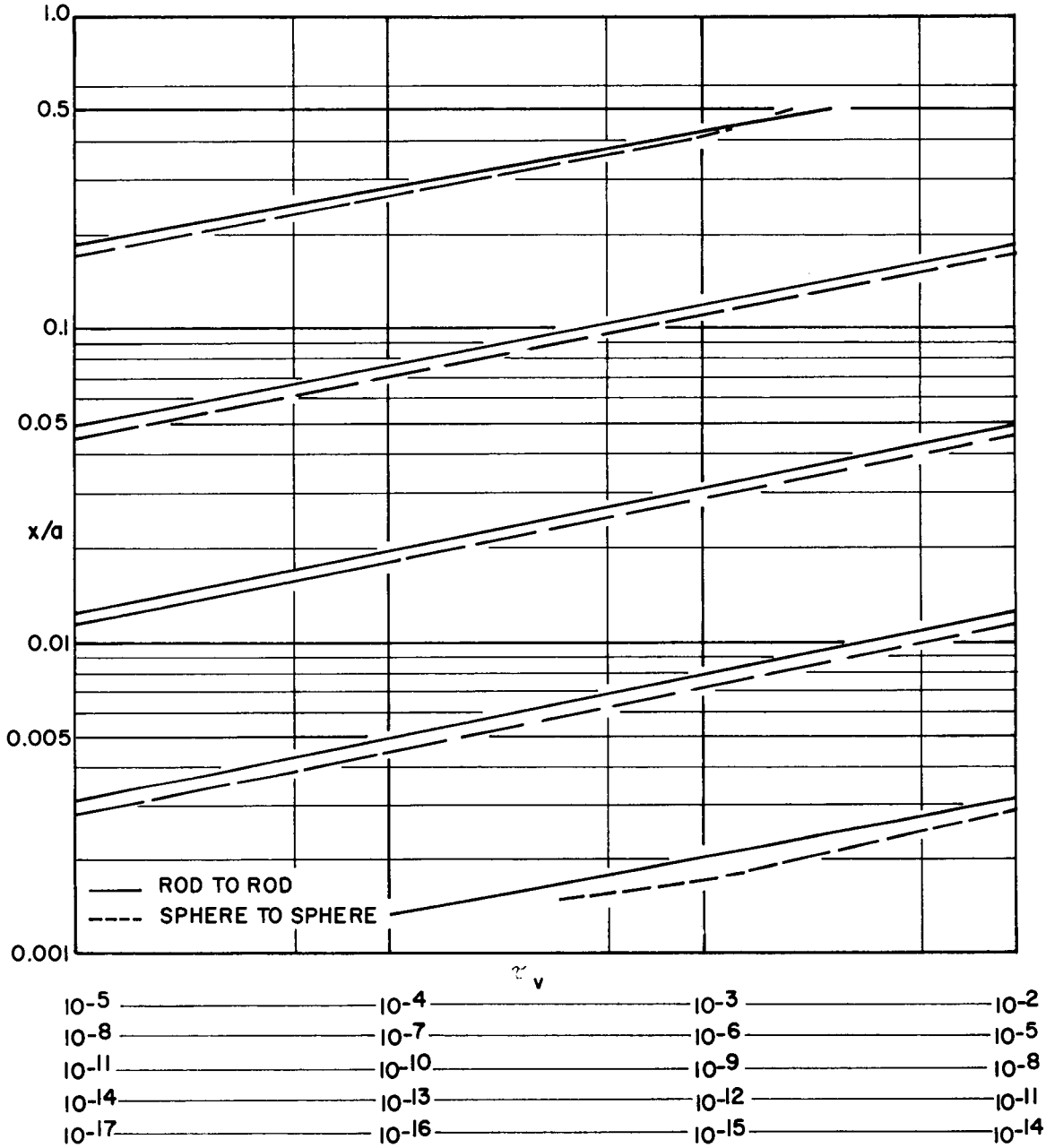

Fig. 2. Plot of x/a versus τ_v for Rod-to-Rod and Sphere-to-Sphere Sintering by Volume Diffusion.

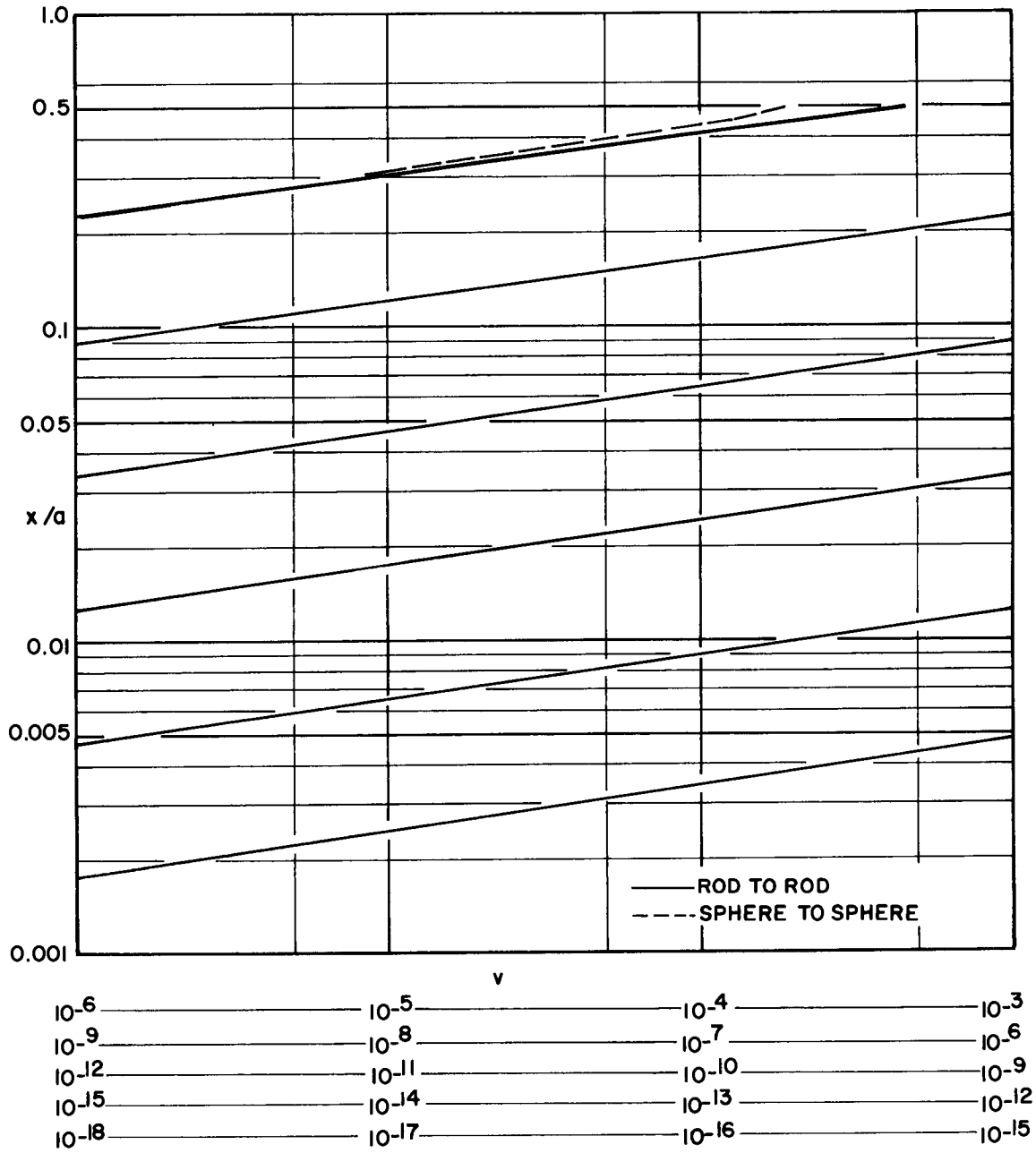

Figure 3. Plot of x/a versus τ_s for Rod-to-Rod and Sphere-to-Sphere Sintering by Surface Diffusion.

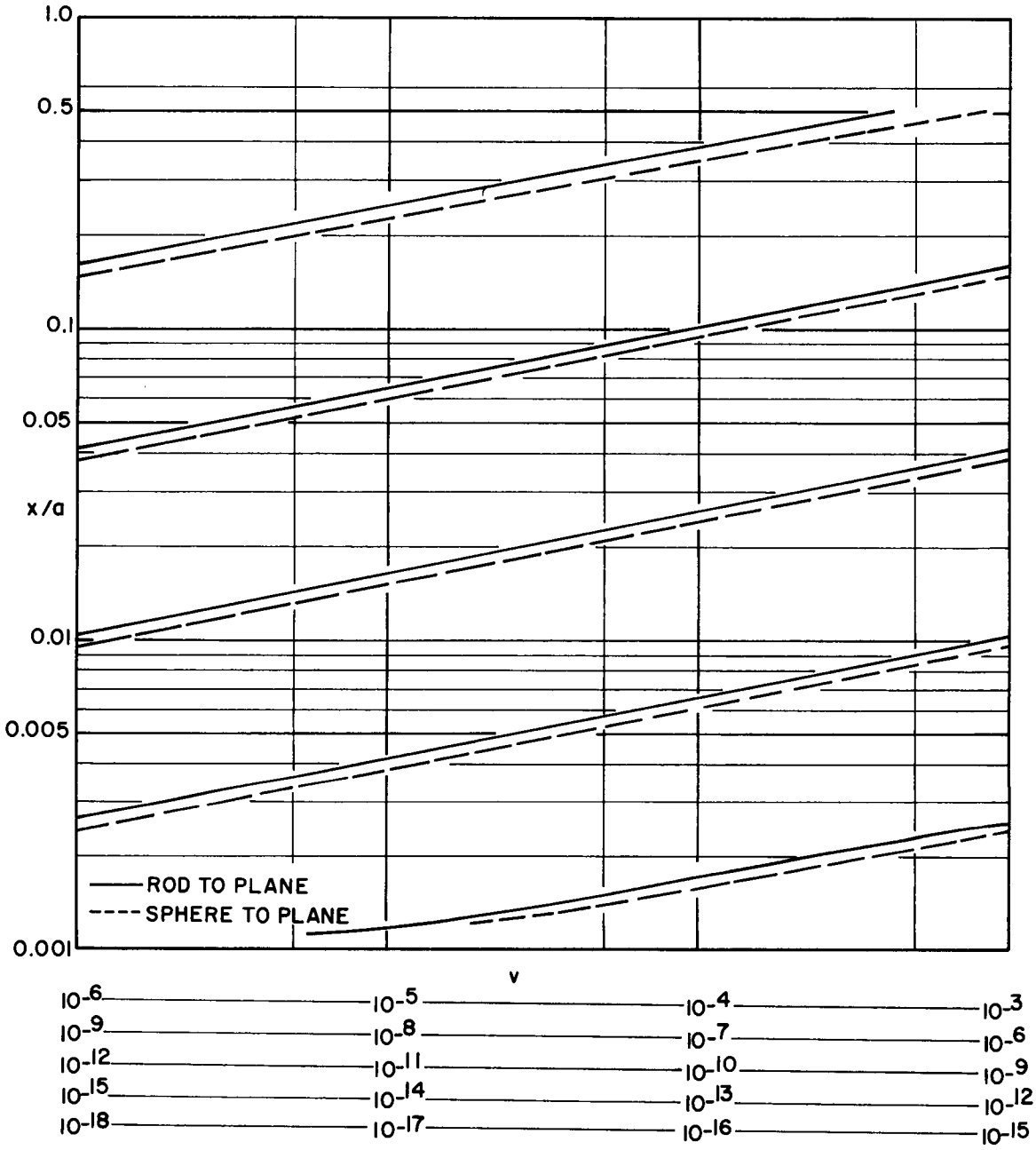

Fig. 4. Plot of x/a versus τ_v for Rod-to-Plane and Sphere-to-Sphere Sintering by Volume Diffusion.

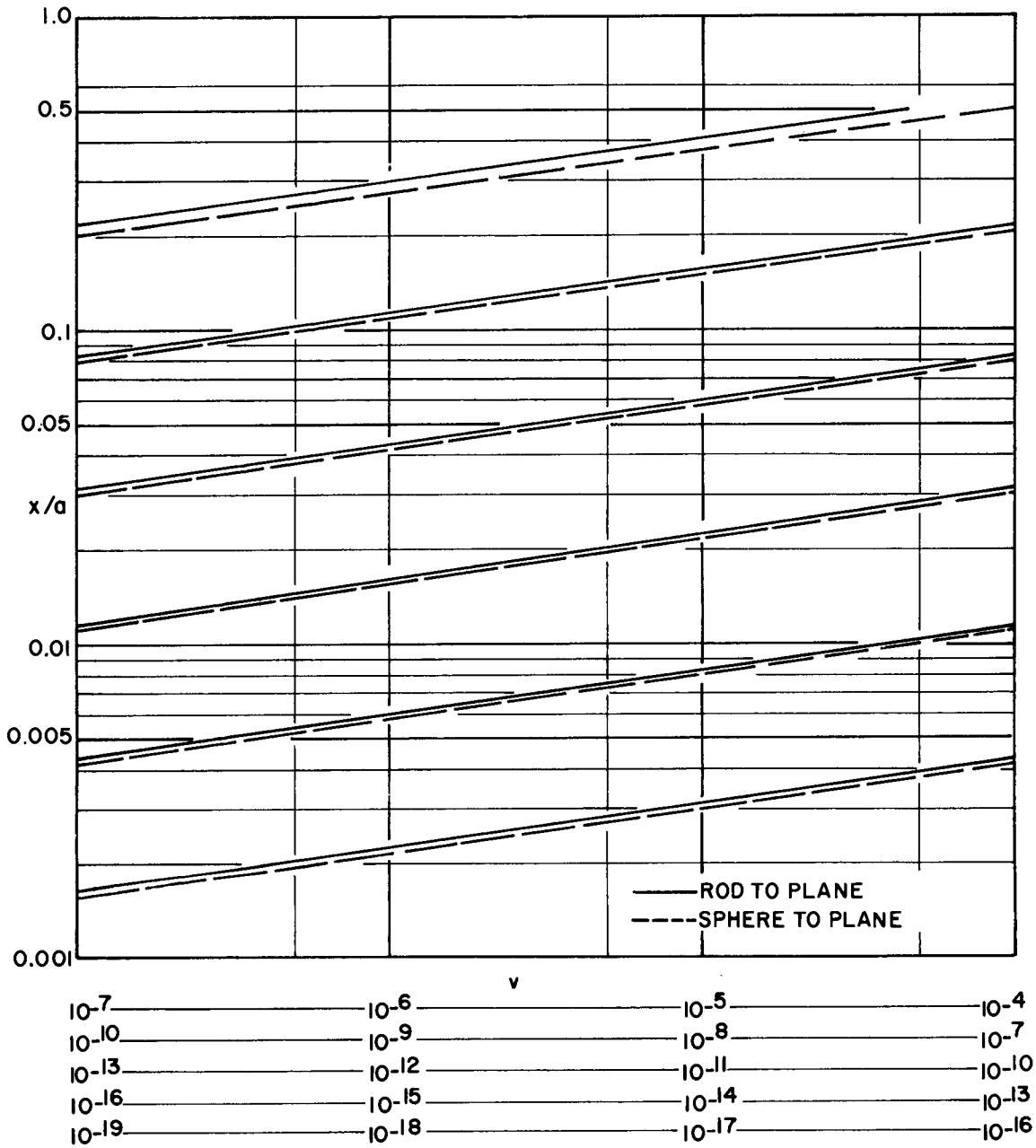

Fig. 5. Plot of x/a versus τ_s for Rod-to-Plane and Sphere-to-Plane Sintering by Surface Diffusion.

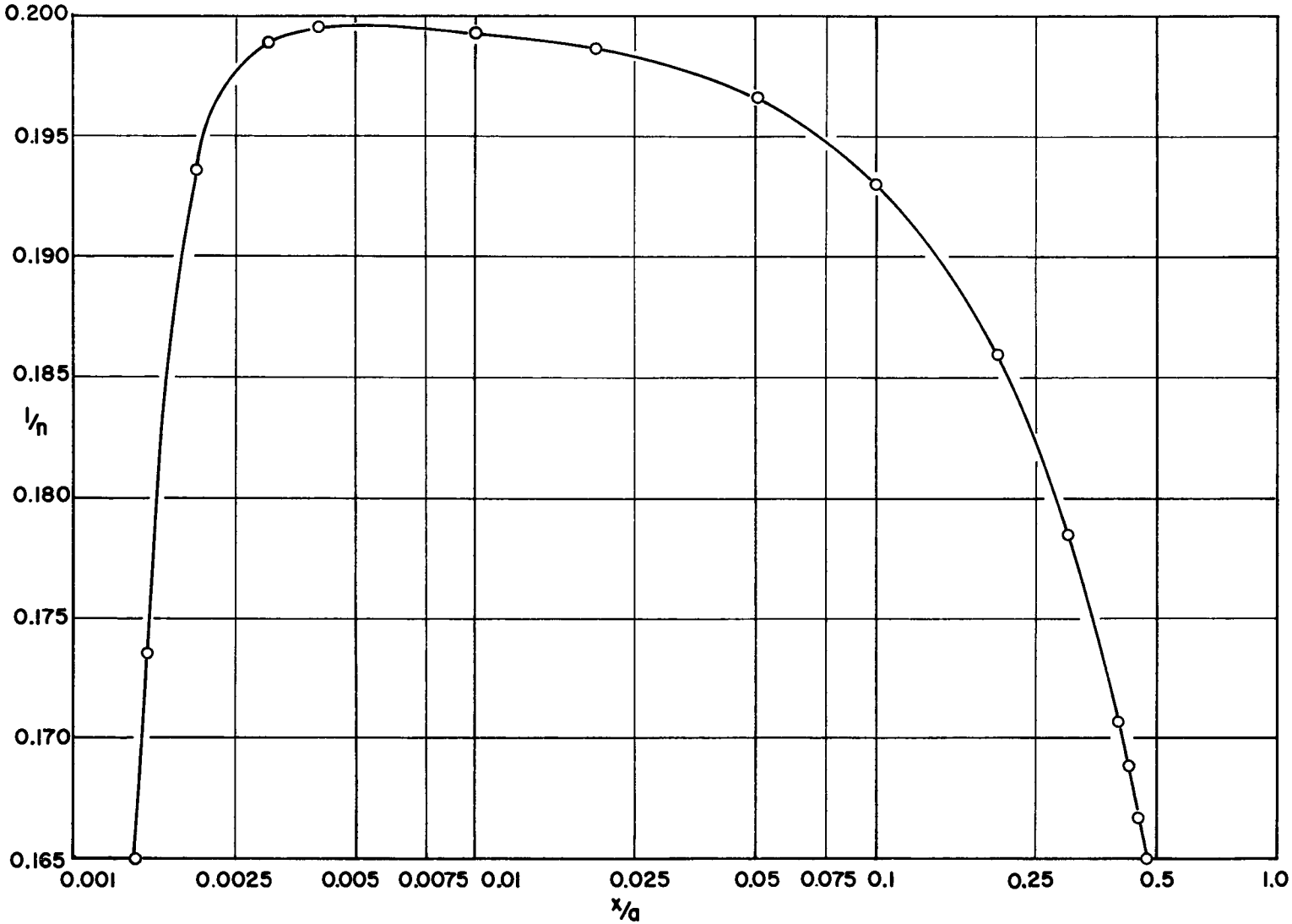

Fig. 6. Plot of 1/n versus x/a for Rod-to-Rod Sintering by Volume Diffusion.

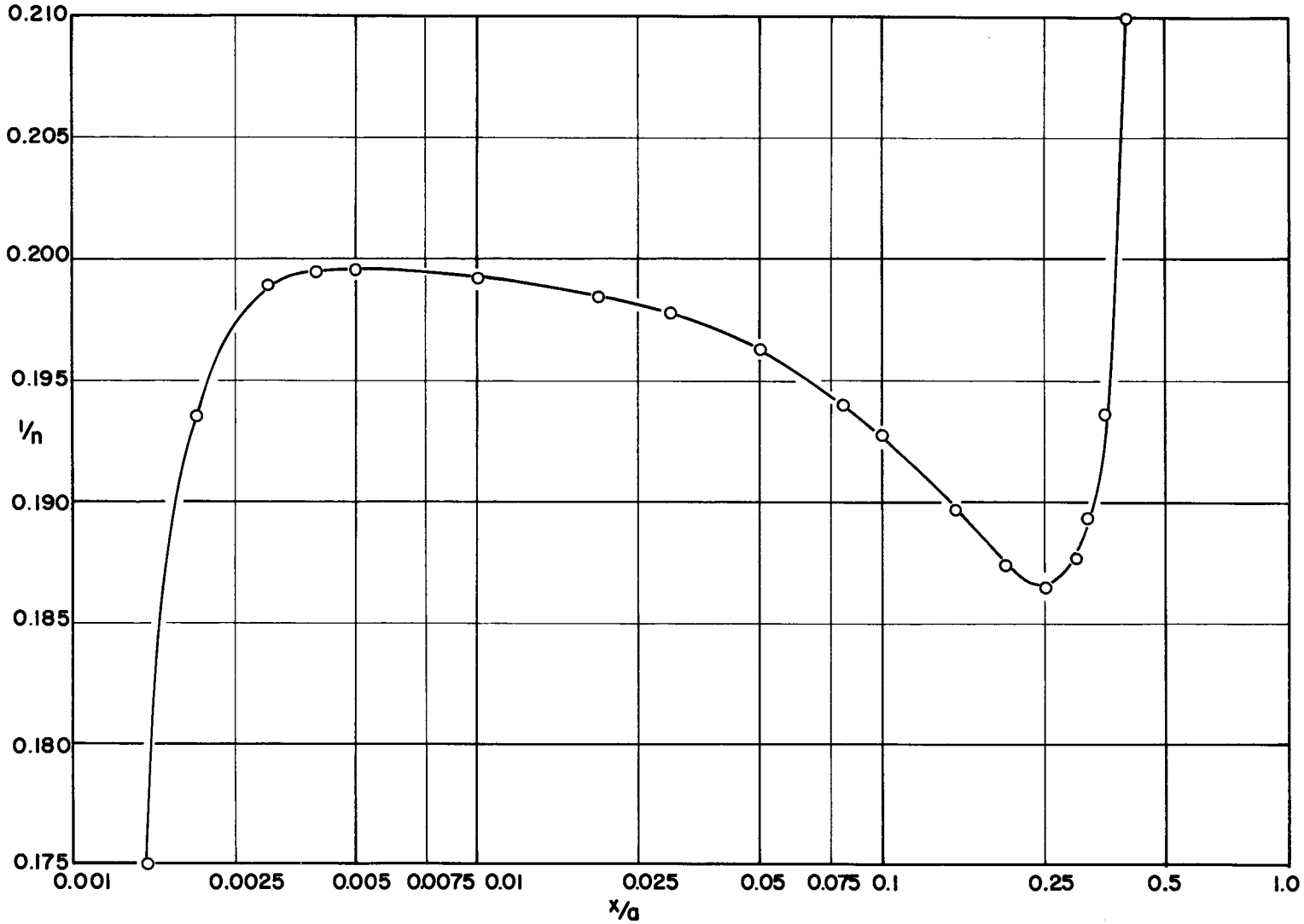

Fig. 7. Plot of 1/n versus x/a for Sphere-to-Sphere Sintering by Volume Diffusion.

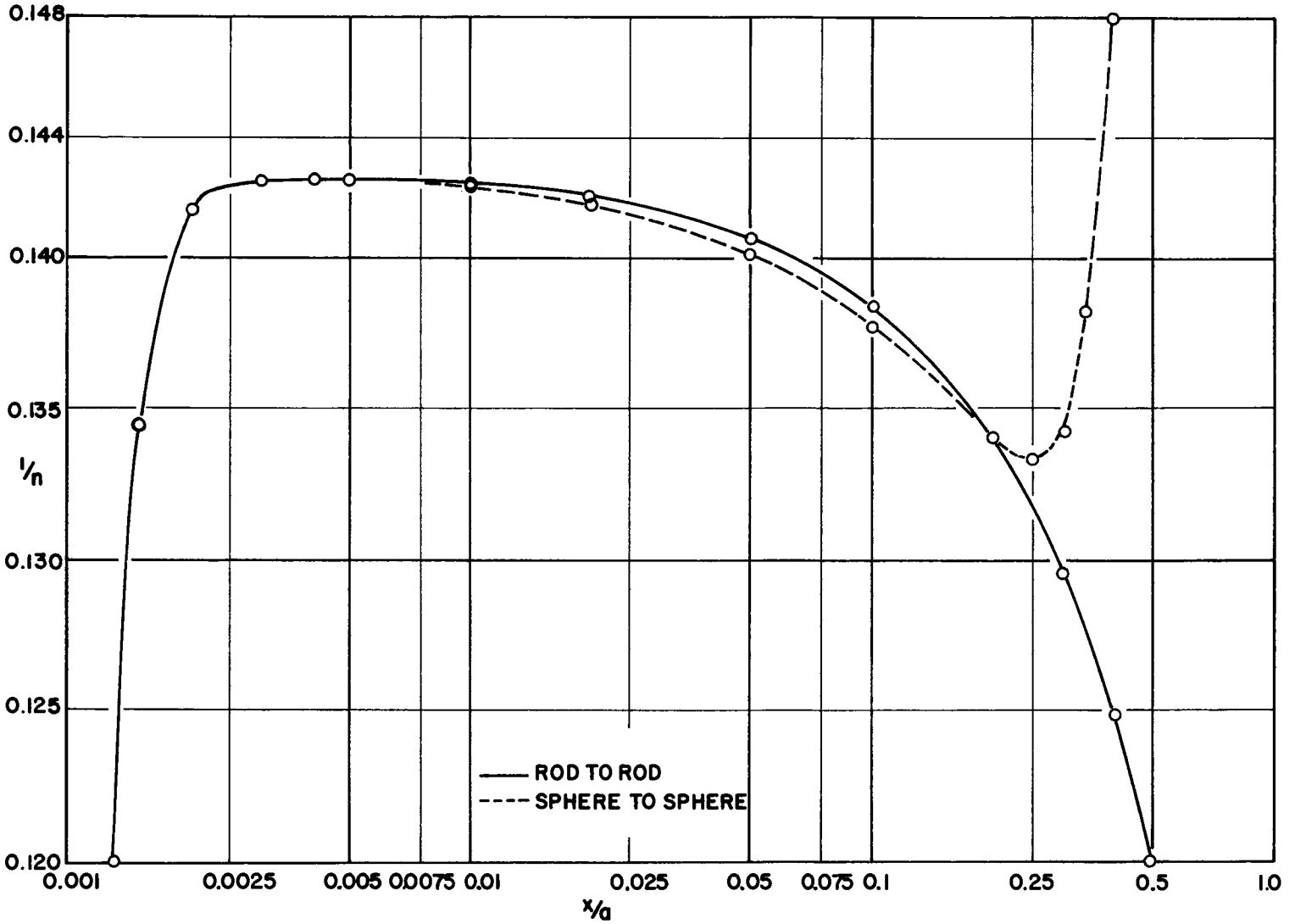

Fig. 8. Plot of 1/n versus x/a for Rod-to-Rod and Sphere-to-Sphere Sintering by Surface Diffusion.

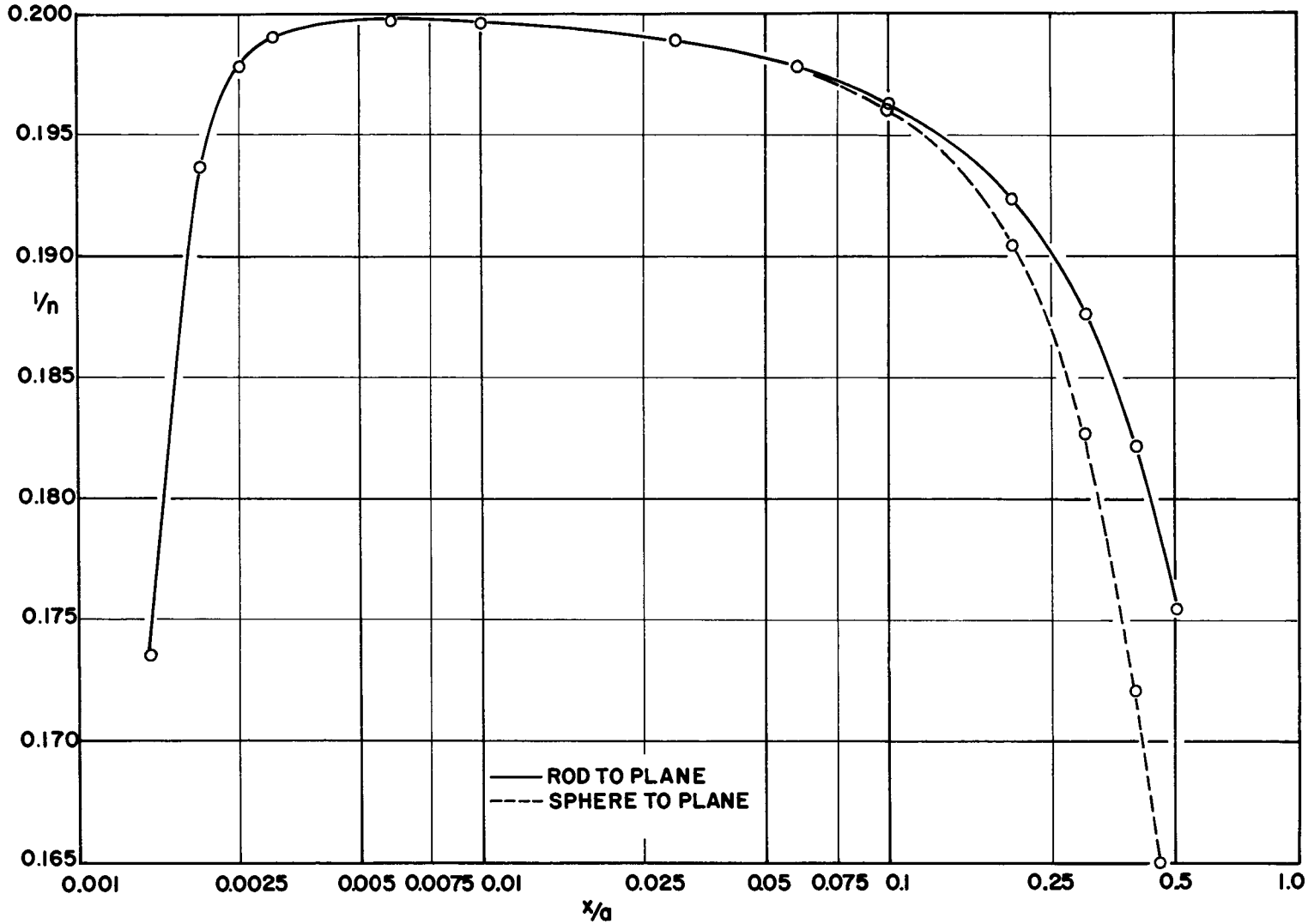

Fig. 9. Plot of 1/n versus x/a for Rod-to-Plane and Sphere-to-Plane Sintering by Volume Diffusion.

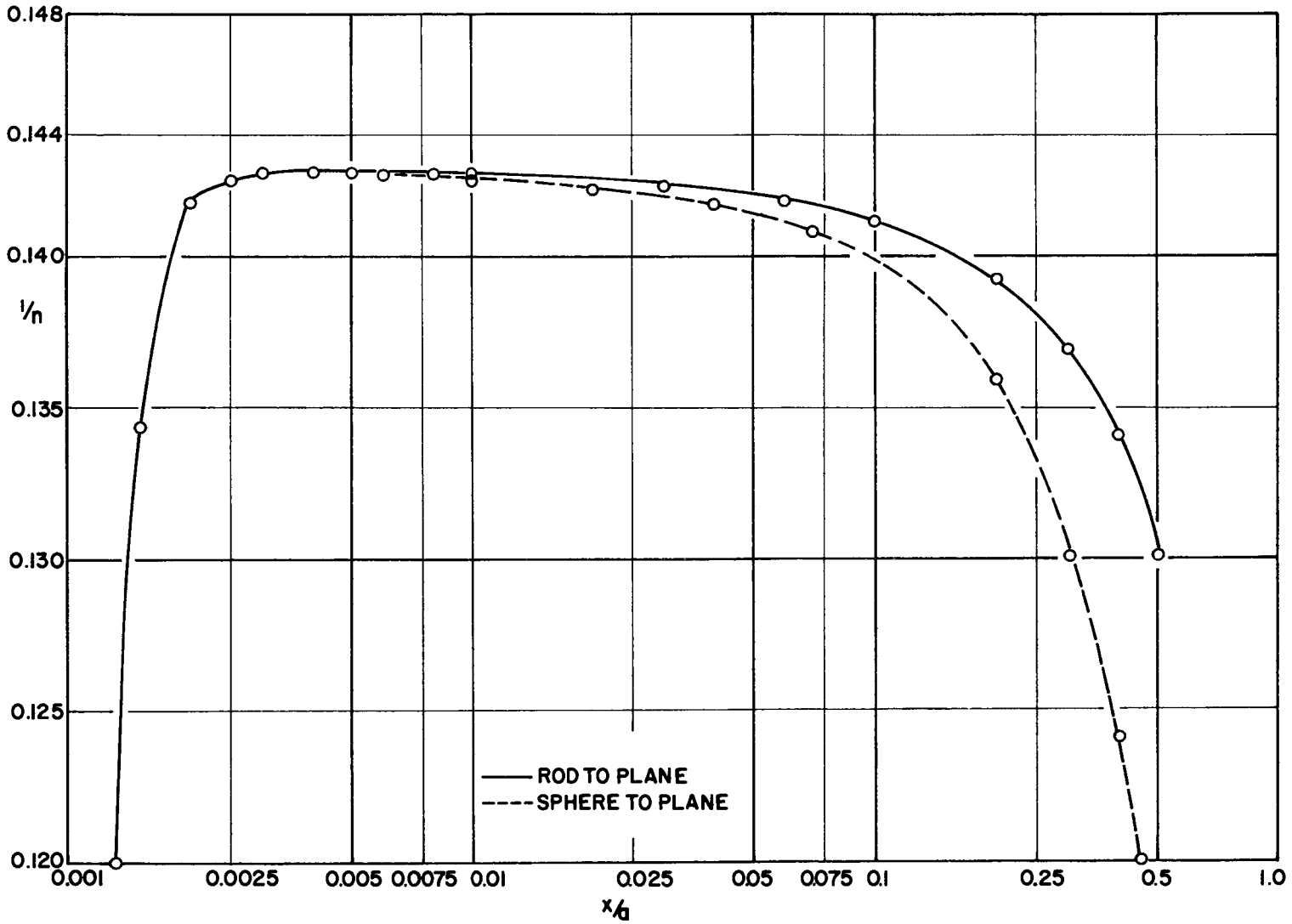

Fig. 10. Plot of 1/n versus x/a for Rod-to-Plane and Sphere-to-Plane Sintering by Surface Diffusion.

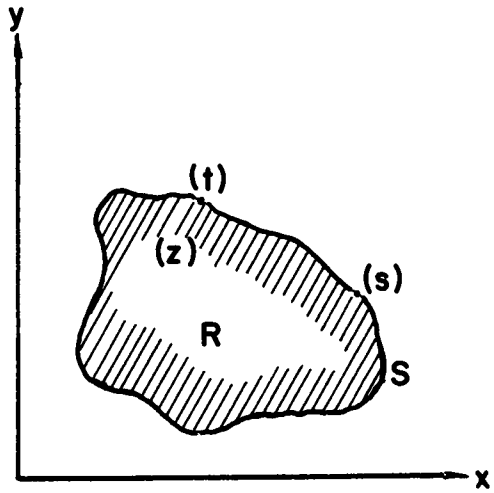

Fig. 11. Construction for Cauchy Integral Equation.

It will be noted that as $x/a \rightarrow 0$, the slopes do not approach the values 1/5 and 1/7 for volume- and surface-diffusion cases, respectively. This behavior results from the boundary condition of Eq. (13), that the initial $x/a \neq 0$ and initial $t' \neq 0$. It is a transient effect resulting from the mathematical method of solving Eq. (12) and has no bearing on any physical sintering process. The solutions to Eq. (12) have been obtained on a time scale t' where

$$t' = t - t_o = t[1 - (t_o/t)] \ . \tag{14}$$

The effect of t_o, which is essentially an artificial shift of the time base, decreases rapidly, as the last equality of Eq. (14) indicates. When $t = 100t_o$ the effect of t_o on t' is a 1% alteration of the time base. Further, if $U^5 \propto t$ or nearly so, then when $U = 2.51\ U_o$, the effect of the shifted time base has negligible effect on a calculated $d \ln U/d \ln t$. Therefore the slopes on Figs. 5 through 11 for $U < 0.0025$ are meaningless and should be ignored.

The points of interest thus gleaned from examining solutions to various sintering problems in which Kuczynski's "geometrical assumptions" are maintained but the "small neck assumptions" are relaxed are: (1) The 1/n slope values predicted by this analysis are not constant for $x/a > 0.1$. (2) The constant n tends to increase in these solutions with increasing x/a. (3) In order to eliminate the effects of initiating a solution to a volume diffusion controlled sintering process at $x_o \neq 0$ for $t' = t - t_o = 0$, x_o must be $< 2.51\ x_1$, where x_1 is the smallest neck diameter for which a numerical value of $d\ [\ln(x/a)]/d\ (\ln t)$ is desired.

(4) Thus, most experimental observations have been made over a range of x/a for which n varies, and since surface diffusion may contribute substantially to neck growth at small x/a, the time scale for computing $1/n$ may be shifted by some t_o.

These four points, coupled with Nichols' results indicating that Kuczynski's geometrical assumptions are not correct for sintering by surface diffusion, provide adequate justification for the remainder of this work, which is concerned with solving numerically for the rate of sintering of a rod to a rod and a rod to a plane by a volume-diffusion mechanism. The solutions to be developed do not impose an interface morphology on the neck region. Rather, whatever morphology develops naturally is used as a basis for computation.

NUMERICAL METHOD FOR SOLUTION OF SINTERING VOLUME DIFFUSION IN TWO DIMENSIONS

Physical Assumptions

The general problem of interface migration controlled by volume diffusion reduces to the specific problem of determining the flux of some diffusing species normal to the interface everywhere on the interface. In this treatment of sintering, vacancies are considered to be the mobile species.

Several important assumptions are made in order to facilitate the solution of the problem. The surface tension, γ, and the diffusion coefficient for vacancies D_v are assumed isotropic. It is assumed that local equilibrium obtains, and that concentration of vacancies just below the surface of the sintering body is determined by the Gibbs-Thompson

relationship [Eq. (2)]. The most important assumption made here to obtain a numerical solution is that the velocity of the most rapidly migrating portion of the interface is small compared to that of a vacancy. Under these conditions, an equilibrium concentration of vacancies exists throughout a sintering body at all stages of interest during sintering. This assumption may be simply justified as follows: if the jump frequency of a vacancy near the melting point of a real material, Γ_v, is about 10^{11} sec^{-1}, and a jump distance, α, of 3×10^{-8} cm is assumed; then the most probable displacement of a vacancy per second is $\alpha(\Gamma_v t)^{1/2}$ or 9×10^{-3} cm/sec. One may use Eq. (7) to approximate the rate of migration of the neck root (the most rapidly migrating surface region during sintering). Using typical values of $\gamma\Omega/kT = 10^{-7}$, $a = 10^{-3}$ cm, and a mole fraction of 10^{-3} for vacancies, it may be shown that the neck root velocity is approximately 4×10^{-5} cm/sec when $x/a = 0.1$. The equilibrium assumption is better for larger x/a and larger a, which is in the range of physical parameters for which volume diffusion is expected to become dominant. The fact that vacancies migrate about two orders of magnitude more rapidly than the neck root under the conditions described above is considered adequate justification for the assumption that vacancies are distributed in an equilibrium fashion during the periods of sintering which are of interest.

The justification offered above is equivalent to the arguments used previously by Mullins and Sekerka in justifying the use of Laplace's equation in treating slowly moving interfaces (20,21).

Method of Solving for the Concentration Gradient of Vacancies Normal to an Arbitrary Interface

Fick's second law reduces to the following form if the diffusion coefficient, D, is independent of concentration:

$$dc/dt = D\left(\frac{\partial^2 C_R}{\partial x^2} + \frac{\partial^2 C_R}{\partial y^2}\right) . \tag{15}$$

However, the assumption that vacancies are distributed in an equilibrium fashion throughout a sintering body at any stage of the sintering process implies that $dc/dt \sim 0$. Thus, the concentration of vacancies in a two-dimensional-sintering body must satisfy Laplace's equation,

$$\nabla^2 C_R(x,y) = \frac{\partial^2 C_R}{\partial x^2} + \frac{\partial^2 C_R}{\partial y^2} = 0 . \tag{16}$$

Since the concentration of vacancies is specified just under the surface by the Gibbs-Thompson equation, the problem of determining $C_R(x,y)$ at any stage of sintering is the classical Dirichlet problem.

The Dirichlet problem is the determination of a function which satisfies Laplace's equation, and which assumes preassigned values $C_R = C_R(s)$ on the boundary S of some simply connected region R. Here, we identify S with the two-dimensional profile of the sintering body and R with the region enclosed by S (that is, the body). The boundary values $C_R(s)$ are identified with the vacancy concentrations very near to the surface and are specified by the Gibbs-Thompson relation.

It is not necessary to solve the Dirichlet problem in order to determine the velocity of each element of surface. Rather, simply solving for $\partial C_R/\partial n$, the concentration gradient of vacancies normal to the boundary where n is the outward normal to the surface, provides all the information necessary to handle the migrating interface problem. There are a number of mathematical approaches which are plausible. The approach used in this work stems from the fact that since $C_R(x,y)$ is a harmonic function at any time, it is possible to construct an analytic function, $F(Z)$, such that

$$F(Z) = C_R(x,y) + i\, C_I(x,y) \ . \tag{17}$$

Further, since $F(Z)$ is analytic, it may be shown that the real and imaginary parts of $F(Z)$ have partial derivatives of all orders, and the first partial derivatives of the real and imaginary parts are related by the Cauchy-Riemann equations (20),

$$\frac{\partial C_R}{\partial x} = \frac{\partial C_I}{\partial y} \tag{18a}$$

$$\frac{\partial C_R}{\partial y} = -\frac{\partial C_I}{\partial x} \ . \tag{18b}$$

If the x-axis coincides with the outward normal to the interface, then the y-axis coincides with the line tangent to the interface. Thus, adopting the convention that the positive direction along the boundary is defined as counterclockwise with the body on the left, we may write that

$$\frac{\partial C_R}{\partial n} = \frac{\partial C_I}{\partial s} \ . \tag{19}$$

Thus, the required solution for $\partial C_R/\partial n$ may be obtained by solving for $\partial C_I/\partial s$.

The analytic function F(Z) at some point (Z) may be constructed within a simply connected region R bounded by curve S according to the Cauchy integral formula* (see Fig. 11) from a function C(s) defined on S by (21):

$$F(Z) = \frac{1}{2\pi i} \oint \frac{C(s)}{s - Z} \, ds \ . \tag{20}$$

Further, Mikhlin (23) shows that as Z tends from some point in R to a point t on the contour S, that F(Z) tends to a limit F(t) where F(t) is given by the singular integral equation

$$\lim_{Z \to t} F(Z) = F(t) = \frac{1}{2} C(t) + \frac{1}{2\pi i} \oint \frac{C(s)}{s - t} \, ds \ . \tag{21}$$

In general, the principal value of the integral of Eqs. (20) and (21) must be taken.

Mikhlin (23) makes another significant point. Equation (20) is valid (for a nonclosed integral) even if S is a simple arc rather than a closed curve. If we choose C(s) to be continuous, then Eq. (21) becomes (24):

$$C(t) = -\frac{1}{\pi} \oint \frac{C(s)}{s - t} \cdot ds \ . \tag{22}$$

---

*Note that Eq. (20) guarantees that the solution which is constructed will be analytic if C(s) is continuous (22).

By taking the imaginary parts of both sides of Eq. (22), it may be shown that

$$\mathrm{Im}[C(t)] = \mathrm{Im}\left[-\frac{i}{\pi} \oint \frac{C(s)}{s-t}\, ds \right]$$

$$C_I(t) = -\frac{1}{\pi} \oint \left[C_R(s) \cdot \mathrm{Re}\, \frac{ds}{s-t} - C_I(s)\, \mathrm{Im}\left(\frac{ds}{s-t}\right) \right] \quad (23)$$

The real and imaginary parts of $ds/(s-t)$ may be determined as follows: Let $\vec{ds}$ be a directed line segment of length $|ds|$ making an angle θ_1 with the x-axis, and $\overrightarrow{s-t}$ be a directed line segment making angle θ_2 with the x-axis [see Fig. 12(a)]. The value of $|\vec{ds}/(\overrightarrow{s-t})|$ is given by

$$\frac{|ds|}{|s-t|} = \frac{|ds|}{|s-t|} [\cos(\theta_1 - \theta_2) + i \cdot \sin(\theta_1 - \theta_2)] . \quad (24)$$

Now, we may define $\vec{r} = -(\overrightarrow{s-t})$ and define the angle $<(r\upsilon)$ as shown in Fig. 12(b), where $\vec{\upsilon}$ is a unit outward normal to S. The angle $<(r\upsilon)$ is obtained by the counterclockwise rotation of $\vec{r}$ into $\vec{\upsilon}$.

$$\theta_1 - \theta_2 = (r\upsilon) - \pi/2 . \quad (25)$$

By substituting Eq. (25) and Eq. (24) into Eq. (23), the following singular linear integral equation is obtained for $C_I(t)$:

$$C_I(t) = -\frac{1}{\pi} \oint \frac{C_R(s) \sin(r\upsilon)}{|\vec{r}|}\, ds - \frac{1}{\pi} \oint \frac{C_I(s) \cos(r\upsilon)}{|\vec{r}|}\, ds . \quad (26)$$

It is demonstrated by Lovitt (25) that

$$\lim_{|\vec{r}| \to 0} \cos \frac{(r\upsilon)}{|\vec{r}|} = \frac{1}{2} K(t) \quad (27)$$

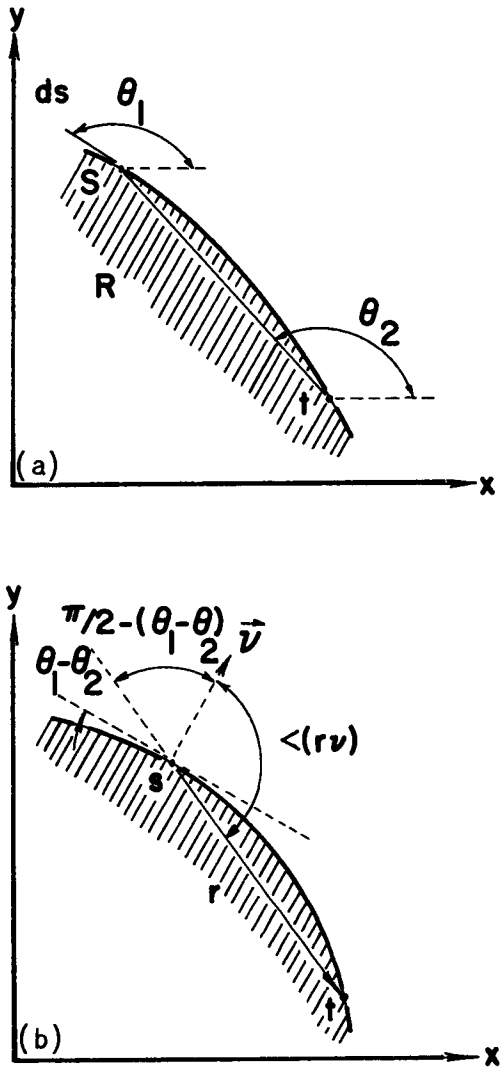

Fig. 12. Construction Used to Define (a) Real and Imaginary Parts of ds/(s-z) and (b) the Angle (rυ).

where $K(t)$ is the local curvature at point t.* Although the kernel $\sin(r\upsilon)/|\vec{r}|$ is singular, a method of dealing with this problem is discussed in the next section of this work.

Cauchy Principal Value for the Singular Kernel

If an integrand $f(s)$ has a singularity at $s = 0$, then the Cauchy principal value of the improper integral from $-a$ to a is defined as (26):

$$\int_{-a}^{a} f(s)ds = \lim_{\epsilon \to 0}\left[\int_{-a}^{-\epsilon} f(s)ds + \int_{\epsilon}^{a} f(s)ds\right] . \tag{28}$$

It is important that Eq. (26) is valid if the Cauchy principal values of any improper integrals are taken (26).

To evaluate the Cauchy principal value of the integral of Eq. (28), a new function $g(s)$ is defined and expanded in a Taylor series about $s = 0$:

$$g(s) = s \cdot f(s) = g(0) + g'(0) \cdot s + g''(0) \cdot \frac{s^2}{2!} + \ldots + g^{(n)}(0)\frac{s^n}{n!} + \ldots .$$

Hence,

$$\int_{-a}^{a} f(s)ds = \int_{-a}^{a} \frac{g(s)}{s}\, ds = \int_{-a}^{a} \left[\frac{g(0)}{s} + g'(0) + g''(0)\frac{s}{2!} + \ldots\right] ds .$$

However, the integrals of the terms involving $g^{(n)}(0)$ are zero due to symmetry for even values of n. Neglecting terms in $g^{(3)}(0)$ and higher, Eq. (28) becomes

$$\int_{-a}^{a} f(s)\, ds \cong \int_{-a}^{a} g'(0)ds = 2\, ag'(0) . \tag{29}$$

---

*The local curvature may be obtained from $1/r = d\theta/ds$ for a two-dimensional body where θ is the angle between a normal to the curve and the x-axis.

Since it is anticipated that the solution to Eq. (26) will be obtained numerically by discretizing the boundary representation to a set of arc segments of length Δs, it is desirable to approximate $g'(0)$ by a centered difference:

$$g'(0) \cong [g(a) - g(-a)]/(2\Delta s) \ .$$

Therefore a useful numerical approximation to the improper integral considered in Eq. (28) is given as:

$$\int_{-a}^{a} f(s)\ ds \cong a[f(a) + f(-a)] \ . \tag{30}$$

Replacing the Integral Equation with a System of Linear Equations

Equation (26) is a classical integral equation of Fredholm of the second kind. The inhomogeneous term is an integral whose value may be determined. By using methods described by Fox and Goodwin (27) or Kantorovich and Krylov (28), solutions may be obtained according to the techniques described below. Several other methods have been described by these and other authors, but the use of the high speed digital computer makes the techniques described here particularly attractive.

Any contour in question is divided into n arc segments of equal length Δs, and the parameter s defined from some starting point such that $s_k = k\Delta s$. The x and y coordinates (x_k, y_k) and the normal angle θ_n for the set of points P_k which determine such a system are shown in Fig. 13. The integrals may now be replaced by a quadrature approximation of the form

$$\int_a^b f(s)\ ds \cong \sum_{k=0}^{n} A_k\ f(s_k)\ \Delta s + e \ , \tag{31}$$

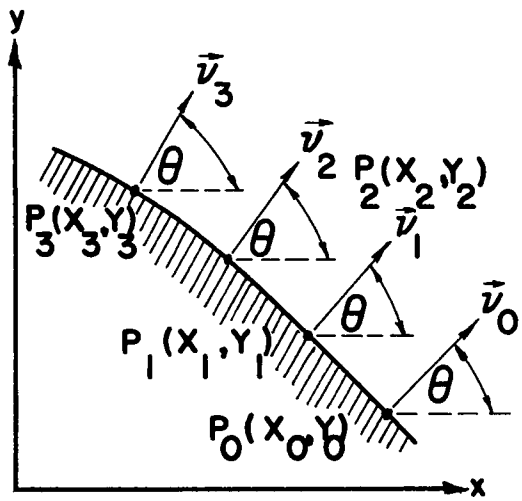

Fig. 13. Partitioning of the Continuous Contour S.

where e is the error introduced by the quadrature. This error term will be discussed later. The terms A_k and s_k are constant for any particular integral and for any particular quadrature formula. Among the quadrature formulae which may be used are the rectangular, trapezoidal, Simpson, Chebyshev, and Gaussian formulae. Although the latter two formulae are generally the most accurate, the s_k are not evenly spaced in arc length, making them somewhat difficult to apply in the schemes which were used in solving the integral Eq. (26). The rectangular and trapezoidal schemes were judged to be too inaccurate for the purposes of this work, leaving the Simpson quadrature formula as the most promising scheme. (In fact, this statement is supported by work in which the trapezoidal formula was used. As might be expected, the error of the trapezoidal quadrature was larger than that of the Simpson quadrature, and decreased much more slowly as Δs was decreased.)

In the usual Simpson formulae, where the range of integration is broken into n segments of arc length Δs, the $s_k = K\Delta s$, and the A_k are defined by the following equations:

$$A_1 = A_n = (b - a)/3$$

$$A_2 = A_4 = A_6 = \ldots. = A_{n-1} = 4(b - a)/3$$

$$A_3 = A_5 = A_7 = \ldots. = A_{n-2} = 2(b - a)/3 \ . \qquad (32)$$

Kantorovich and Krylov discuss the maximum error, σ, of the Simpson quadrature. Evaluation of this error is not simple, since it depends upon the derivatives of both the function $C(s)$ and the kernel. For this reason, only a numerical analysis of the error involved in solving the

integral equation will be attempted. It is of interest, however, to note the dependence of σ on the range and number of segments. Here, $T^{(4)}$ is an unevaluated term involving the derivatives mentioned earlier:

$$\sigma \leq \frac{1}{90} (b - a)^5 \frac{T^{(4)}}{(n - 1)} 4 .$$

The second order Simpson quadrature formula has the accuracy of a third order polynomial quadrature formula.

For any two points, P_i and P_j, the numerical values of the kernels may be obtained as follows (see Fig. 14). Suppose that Eq. (26) is written for point P_i, and that P_j is one of the points on the integration path. Then the following definitions may be made:

$$K'_s(i,j) = \frac{\sin (r\upsilon)_{i,j}}{|\vec{r}_{i,j}|} = \frac{\vec{r} \times \vec{\upsilon}}{|\vec{r}| \cdot |\vec{\upsilon}| \cdot |\vec{r}|}$$

$$= \frac{(x_i - x_j) \sin \theta_j - (y_i - y_j) \cos \theta_j}{(x_i - x_j)^2 + (y_i - y_j)^2} , \qquad (33)$$

$$K'_c(i,j) \frac{\cos (r\upsilon)_{i,j}}{|\vec{r}_{i,j}|} = \frac{\vec{r} \cdot \vec{\upsilon}}{|\vec{r}| \cdot |\vec{\upsilon}| \cdot |\vec{r}|}$$

$$= \frac{(x_i - x_j) \cos \theta_j + (y_i - y_j) \cdot \sin \theta_j}{(x_i - x_j)^2 + (y_i - y_j)^2} . \qquad (34)$$

For convenience, the further definition is made that the unprimed $K_s(i,j)$ and $K_c(i,j)$ are the products of $K'_s(i,j)$ and $K'_c(i,j)$ with the appropriate values A_k for the integration under consideration.

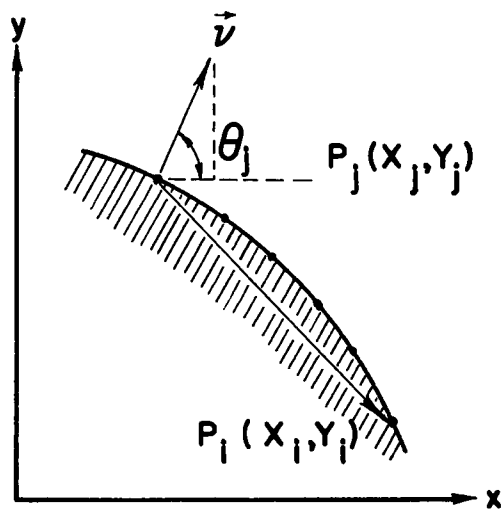

Fig. 14. Construction Used in Defining Kernels Numerically.

$$K_s(i,j) = \frac{1}{\pi} A(i,j) \cdot K'_s(i,j) \, \Delta s \ , \tag{35}$$

$$K_c(i,j) = \frac{1}{\pi} A(i,j) \cdot K'_c(i,j) \, \Delta s \ , \tag{36}$$

Note that these $A(i,j)$ must take account of the approximation to the singular term $K_s(i,i)$ [Eq. (30)] and the limiting value of $K'_c(i,i)$ as given in Eq. (27). For the detailed description of the arrays thus defined for the cases of closed and nonclosed contours, see Appendix 2.

Under these limitations, it is now possible to replace the system of integral equations represented by Eq. (26) by the following system of linear equations:

$$C_I(i) \cong \phi_I(i) = \sum_{j=1}^{n} K_s(i,j) C_R(j) + \sum_{j=1}^{n} K_c(i,j) \cdot \phi_I(j) \tag{37}$$

where $\phi_I(i)$ is the approximate solution obtained from the set of linear equations.

The methods of solution of this system of equations will be the next consideration.

Solving the Set of Linear Equations

Almost all texts on linear integral equations describe a method of successive approximations for determining $\phi_I(i)$ by expanding $\phi_I(i)$ and using the so-called iterated kernels. However, solutions may be obtained much more rapidly on a digital computer by rewriting Eq. (37) as a matrix equation in which the values $\phi_I(i)$ and $C_R(i)$ are treated as elements of

one-dimensional arrays and $K_s(i,j)$ and $K_c(i,j)$ are treated as elements of two-dimensional arrays, or, as vectors and matrices, respectively. Retaining the same notation, Eq. (37) becomes

$$\vec{\phi}_I = \underset{\sim}{K}_s \cdot \vec{C}_R + \underset{\sim}{K}_c \cdot \vec{\phi}_I \qquad (38)^*$$

By rearranging Eq. (38) a solution may be obtained directly by matrix inversion.

$$\vec{\phi}_I = (\underset{\sim}{I} - \underset{\sim}{K}_c)^{-1} \cdot \underset{\sim}{K}_s \cdot \vec{C}_R \ . \qquad (39)$$

The matrix $\underset{\sim}{I}$ is the identity matrix. Fortunately, in all of the systems which have been investigated to date, $(\underset{\sim}{I} - \underset{\sim}{K}_c)$ is a well-conditioned matrix. Thus, it may be inverted accurately, even when the order of the matrix is 90 or higher. On both the Bendix G-21 computer and the CDC-1604 computer, the $(\underset{\sim}{I} - \underset{\sim}{K}_c)$ matrix has been inverted using Gauss-Jordan reduction methods on matrices of order 90 for elliptical contours and for the contours generated during the sintering of a rod to a rod. The products of $(\underset{\sim}{I} - \underset{\sim}{K}_c)$ and its inverse have been formed, and found to be equal to the identity matrix to at least seven significant places.

Matrix inversion is a time consuming process on a digital computer, and the method of successive substitutions may be used in solving for $\vec{\phi}_I$ to avoid using matrix inversion. If an approximation to $\vec{\phi}_I$ is known

---

*Matrix notation: textbook style calls for bold-face type. Suggested that "small m" underscore be replaced by wavy underscore, example: $\underset{\sim}{K}_s \cdot \vec{C}_R$.

(from matrix inversion for a similar contour, in most cases) called $\vec{\phi}_I^0$, then the sequence of successive substitutions

$$\vec{\phi}_I^1 = \underset{\sim}{K}_s \cdot \vec{C}_R + \underset{\sim}{K}_c \cdot \vec{\phi}_I^0 \tag{40a}$$

$$\vec{\phi}_I^{(j+1)} = \underset{\sim}{K}_s \cdot \vec{C}_R + \underset{\sim}{K}_c \cdot \vec{\phi}_I^{(j)} , \tag{40b}$$

produces a set of $\vec{\phi}_I^{(j)}$ which converge rapidly to $\vec{\phi}_I$. An example of this convergence will be given later.

Tests of the Methods Used

Decay of an Ellipse by Volume Diffusion

The decay of an ellipse by volume diffusion was selected as a test case for the numerical techniques described earlier. The remarks in Appendix 2 used in defining $\underset{\sim}{K}_s(i,j)$ and $\underset{\sim}{K}_c(i,j)$ for a closed contour apply to this geometry. The ellipse contour was defined by the standard equations. (See Fig. 15.)

$$r = R_o + \delta \sin (2\theta - \pi/4)$$

$$k = 2(R_o\delta)^{1/2}/(R_o + \delta)$$

where k is the eccentricity of the ellipse. The points P_i were spaced at equal arc intervals around the contour, using several terms of a series expansion of the following integral to accomplish the spacing.

$$s = (R_o + \delta) \int_0^{\phi} (1 - k^2 \sin^2 \theta)\, d\theta .$$

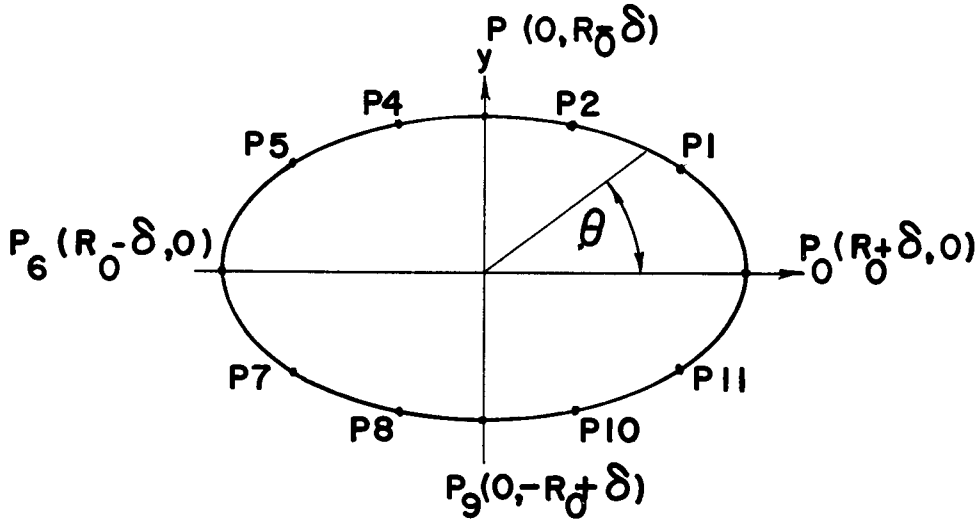

Fig. 15. Ellipse Geometry of Test Case.

Solutions were obtained for three values of k, with 8, 16, 24, 32, and 40 points spaced about the contour for each value of k.

The solutions were obtained by solving for $\vec{\phi}_I$, and approximating

$$\left.\frac{\partial C_R}{\partial n}\right|_{P_i} \cong \left.\frac{\partial \phi_I}{\partial s}\right|_{P_i} \cong \frac{\phi_I(i+1) - \phi_I(i-1)}{2\Delta s} \tag{41}$$

where Δs is the arc spacing between points. The velocity of the point P_i is obtained by a material balance as:

$$v_i = \frac{D_v \partial C_R/\partial n}{[1 - C_R\ (i)]} \cong \frac{D_v[\phi_I(i+1) - \phi_I(i-1)]}{2\Delta s[1 - C_R(i)]} \ . \tag{42}$$

Nichols (29) has given the solution of this problem for a small perturbation value of k, which may be condensed to

$$\frac{\dot{\delta}}{D_v \delta} = -\frac{\gamma \Omega C_o}{kTR_o} \frac{6}{R_o}^{3} \ .$$

For a fixed set of physical parameters, $R_o = 1$, $(\gamma\Omega C_o)/(kT) = 10^{-3}$, the term $\dot{\delta}/(D\Omega\delta)$ should equal 6×10^{-3}.

The results of the numerical scheme are tabulated in Table 2 to illustrate the very small difference (less than 0.1%) in results obtained when $\delta = 2.7466 \times 10^{-5}$ and $\delta = 2.7466 \times 10^{-4}$. A plot of $\dot{\delta}/(D_v\delta)$ versus the reciprocal of the square of the number of points P_i used to define the contour, which is a measure of $(\Delta s)^2$ is also given in Fig. 16. It is seen that in the limits as δ approaches zero and Δs approaches zero,

Table 2. Tabulated Values of $\dot{\delta}/(D_v\delta)$ for Decay of Ellipse by Volume Diffusion

Number of Points on Contour	$\delta = 2.7466 \times 10^{-3}$	$\delta = 2.7466 \times 10^{-4}$	$\delta = 2.7466 \times 10^{-5}$
	$\times 10^{-3}$	$\times 10^{-3}$	$\times 10^{-3}$
8	1.789	1.789	1.789
16	4.704	4.685	4.683
24	5.443	5.413	5.410
32	5.710	5.674	5.671
40	5.834	5.795	5.791

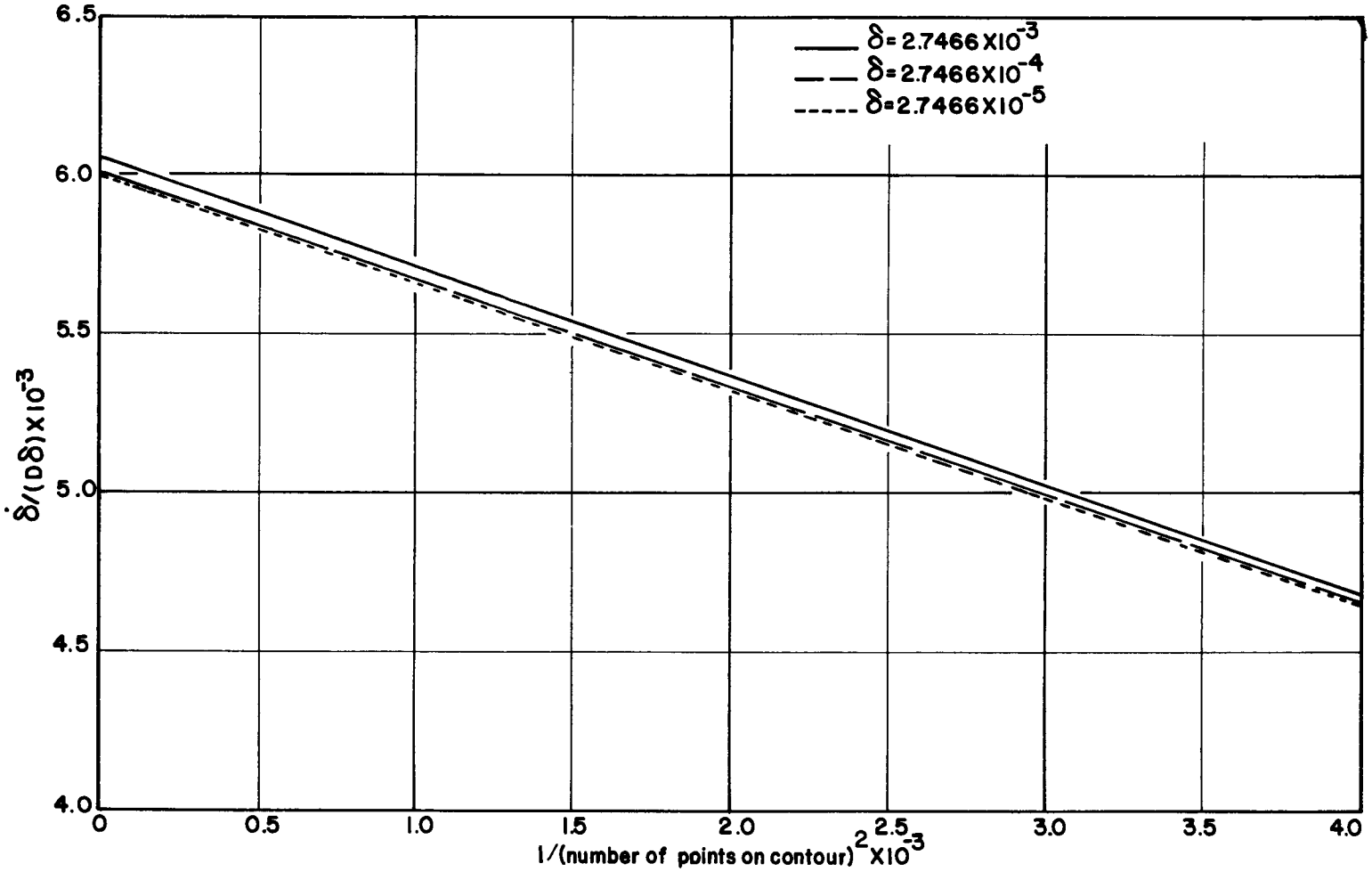

Fig. 16. Plot of $\dot{\delta}/(D_v\delta)$ for the Decay of an Ellipse by Volume Diffusion versus $1/(\text{number of points on contour})^2$.

the numerical solutions converge to the value predicted by Nichols for small perturbations.

The results further indicate that the velocities of each of the points P_i are nearly proportional to cos (2θ), which is the functional dependence predicted by Nichols' analysis. The deviation from this dependence decreases with decreasing Δs.

This test is felt to be an adequate demonstration that the numerical techniques described previously yield suitable solutions for the velocities of points on migrating interfaces, and that the accuracy of the solutions may be improved by decreasing Δs. A further test of the linear integral equations is provided in the next section.

Planar Analog of Sintering Using a Nonclosed Contour

Imagine "flattening" the rod-to-rod neck profile adopted by Kuczynski to a plane; this is shown schematically in Fig. 17 if one understands that the region $-b \leq s \leq b$ corresponds to a neck, and that each of the regions $s \leq b$ and $s \geq b$ are "rods." A short discussion of this problem lends valuable insight into the sintering problem.

The solution $C_I(t)$, is required to satisfy the following boundary conditions (see Fig. 17):

$$C_R = 0, \quad s > b \text{ or } s < -b$$

$$C_R = C', \quad -b \leq s \leq b$$

Because $\cos (r\upsilon)_1 = \cos (r\upsilon)_2 = 0$, while $\sin (r\upsilon)_1 = -\sin (r\upsilon)_2 = 1$, Eq. (26) may be written for the limits of integration $s = -\infty$ to $s = \infty$ and reduced to

$$C_I(t) = \frac{C'}{\pi} \int_{-b}^{b} \frac{ds}{|s - t|} = -\frac{C'}{\pi} \ln \left(\frac{t - b}{t + b}\right) . \tag{44}$$

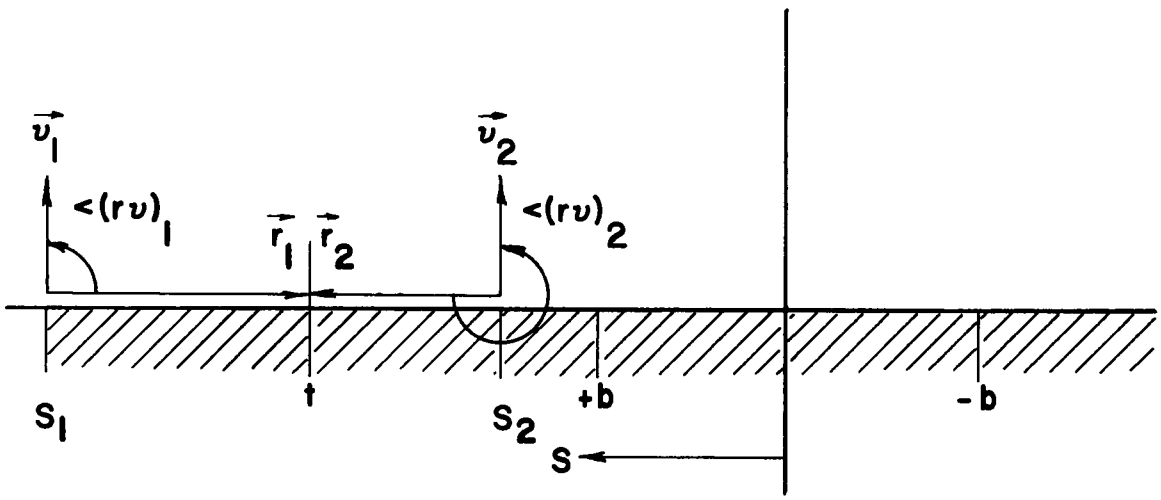

Fig. 17. The Planar Analog of Rod-to-Rod Sintering.

Differentiation yields

$$\frac{\partial C_I(s)}{\partial s} = -\frac{C'}{\pi}\left(\frac{1}{s-b} - \frac{1}{s+b}\right) . \tag{45}$$

These results may be obtained by the method of Fourier integrals as well.

Both $C_I(t)$ and $\partial C_I(s)/\partial s$ are plotted schematically in Fig. 18. Several interesting points may be gleaned from examining these plots. First, at $s = b$ and $s = -b$, where $C_R(s)$ is discontinuous, $C_I(s)$ is singular and $\partial C_I(s)/\partial s$ is discontinuous. The velocity of each point on the contour may be computed directly from Eq. (42).

Consequently, the velocity $v(s)$, goes to zero as S approaches $+\infty$ or $-\infty$ (Ref. 3). The requirement of conservation of volume as the contour migrates is stated

$$\int_0^\infty v(s)\, ds = \int_0^\infty \partial C_I(s)/\partial s \cdot ds .$$

Since $C_I(s)$ approaches zero as s becomes large, this requirement is satisfied.

It is expected that the solutions to the rod-to-rod and rod-to-plane sintering problems will behave in a manner analogous to this solution.

Initial Profile Migration Behavior in Rod-to-Rod Sintering

The Nonclosed Contour

The initial morphology is that described by Kuczynski's geometrical assumptions. The contour is considered to be composed of segments of arc length Δs. However, if the integral of Eq. (26) were approximated over

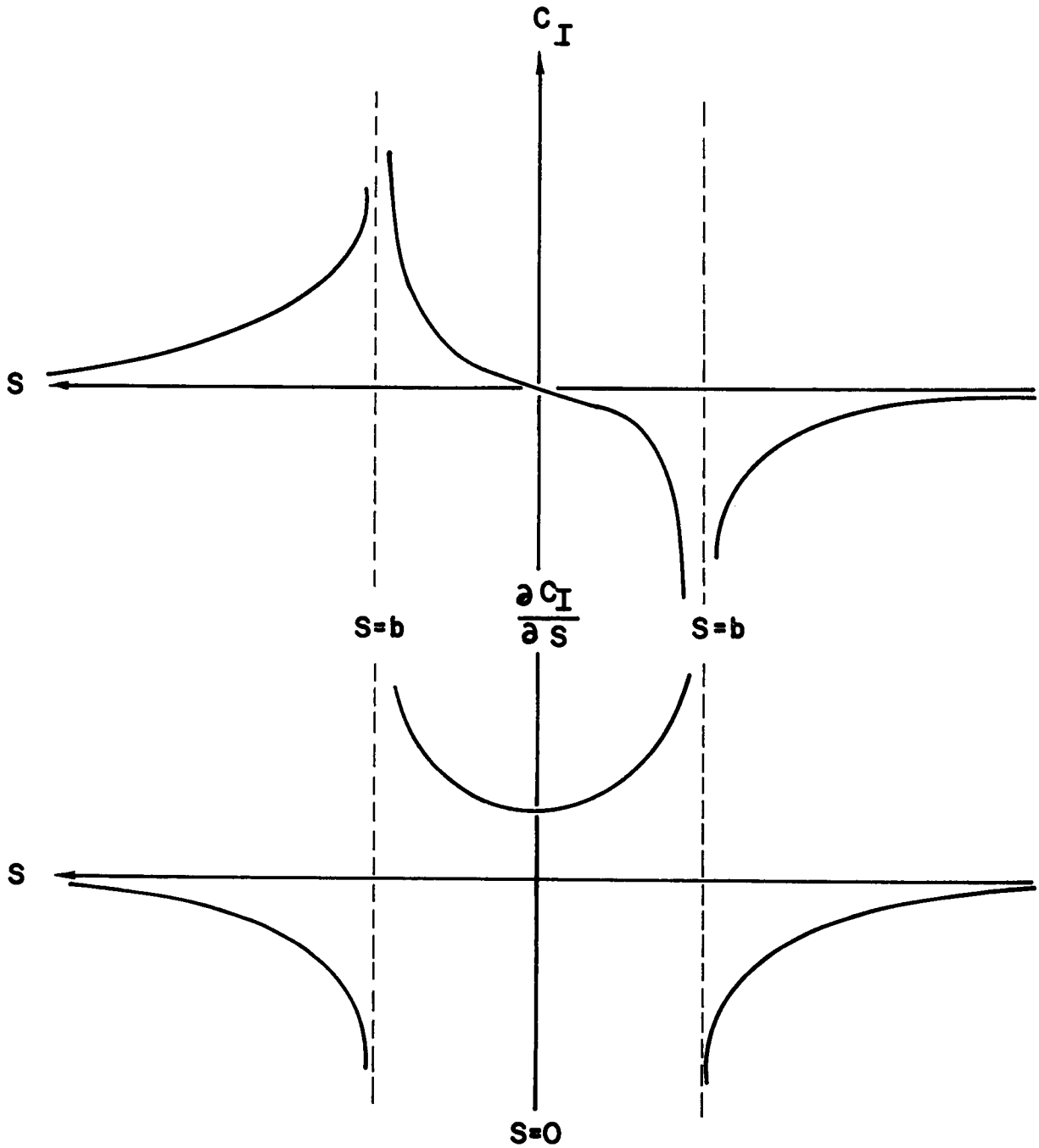

Fig. 18. Schematic Plots of $C_I(s)$ and $\partial C_I(s)/\partial s$ for the Planar Analog Problem.

the entire contour by Eq. (37) and Δs were sufficiently small to yield an accurate numerical solution for $x/a \leq 0.1$, the number of arc segments would be unmanageably large and computation time would be excessive on even the most modern digital computer. The region S′ is the "top half" of the neck root region and is defined by the array of points P_1, P_2, $\ldots P_{n'}$, $\ldots P_{n-1}$, P_n. The point $P_{n'}$ lies on the symmetry plane at which the sintering bodies make initial contact; thus, $P_{n'}$ is always at the neck root. The distance parameter "s" is set to be zero at $P_{n'}$, so that $s_i = (i - n')\Delta s$. Points P_1 and P_n are therefore symmetric about $P_{n'}$.

The contour may now be divided into three intervals, S′, S″, and S‴. The region S‴ is the "bottom half" of the neck root, and is the reflection of S′ across the plane joining the centers of the rods. All parts of the contour not on S′ or S‴ lie on S″.

The first attempt at a solution considers only the region S′ of the total closed contour. A solution based on S′ is feasible for the following two reasons. (1) Since only differences in C_R, the real concentration, are of interest, C_R may be redefined using as a "standard state" the concentration just under the main rod body of curvature 1/a″

$$C_R = C_R^K - C_R^a = \frac{\gamma\Omega C_o}{kT}\left(\frac{1}{a} - \frac{1}{K}\right) . \tag{47}$$

where C_R^K is the concentration under a segment of contour of curvature K. Thus, the first term on the right hand side of Eq. (26) vanishes everywhere on S″.

$$-\frac{1}{\pi}\int_{S''} \frac{C_R(s)\sin(r\upsilon)}{|\vec{r}|}\, ds = 0 . \tag{48}$$

(2) The solution anticipated (on the basis of this section, pages 47 and 49) for $C_I(s)$ for the closed contour has the general characteristics illustrated in Fig. 19. Vacancies from the neck migrate to the nearby rod surface, causing rapid growth of the neck at the expense of the receding boundary of the nearby rod. However, at some distance sufficiently removed from $P_{n'}$, the surface is not affected significantly by the presence of the neck. This follows directly from the 1/r dependence of both kernels. Also, $C_I(s)$ does approach zero far from the neck, so that the second term on the right hand side of Eq. (26) is nearly zero on S″.

$$-\frac{1}{\pi}\int_{S''} \frac{C_I(s)\cos(r\upsilon)}{|\vec{r}|}\,ds = 0 \,. \tag{49}$$

In the discretized form this equation reads exactly as Eq. (37). Three points deserve attention here: (1) the exact usage of the quadrature formulae at P_1 and P_n is not trivial and is discussed in the appendix. (2) In addition to errors introduced by the finite arc length, a second set of errors is introduced based on the approximation in Eq. (49). It is assumed at this stage that the reflection of the neck across the centerline in Fig. 20, S‴ does not influence the solution. Although these effects will be correctly considered later, their magnitude is of very real interest. (3) In the continuous problem, the discontinuity in curvature at the neck-rod junction, which results from assuming the Kuczynski geometry, causes the flux of material normal to the surface to approach positive and negative infinity in the neck and rod at the junction, respectively. As the surface develops its preferred morphologies

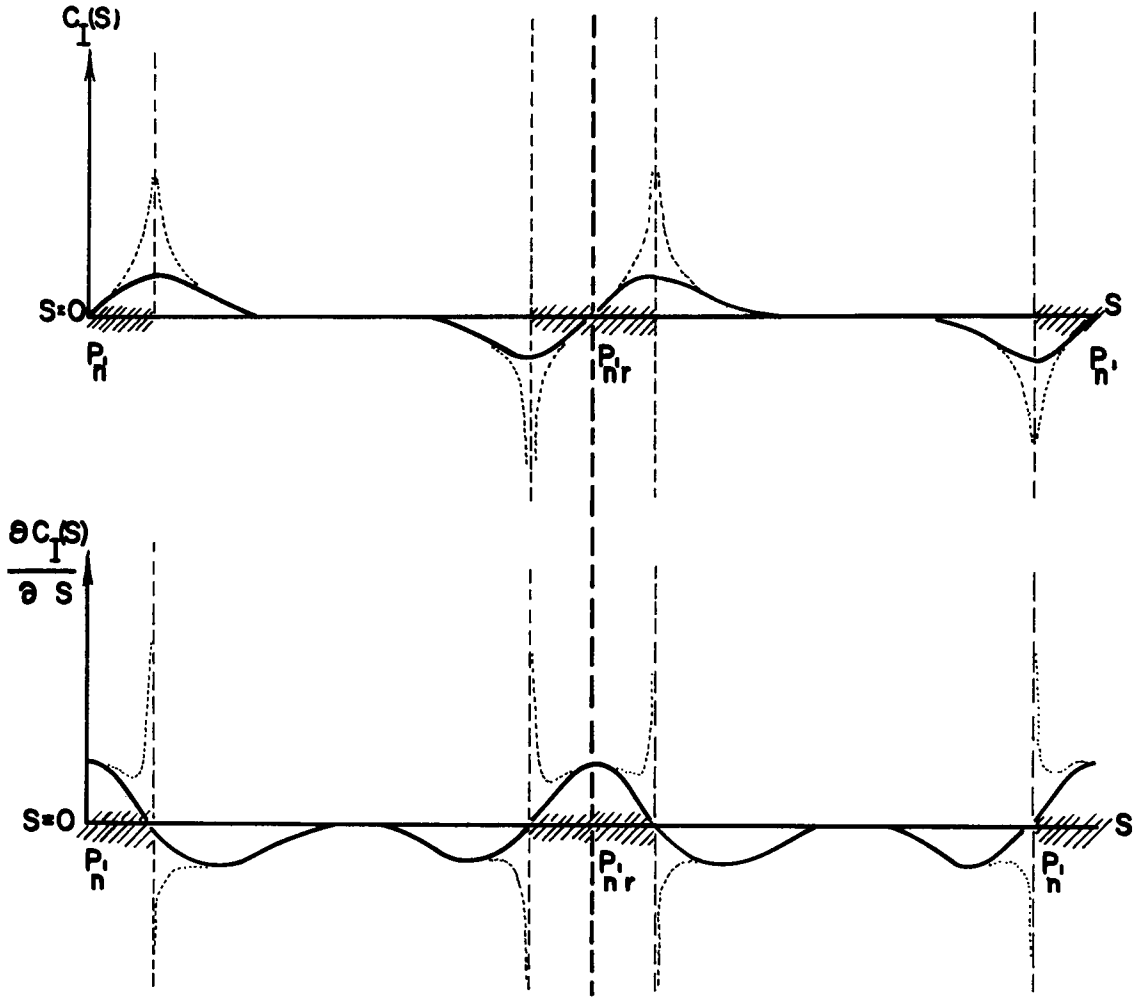

Fig. 19. Schematic Plot of Anticipated $C_I(s)$ and $\partial C_I(s)/\partial s$ for Rod-to-Rod Sintering. Discontinuous behavior dotted, numerical solution full lines. Cyclic boundary conditions shown fully. Shaded regions are neck regions.

during sintering, this artificial discontinuity is quickly smoothed. The solutions to the discretized problem never become discontinuous for any finite Δs because of the difference technique used to approximate the local curvature at the ith point:

$$K_i \cong (\theta_{i+1} - \theta_{i-1})/2\Delta s \ . \tag{50}$$

However, the behavior of the solutions of the discretized problems approach the discontinuous behavior of the solution of the continuous problem as Δs approaches zero. The smooth and discontinuous functions are represented for the reader's convenience in Fig. 19; the discontinuous behavior occurs only in the formal mathematical solution of the continuous problem.

Errors Arising from the Nonclosed Contour and Finite Arc Spacing

The following discussion deals with the major problem of determining how much of the error for any solution of Eq. (47), in which Eq. (47) is written only for the contour S', is due to discretization (the finite value of Δs) and how much error is due to not allowing S' to include the entire closed contour.

Examination of Fig. 20 indicates that if S_n, the distance coordinate of the last point of S', remains constant, the various values of n will produce different arc spacing, Δs. On the other hand, if Δs be held constant and n allowed to vary, then the range of S' is increased at constant arc spacing.

Let S_q be the distance along the contour between the neck root and the rod-neck junction. This distance may be divided into m segments of arc length Δs, or $\Delta s = s_q/m$, where m = 1, 2, 3 ... The values of n and

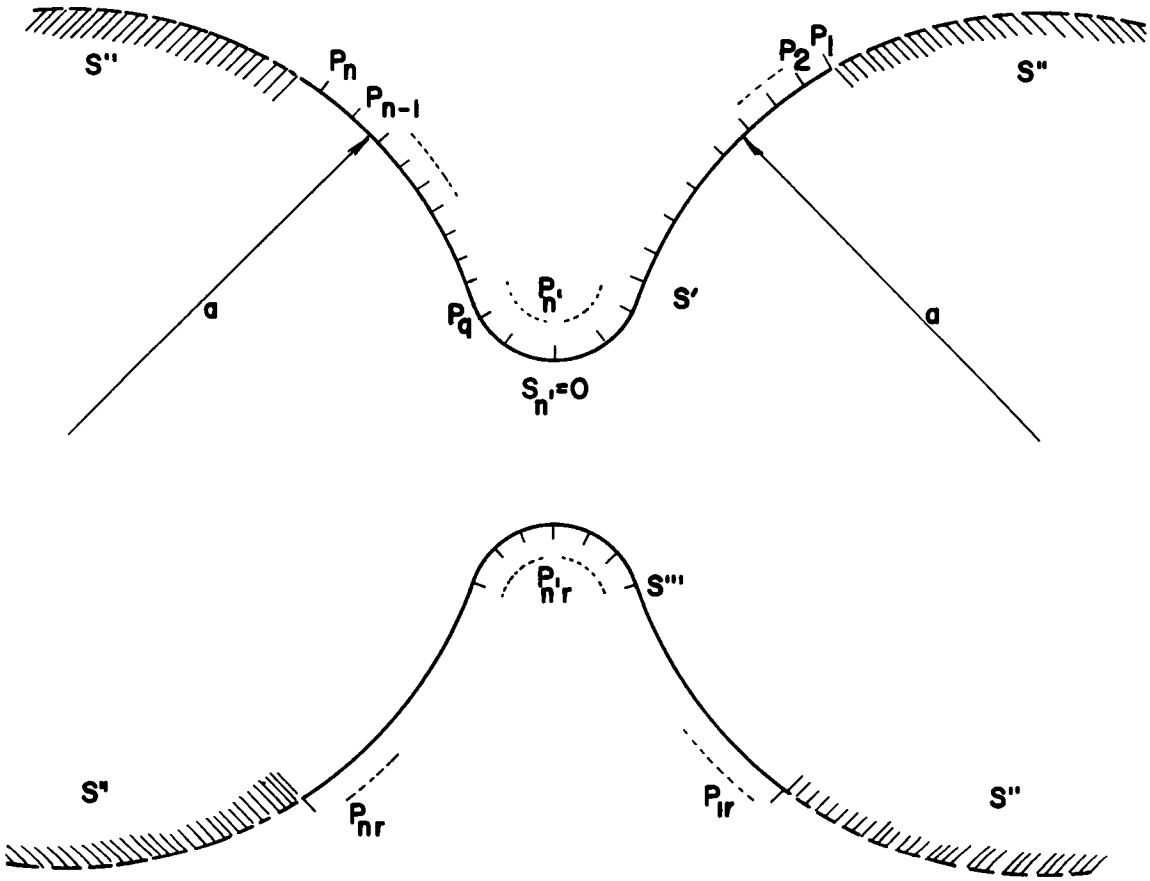

Fig. 20. Initial Morphology Assumed for Rod-to-Rod Sintering. $P_{n'r}$ is the reflection of $P_{n'}$. S_q is the contour distance from $P_{n'}$ to P_q.

s_n were always selected so that $s_n = ks_q$, $k = 1, 2, 3 \ldots$ Thus, for any initial x/a all contour representations of given m have constant arc spacing Δs, whereas all contour representations of given k have the same range of S', or the same value of S_n.

A solution for a particular contour representation (k,m) involves determining the velocity $v_i(k,m)$ of each point P_i for that representation. Sets of solutions were computed by direct matrix inversion of Eq. (38) for initial neck profiles having $x/a|_o = 0.05$, 0.10, and 0.30. For each initial profile, subsets of solutions were computed at constant m (constant Δs) for various values of k, and at constant k (constant range of S') for various values of m.

The velocity of greatest interest is that at the neck root, $v_{n'}(k,m)$. A dimensionless "modified velocity," $Q(k,m)$, is defined as

$$Q(k,m) = av_{n'}(k,m)/D_v \ . \tag{51}$$

Figure 21 illustrates the results for $x/a|_o = 0.1$. The $Q(k,m)$ is plotted as a function of $(\Delta s)^2$ or $(1/m)^2$ and smooth curves are drawn through the subsets $Q(k,m)$ of constant k. This set of curves indicates the effect of varying Δs for constant ranges of S'. Extrapolating the curves to $\Delta s = 0$ yields the set of "modified velocities" $Q(1,\infty)$, $Q(2,\infty)$, $Q(3,\infty)$ ... The set of $Q(k,\infty)$ represents the effect of varying k on the solution in the limit as Δs approaches zero.

The $Q(k,m)$ are plotted as a function of $(1/k)$ in Fig. 22 for $x/a|_o = 0.10$. Smooth curves are drawn through subsets of constant m (or Δs). This set of curves indicates the effect of the range of S' for constant values of Δs. Extrapolating these curves to $1/k \sim 0$ yields the

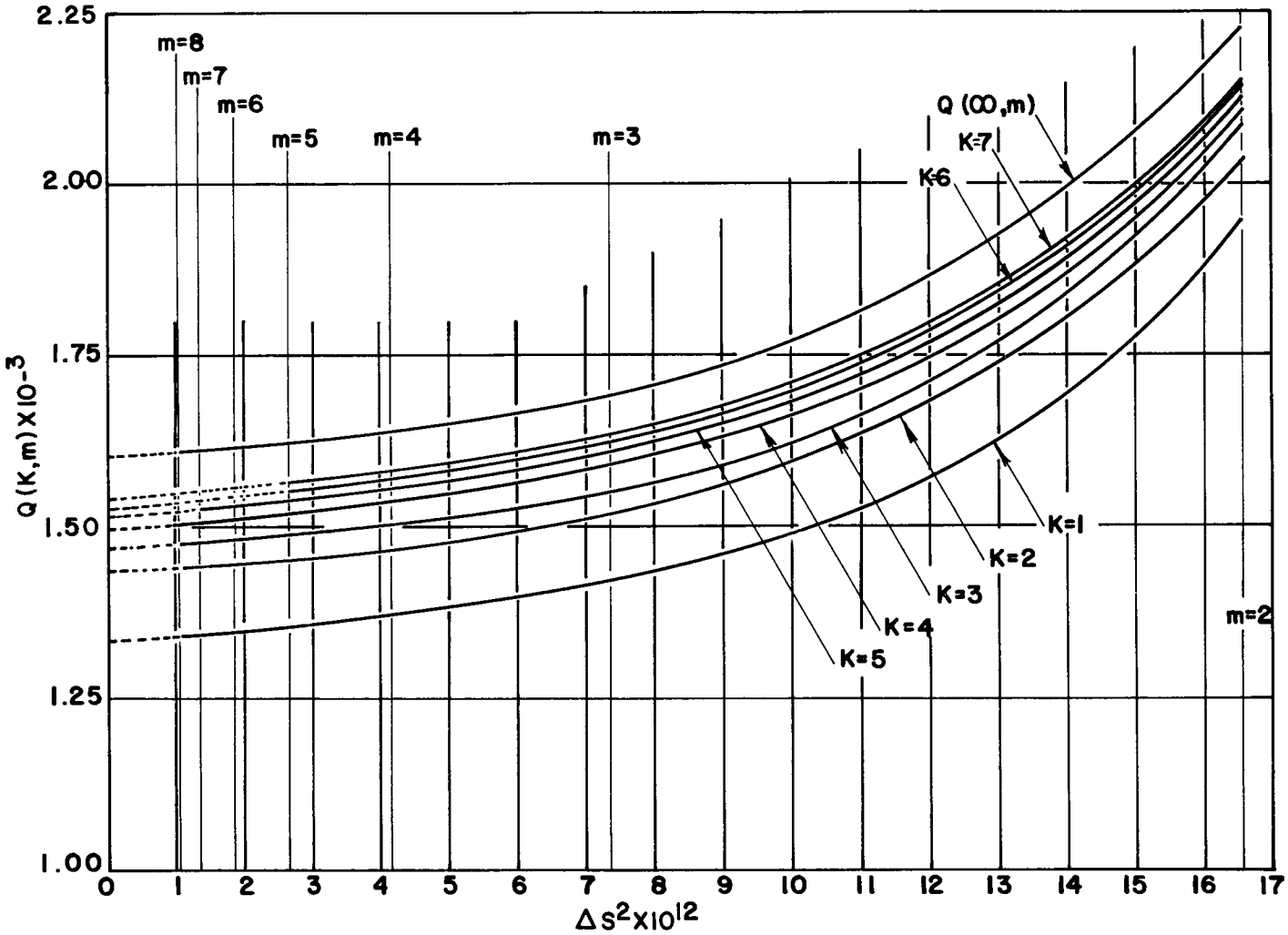

Fig. 21. Plot of Q(k,m) versus $(\Delta s)^2$ for Rod-to-Rod Sintering, $x/a|_o = 0.10$.

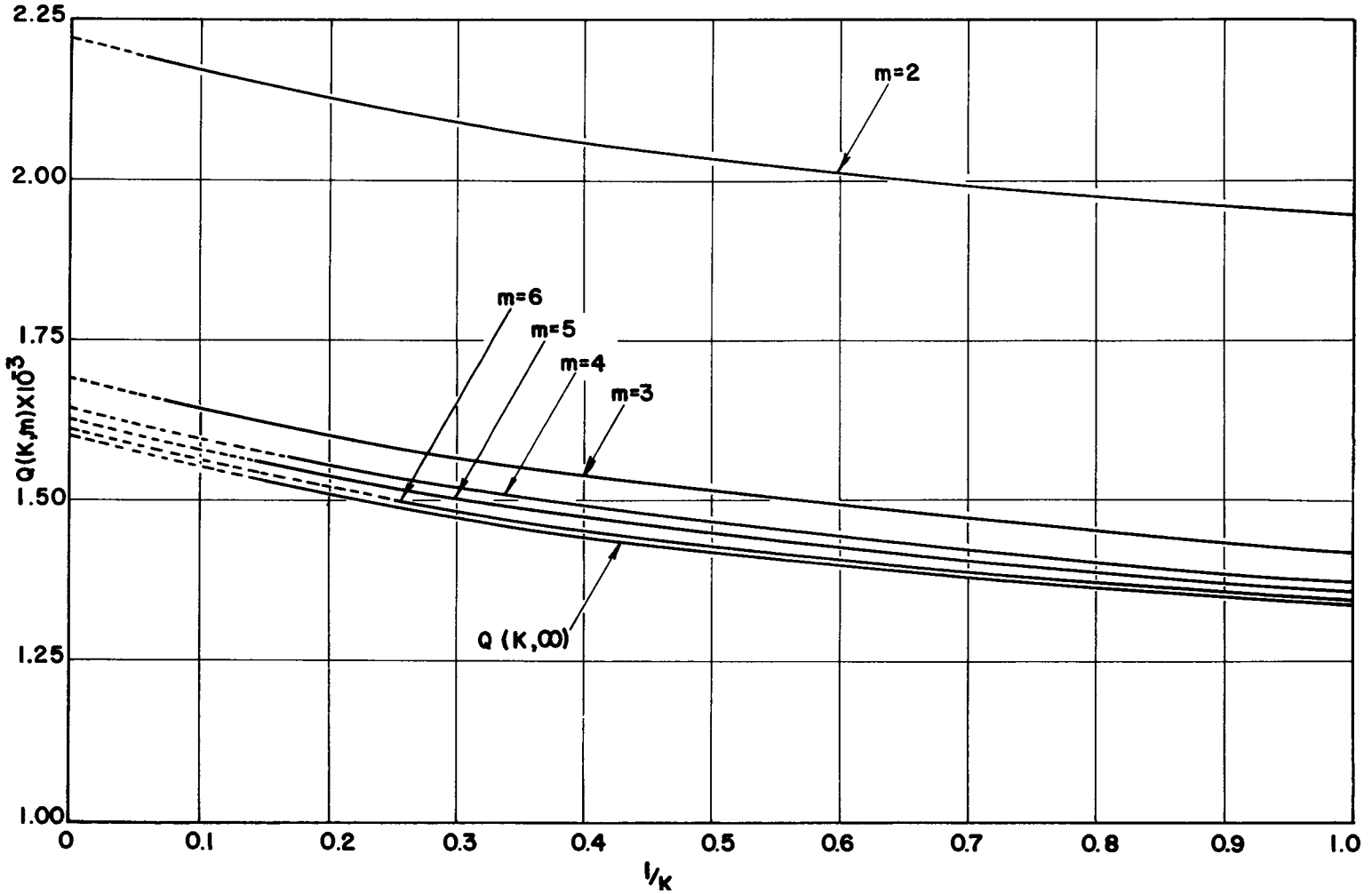

Fig. 22. Plot of Q(k,m) versus (1/k) for Rod-to-Rod Sintering, $x/a\big|_o = 0.10$.

set of "modified velocities" $Q(\infty,2)$, $Q(\infty,3)$, $Q(\infty,4)$, ... This set of $Q(\infty,m)$ represents the effect of varying Δs on the solution in the limit as S' is extended to include the entire contour except S'''.

These two sets of curves are closely interrelated. Plotting the $Q(k,\infty)$ on Fig. 21 yields a curve which, when extrapolated to $1/k = 0$, allows a value $Q(\infty,\infty)$ to be estimated. The "true" value is $Q(\infty,\infty)$ which should be obtained if the continuous problem admitted solution over the entire closed contour, excluding the reflected root. The solutions which have been obtained are internally consistent in that a plot of $Q(\infty,m)$ on Fig. 22 yields the same value of $Q(\infty,\infty)$ by extrapolation to $\Delta s = 0$ which was obtained by plotting $Q(k,\infty)$ on Fig. 21.

It may be seen that for $m \geq 3$ (that is, three or more arc segments between the neck root and the rod-neck junction) small changes in k lead to greater error in the solution $Q(k,m)$ than small changes in m. Thus, the over-all accuracy of any solution can be improved at least as much by correcting for the effect of S'', the contour whose influence is not included in the computation of Φ_I, as it can be improved by refining Δs. Subsequent discussions will be directed toward this goal. Other numerical experiments similar to that described above have been performed at $x/a|_o = 0.05$ and 0.30. Although these remarks regarding the relative effects of variations of k and m are also valid when $x/a|_o = 0.05$, it may be shown that $Q(k,m)$ varies as rapidly with unit changes in m as it does with k at $x/a|_o = 0.30$.

Equation (7) may be differentiated and used to predict the "modified velocity" Q_k from a Kuczynski-type analysis. Computation of Q_k has the

same values of parameters ($\gamma\Omega C_v^\circ/kT = 10^{-10}$, $a = 10^{-3}$) that were used to compute $Q(\infty,\infty)$.

$$Q_k = \frac{a}{D_v}\frac{dx}{dt} = \frac{2}{}\left(\frac{x}{a}\right)^{-4}\left(\frac{\gamma\Omega C_v^\circ}{kT}\right) . \tag{52}$$

Tabulated results from this computation are compared below with $Q(\infty,\infty)$ for $x/a|_o = 0.05$, 0.10, and 0.30.

$x/a\|_o$	Q_k	$Q(\infty,\infty)$
0.05	3.2×10^{-2}	2.75×10^{-2}
0.10	2.0×10^{-3}	1.60×10^{-3}
0.30	2.469×10^{-5}	1.56×10^{-5}

As $x/a|_o$ approaches small values, the difference between $Q(\infty,\infty)$ and Q_k decreases.

Figure 23 is a plot of the imaginary function, $\phi_I(s)$, obtained by direct matrix inversion at constant $k = 4$ for a range of $m(\Delta s)$. It will be noted that $\vec{\phi}_I$ approaches zero far from the neck. Further, as Δs is refined it is apparent that $\vec{\phi}_I$ more nearly simulates the singularity expected for the solution of the continuous problem at the rod-neck junction.

Correcting the Solution for the Nonclosed Contour and Reflected Neck

Since a substantial amount of error is introduced into the solutions by the limited range of S', it is particularly desirable to develop a

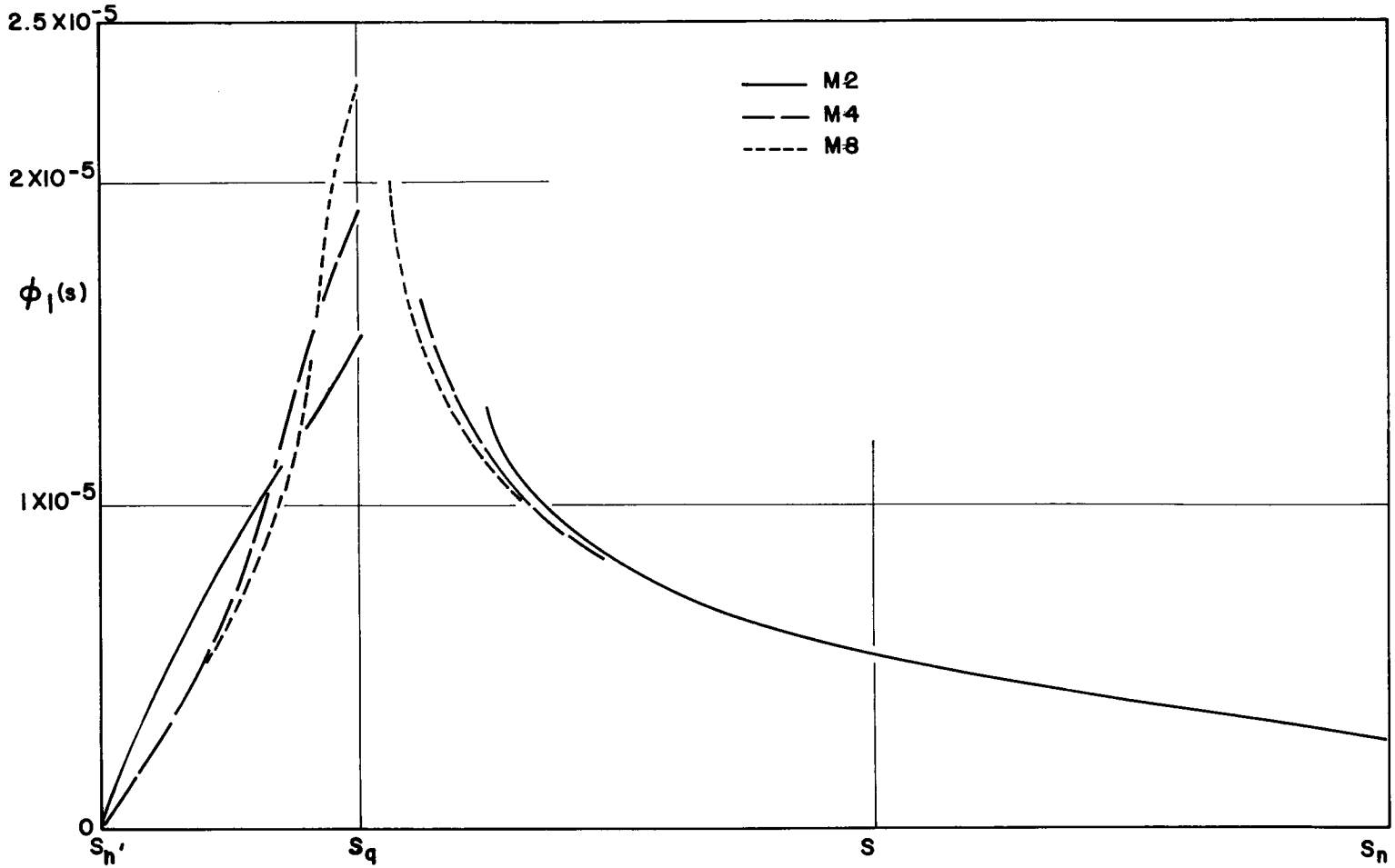

Fig. 23. Plot of $\phi_I(s)$ versus s for $x/a|_o = 0.10$.

technique for correcting this error. Fortunately, the techniques for making this correction allow easy correction for the presence of the reflected neck region, S'''.

The correction factor is based on the notion behind Eq. (40), that an approximate solution of suitable accuracy may be achieved by successive substitutions. One begins with a solution to Eq. (38) for the contour region S', obtained by matrix inversion, denoted $\vec{\phi}_I^{\circ}(S')$. In addition, the arrays $\vec{\phi}_I(S')$, $\vec{\phi}_I(S_2)$, and $\vec{\phi}_I(S''')$ are defined as the values of $\vec{\phi}_I$ on the regions S', S_2, and S''', respectively. By techniques to be discussed below, $\vec{\phi}_I(S')$ is extrapolated over a portion of S'' which will be denoted S_2. The region S_2 begins at the ends of S' and extends far enough into S'' that $\vec{\phi}_I$ at the end of S_2 is at least four orders of magnitude smaller than its maximum value on S'. Further, $\vec{\phi}_I(S''')$ is assumed to be related to $\vec{\phi}_I(S')$ by the symmetry shown in Fig. 19.

The matrix form [Eq. (38)] of the basic integral equation [Eq. (26)] is then separated to include the three regions S', S_2, and S''' separately. When these integral are approximated in the manner described in Appendix 2, the following result is obtained:

$$\vec{\phi}_I = \underset{\sim}{K}_s(S') \cdot \vec{C}_R(S') + \underset{\sim}{K}_c(S') \cdot \vec{\phi}_I(S') + \underset{\sim}{K}_s(S_2) \cdot \vec{C}_R(S_2) + \underset{\sim}{K}_c(S_2) \cdot \vec{\phi}_I(S_2) + \underset{\sim}{K}_s(S''') \cdot \vec{C}_R(S''') + \underset{\sim}{K}_c(S''') \cdot \vec{\phi}_I(S''') \ . \qquad (53)$$

Equation (47) defined $\vec{C}_R$ in terms of local curvature at each point P_i. The kernel matrices $\underset{\sim}{K}_s$ and $\underset{\sim}{K}_c$ are similarly well defined; the $A(i,j)$ are described in Appendix 2.

The method used to extrapolate $\vec{\phi}_I(S')$ into S_2 is of some interest. At first glance, it would appear that far from the neck a good approximation might be the functional dependence of $\phi_I(s)$ from the planar analogy:

$$\phi_I(s) = K\left(\frac{1}{s - s_q} - \frac{1}{s + s_q}\right) . \tag{54}$$

In fact, if K is computed from the pairs of points on S′ near the end of the range of S′, (P_n, P_{n-1}), (P_{n-1}, P_{n-2}), (P_{n-2}, P_{N-3}), it is found that K varies by 10% or more from pair to pair. Thus, when an extrapolation of this form is used in Eq. (53), the first derivative of imaginary function, approximated by

$$\left.\frac{\partial\phi_I(s)}{\partial s}\right|_{P_i} \cong [\phi_I(i + 1) - \phi_I(i - 1)]/2\Delta s \tag{55}$$

undergoes a sudden change in slope at P_n. The rapid slope change causes unrealistic behavior of the profiles generated later during the solution of the over-all sintering problem.

Several other mathematical functions are justifiable for use in extrapolating $\vec{\phi}_I(S')$. These functions result from closed-form solutions for circles having $\vec{C}_R = 0$ everywhere except in regions corresponding to the neck region of two sintering rods. Unfortunately, all of these easily justified extrapolation functions produce the same sudden change in $\partial\phi_I(s)/\partial s$ that the function of Eq. (54) introduces.

The only extrapolation of the imaginary function on the range S_2 which was investigated and found suitable was

$$\phi_I(s) = K_1/s^2 + K_2/s^4 + K_3/s^6 . \tag{56}$$

The constants K_1, K_2, and K_3 are computed from the imaginary function values at the triplet of points P_{n-2}, P_{n-1}, and P_n.

The preceding discussion has outlined the methods used to define each term on the right side of Eq. (53). The technique for obtaining the corrected solution follows: first, $\vec{\phi}_I^{\circ}(S')$ is found by solving Eq. (38) over the region S′

$$\vec{\phi}_I^{\circ}(s') = [\underset{\sim}{I} - \underset{\sim}{K}_c(S')]^{-1} \cdot \underset{\sim}{K}_s(S') \cdot \vec{C}_R(S') \ . \tag{57}$$

Then $\vec{\phi}_I^{\circ}(S_2)$ and $\vec{\phi}_I^{\circ}(S''')$ are computed from Eq. (54) and symmetry conditions, respectively.

The iterative procedure for computing $\vec{\phi}_I^{(i+1)}(S')$ is to then solve:

$$\begin{aligned}\vec{\phi}_I^{(i+1)}(S') = {} & \underset{\sim}{K}_s(S')\ \vec{C}_R(S') + \underset{\sim}{K}_c(S')\ \vec{\phi}_I^{(i)}(S') + \underset{\sim}{K}_s(S_2)\ \vec{C}_R(S_2) \\ & + \underset{\sim}{K}_c(S_2)\ \vec{\phi}_I^{(i)}(S_2) + \underset{\sim}{K}_s(S''')\ \vec{C}_R(S''') + \underset{\sim}{K}_c(S''')\ \vec{\phi}_I^{(i)}(S''') \ .\end{aligned} \tag{58}$$

The arrays $\vec{\phi}_I^{(i)}(S_2)$ and $\vec{\phi}_I^{(i)}(S''')$ are recomputed from Eq. (54) and symmetry considerations before each iterative application of Eq. (56). The iteration process is repeated until the most rapidly changing value of $\vec{\phi}_I(S')$, which is in fact always that at P_1 or P_n, changes less than one part in 10^4 on successive iteration steps. It has been observed that this criterion leads to changes in $\partial\phi_I(s)/\partial s$ of less than one part in 10^5 on successive iterations. The $\vec{\phi}_I^{(i)}(S')$ converges rapidly to meet this criterion.

The use of this correction technique produces a set of Q values which nearly agree with the $Q(\infty,m)$ extrapolated values. The slight

discrepancy, less than a percent, may be attributed to the visual estimates of $Q(\infty,m)$ or to the effect of those portions of S'' which were not included in S_2 or to the effect of S'''.

Defining the Migrating Boundary on Successive Time Steps

The preceding remarks dealt with the determination of the flux of vacancies normal to a set of points representing a particular contour, with no reference to how the contour changes shape with time. Here it is proposed to allow each point $P_i(x_i,y_i)$ on the contour for which velocities, v_i, are computed from Eq. (42) to migrate normal to the original contour for time Δt to $P_i'(x_i',y_i')$. The loci of all such points defines a new curve after migration, SS (see Fig. 24). Iteration of this calculation constitutes a complete description of the growth process.

However, it is evident from Fig. 24 that, if a smooth curve SS were passed through the points $P_i'(x_i',y_i')$, the curve would not be divided into equal arc segments by the points. Since the techniques for determining the flux of vacancies normal to the contour are based on equal arc segment lengths, it is necessary to define SS by a new set of points $P_i''(x_i'',y_i'')$ which divide it into equal arc segments. Nichols (16) has presented a very interesting technique for dealing with this problem based on finite difference approximations for the change in the (s,θ) coordinates of points $P_i(x_i,y_i)$ which have migrated to $P'(x_i',y_i')$. This technique has been tested and found unsuitable for the relatively large arc spacings and Δt values which must be used to compute a solution in a reasonable time. The net effect of cumulative errors after several time steps is to displace the curve between P_q and the end of S_2 to the right. After

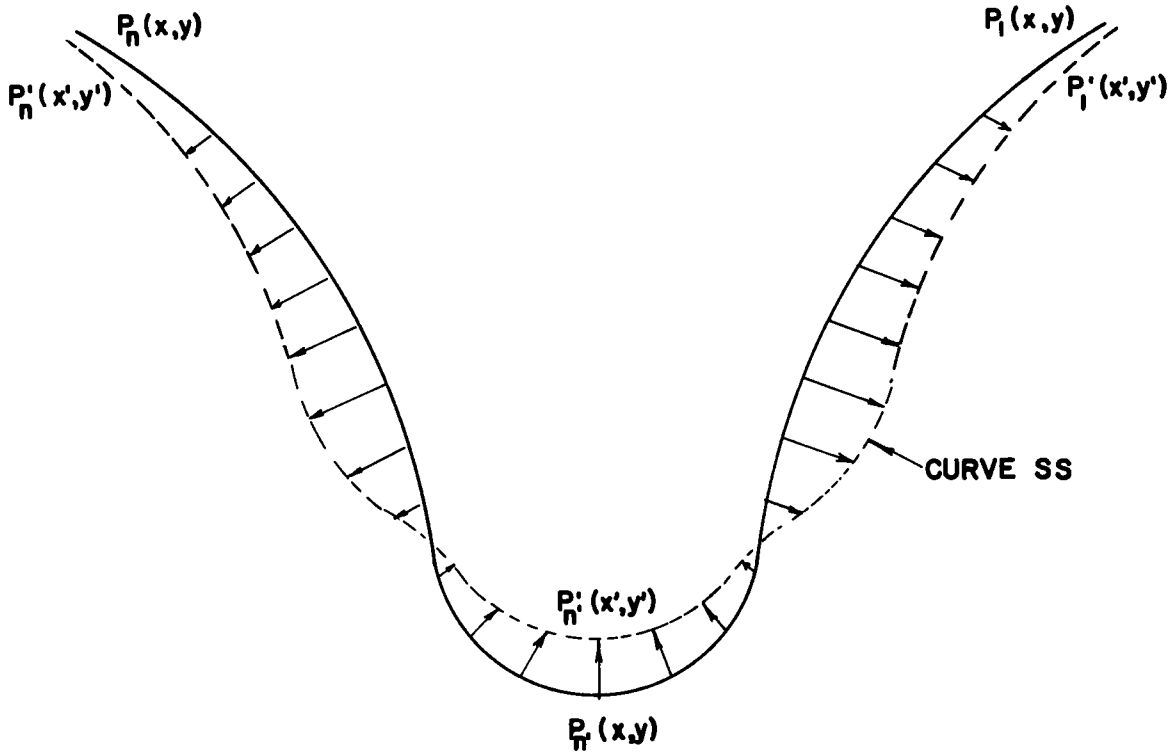

Fig. 24. Migration of $P_i(x_i,y_i)$ on Curve S to $P_i'(x_i',y_i')$ on Curve SS.

a large number of time steps for a test case, the entire curve had "drifted" so much that points which should have fallen on the original contour were displaced more than a rod radius from the original rod contour.

The following techniques have been developed to handle relatively large arc spacings and Δt. Having the set of points $P_i(x_i,y_i)$ and the velocity v_i of each point, the coordinates of the unevenly spaced points $P'_i(x'_i,y'_i)$ are computed from

$$x'_i = x_i + v_i \, \Delta t \cos \theta_i \, , \tag{59}$$

$$y'_i = y_i + v_i \, \Delta t \sin \theta_i \, , \tag{60}$$

where θ_i is the angle between the normal to the original contour at $P_i(x_i,y_i)$ and the x-axis.

A smooth curve was fit to the $P'_i(x'_i,y'_i)$ by passing a cubic through successive sets of points P'_i, P'_{i+1}, and P'_{i+2}

$$y'_i(x) = a_i + b_i x' + c_i (x')^2 + d_i (x')^3$$

where a continuous first derivative was maintained by requiring that

$$dy'_i(x)/dx \big|_{P'_i} = dy'_{i-1}(x)/dx \big|_{P'_i} \, .$$

The fitting technique is begun at point $P'_{n'}$ where $dy'_{n'}(x)/dx = 0$. If $|dy'_{i-1}(x)/dx| > 0.5$ at $P'_i(x'_i,y'_i)$, then a cubic curve of the form $x'_i(y) = a_i + b_i y + c_i (y')^2 + d_i (y')^3$ is fit to the points.

The polynomial coefficients a_i, b_i, c_i, and d_i which define the smooth curve SS may now be used to compute the distance coordinates s'_i on each point $P'_i(x'_i,y'_i)$ measured along the curve. The numerical approximation for the distance between P'_i and P'_{i+1} is made that

$$s'_{i+1} - s'_i = \int_{x'_i}^{x'_{i+1}} \{1 + [dy'_i(x)/dx]^2\}\, dx$$

$$\cong \frac{\Delta x}{24} \sum_{k=0}^{k=\ell} (-R_{i,k-1} + 13\, R_{i,k} + 13\, R_{i,k+1} - R_{i,k+2}) \qquad (61)$$

where

$$\Delta s = (x'_{i+1} - x'_i)/\ell$$

and

$$R_{i,\ell+j} = \left|1 + [dy'_i(x)/dx]^2\right|_{x_i+(\ell+j)\Delta x}.$$

Note that Eq. (61) makes use of values of $dy'_i(x)/dx$ between P'_{i+1} and P'_{i+2}. Therefore one step of the numerical integration in each segment includes multiply-defined $dy'(x)/dx$. Because of the smooth characteristics of the polynomial functions used to determine $y_i(x)$ or $x_i(y)$ for segments of SS, little error is introduced by going outside the range over which $y'_i(x)$ was fitted.

Each point P'_i is now specified by three parameters (x'_i,y'_i, and s'_i). Upon selecting some new value of Δs, a Lagrange interpolation for $x'(s')$ and $y'(s')$ may be used to find equally spaced points $P''_i(x''_i, y''_i)$ on SS, such that $s''_i = (i - n')\Delta s''$.

The new contour is thus defined by points spaced at equal arc intervals and is suitable for computing a new set of velocities v_i for the next time step.

Solution to the Rod-to-Rod Sintering Problem and Errors in the Final Solution

In order to obtain a final solution and arrive at a meaningful estimate of the error in the solution for the rod-to-rod problem, several numerical experiments were performed. Several sources of error require consideration: (1) those arising from the finite arc spacing Δs; (2) those arising from the finite time steps Δt_i employed; and (3) those arising from the finite length of contour used to obtain the precise solution. It has been demonstrated that corrections may be made for the latter source of error to such an extent that such errors are negligible in comparison to errors arising from the former two sources (see section entitled "Initial Profile Migration Behavior in Rod-to-Rod Sintering," page 47). Stability problems of the type encountered by Nichols never arose for any of the parameters used in solving the volume-diffusion problem.

Errors Due to Finite Arc Spacing

The effect of varying Δs on the initial neck profiles has been discussed previously, page 52. In order to determine the effect of varying Δs on the neck velocity over several time steps, solutions to the rod-to-rod system were obtained for $x/a|_o$ = 0.05, 0.09, 0.10, and 0.30 at (k,m) = (4,2), (4,3), and (4,4). (See page 52 for the definition of these terms.) These combinations of parameters represent constant size of the contour regions S', S''', and S_2 (k = constant) and variable Δs (m).

The time increments Δt_i were defined such that the neck-root point displacement was 0.15 Δs on each time step. The arc spacing Δs was set on successive time steps such that a neck of the Kuczynski geometry for that particular x/a would have the region between the neck-root point and the rod-neck junction divided into "m" sections. This procedure, of course, means that the time step variable was not the same for each of the (k,m) systems. However, the procedure is justifiable, since it will be shown in the next section that the results are virtually independent of the size of Δt_i for this small a time step.

Representative results are shown in Fig. 25 for $x/a|_o = 0.09$. This graph demonstrates that as Δs decreases, the product $D_v t$ required to grow a neck of a particular x/a decreases. An equivalent statement is that the computed neck root velocity increases as Δs decreases. The products $D_v t$ are plotted versus $(1/m)^2$ for selected values of x/a in Fig. 26. These curves were extrapolated to $(1/m)^2 = 0$, or to $(\Delta s)^2 = 0$, and the results plotted in Fig. 25 as the extrapolated solution to the problem. If sufficient time and funding were available, such an extrapolation could be performed for all x/a from 0.09 to 0.80, the range of the solution.

The most important conclusions which can be drawn from this analysis are that the finite arc spacing causes the computed solution for $D_v t$ to be approximately 15% too high for the (4,3) system and approximately 8% too high for the (4,4) system. These errors are constant after the first twenty-five time steps for all $x/a|_o$. In view of the uncertainty in existing diffusion and sintering data, the final solution was computed for the (4,3) system.

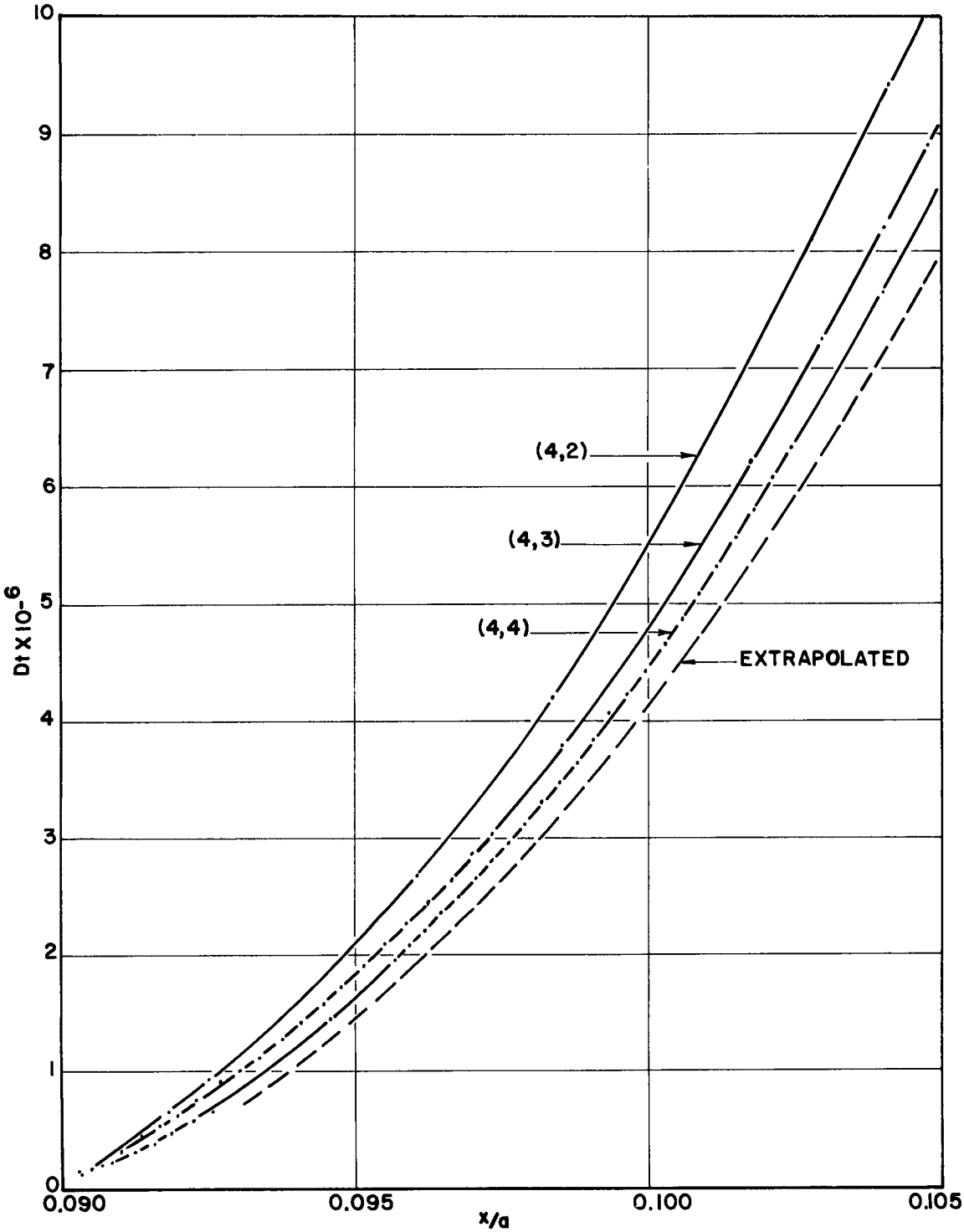

Fig. 25. Plot of $D_v t$ versus x/a for Rod-to-Rod Sintering.

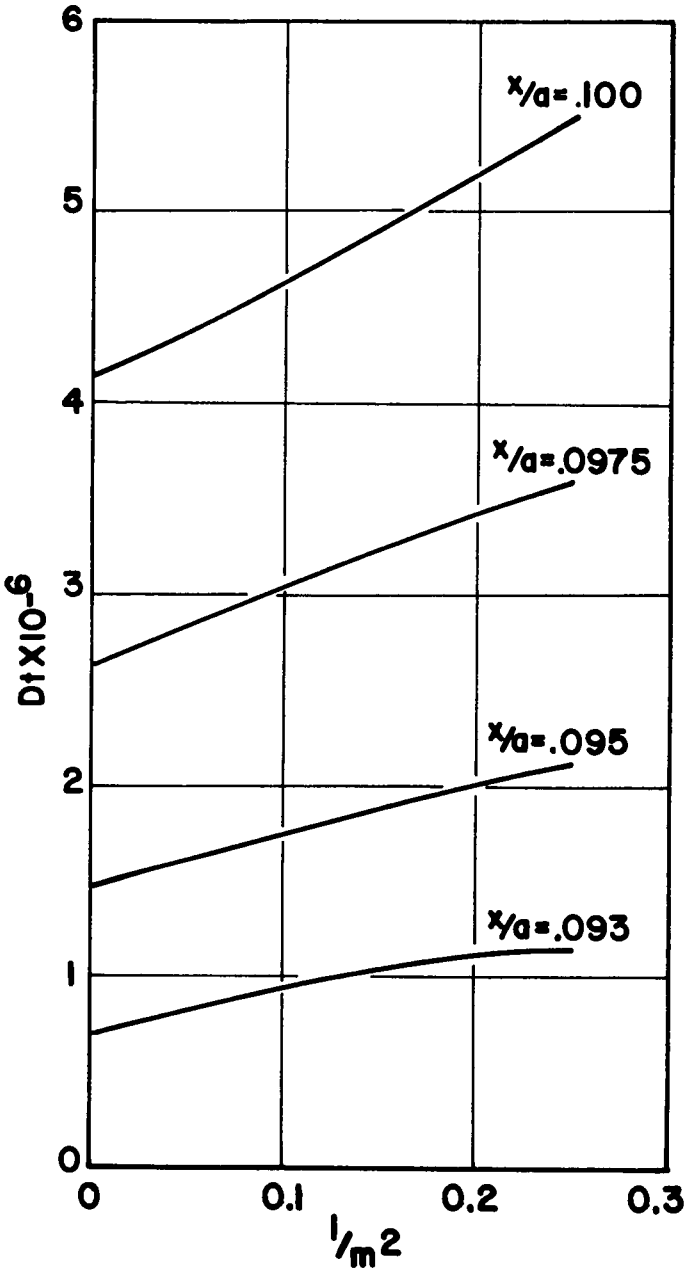

Fig. 26. Extrapolation of $D_v t$ versus $1/m^2$ to Estimate Error in Solution of Rod-to-Rod Sintering Problem.

Errors Due to Finite Time Steps

In order to determine the effect of varying Δt_i, solutions were run for up to forty time steps for various $x/a|_o$ and various (k,m). It was found that if the neck root displacement $\Delta N_{n'}$ on any given time step was less than or equal to 0.15 Δs, no difference could be detected in plots of x/a versus $D_v t$. Figure 27 shows representative data for $x/a|_o = 0.09$ and $\Delta N_{n'} = 0.10$, 0.15, and 0.25 Δs.

Solution to the Rod-to-Rod Sintering Problem

On the basis of the preceding discussion, the system selected for the final solution of the rod-to-rod problem was the (4,3) system. The origin $x/a|_o = 0.09$ was selected because several numerical experiments indicated that by the time x/a = 0.10, the contour assumed is practically identical to that generated from other $x/a|_o < 0.09$. Since Nichols' results indicate that surface diffusion is usually dominant for small x/a, the only interesting region to examine is that for $x/a \gtrsim 0.10$.

Selected contours are shown in Figs. 28 and 29 for the rod-to-rod sintering problem (4,3). Because the time scale varies by about seven orders of magnitude, the results are plotted as ln (x/a) versus ln ($D_v t$) in Fig. 30. In addition, the apparent value of the slope 1/n was computed for each time step and plotted versus x/a (see Fig. 31).

$$\frac{1}{n} = \frac{d \ln(x/a)}{d \ln(t)} \sim \frac{\ln(x/a)_i - \ln(x/a)_{i-1}}{\ln(t_i) - \ln(t_{i-1})} . \tag{62}$$

In accordance with the discussion on page 24, these values are meaningful only for $x/a \gtrsim 0.25$.

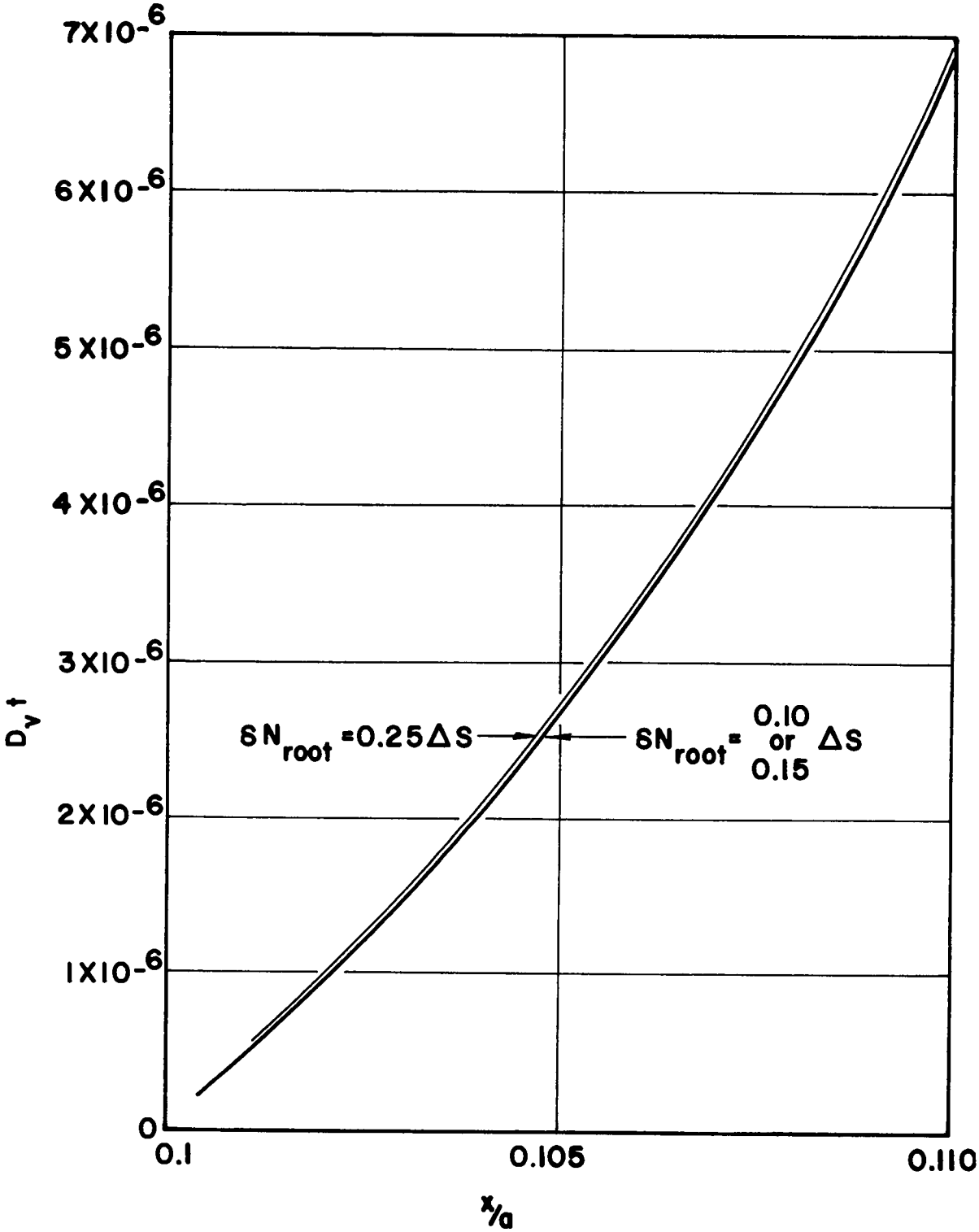

Fig. 27. Plot of $D_v t$ versus x/a for Various Values of $\Delta N_{n'} = d \cdot \Delta s$.

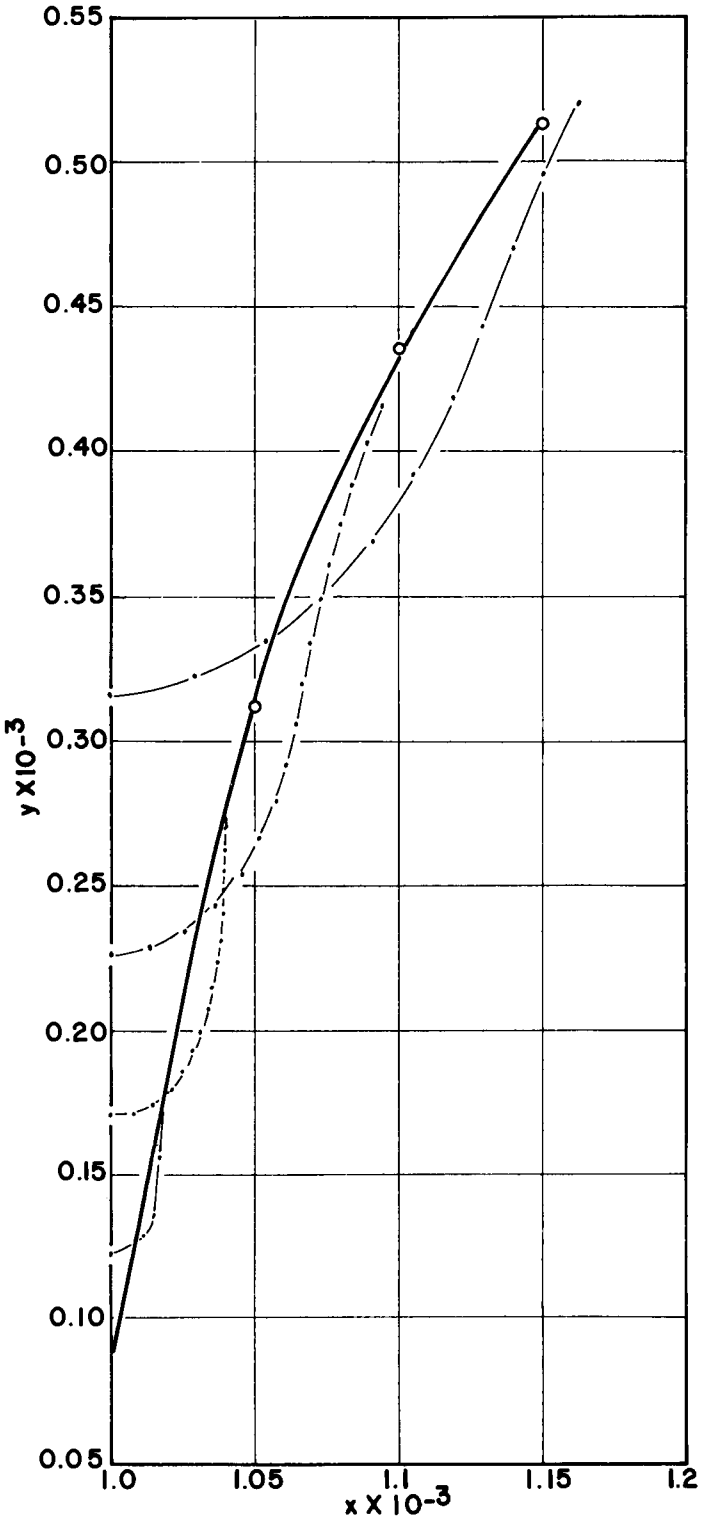

Fig. 28. Contours Generated During Early Stages of Rod-to-Rod Sintering.

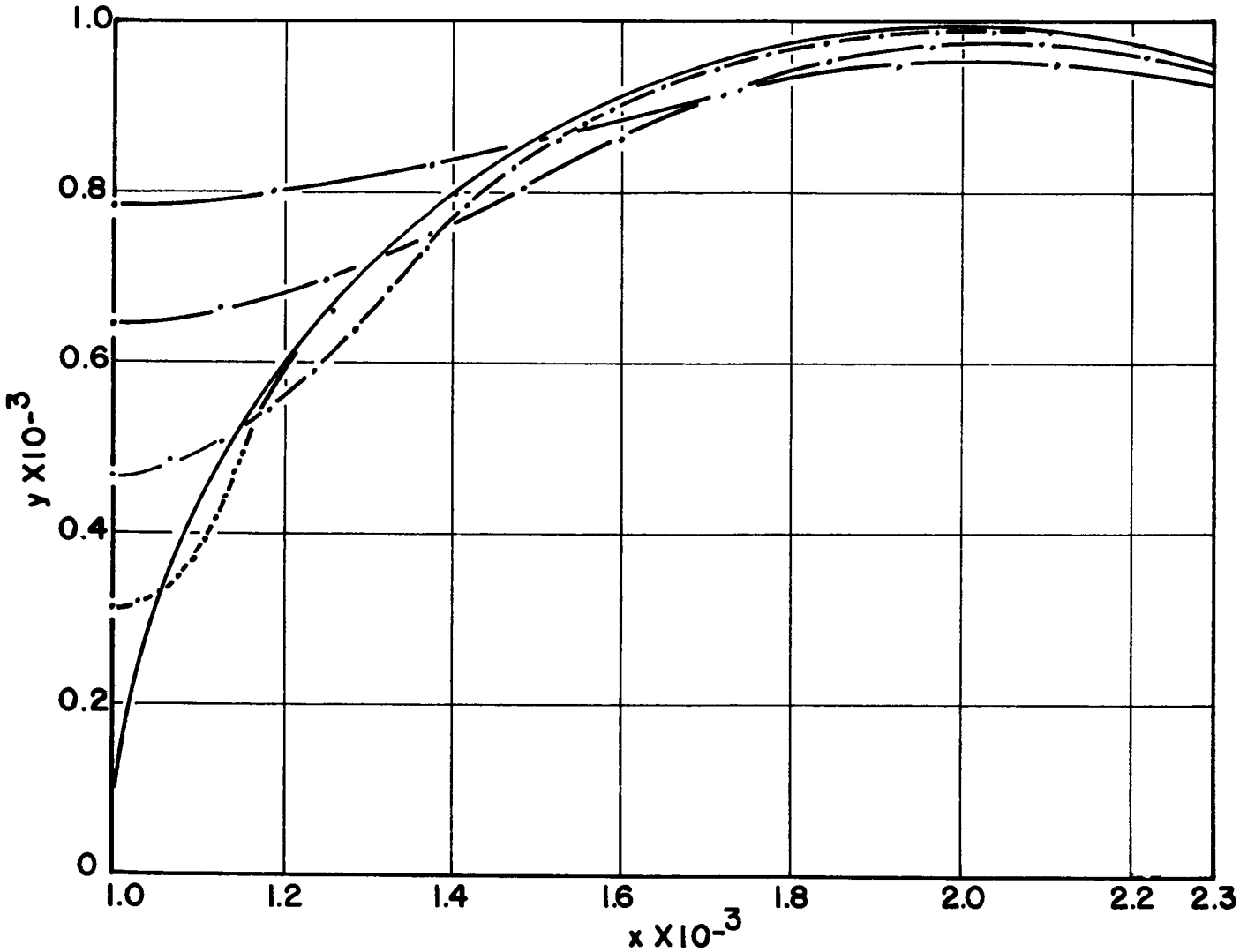

Fig. 29. Contours Generated During Later Stages of Rod-to-Rod Sintering.

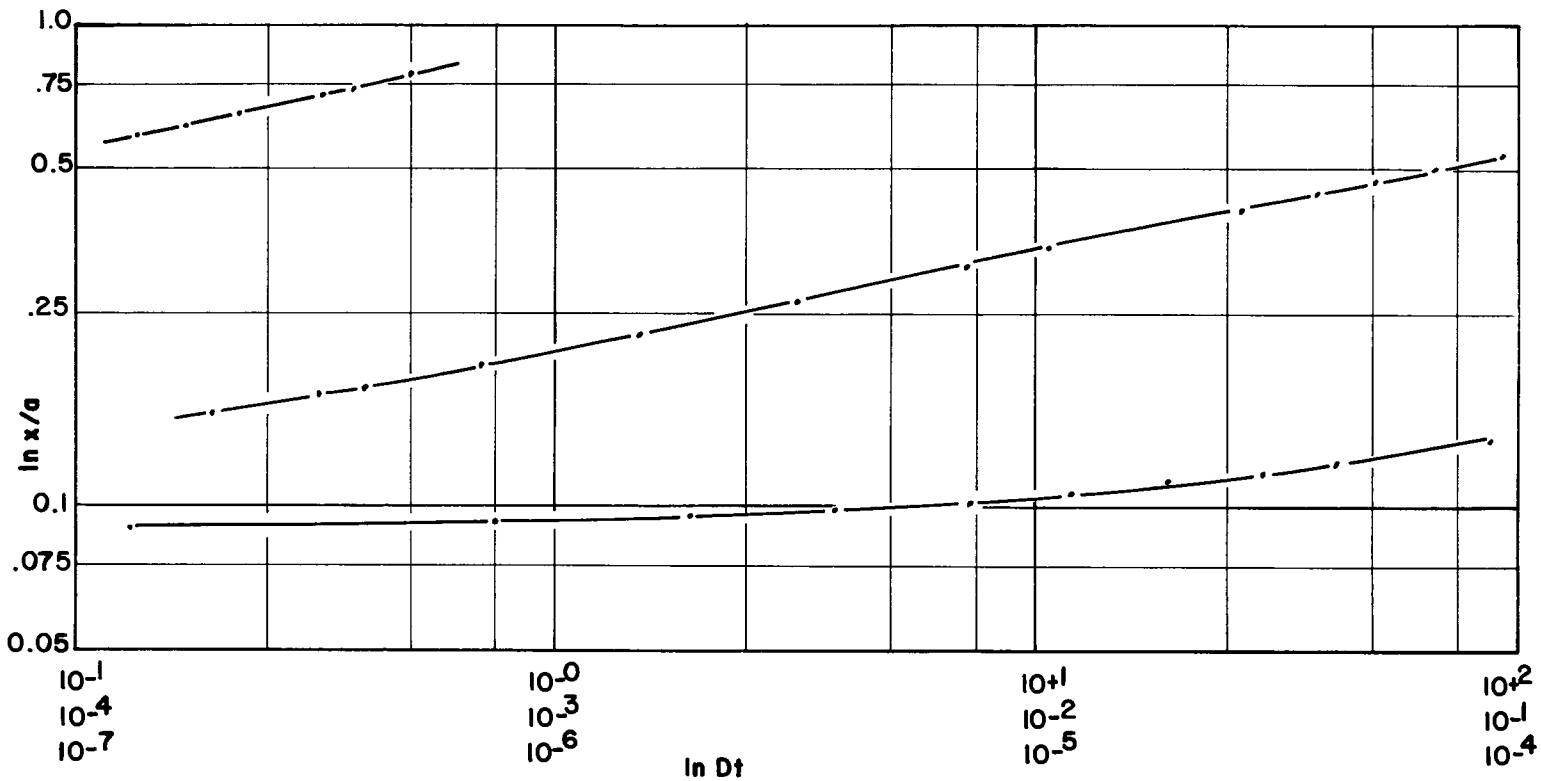

Fig. 30. Log-Log Plot of x/a versus $D_v t$ for Rod-to-Rod Sintering.

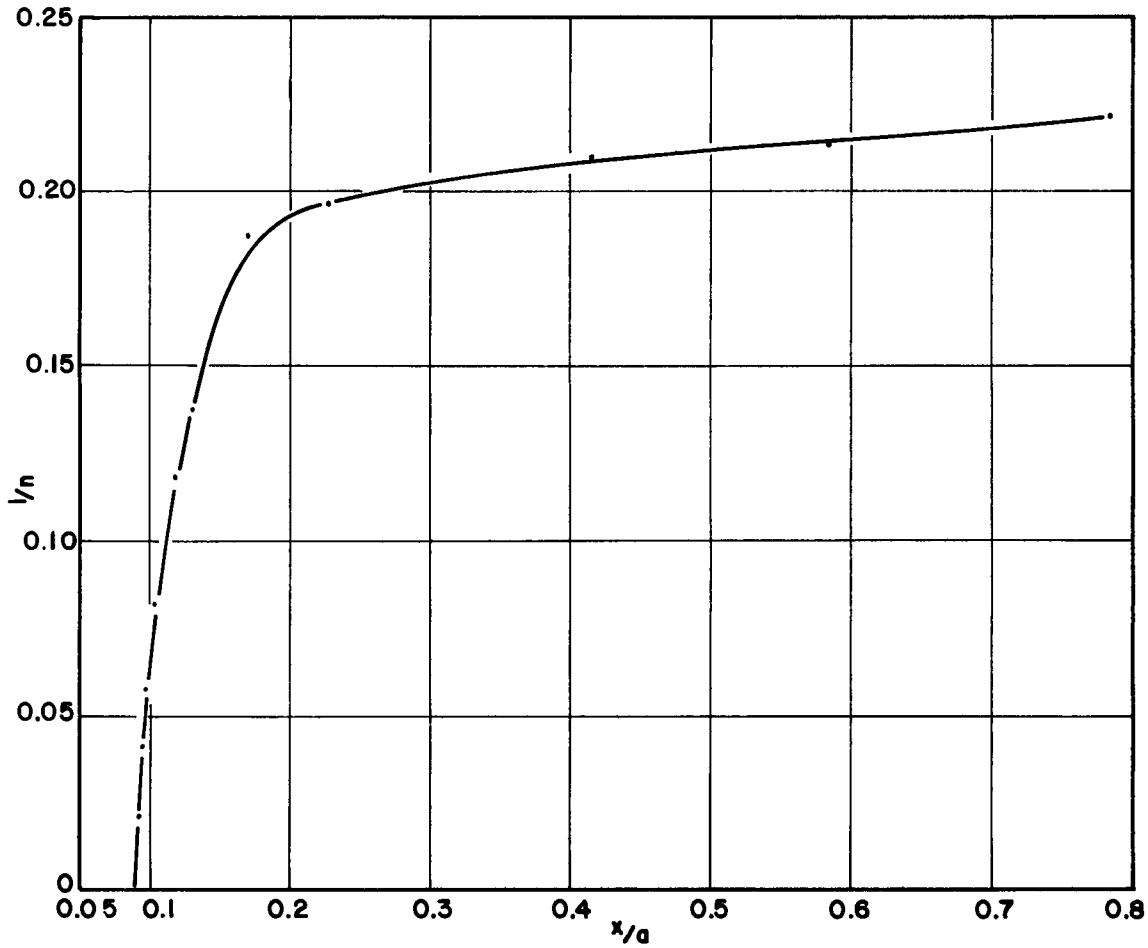

Fig. 31. Plot of 1/n versus x/a for Rod-to-Rod Sintering.

Dimensionless Parameters and Treatment of Experimental Data

For ease of reading, the parameters involved in obtaining a solution have been treated as real physical constants. The arbitrarily assumed values used in obtaining the solutions to the sintering problems given here were:

$$\frac{\gamma\Omega}{kT} = A = 10^{-10}, \quad a = 10^{-3}\ \text{cm}, \quad C_o = 10^{-3}\ . \tag{63}$$

A real material has its own set of parameters which will be denoted in the prime system, of C'_o, $(\gamma\Omega/kt)'$, a', $(D_v t)'$, etc. The dimensionless parameter ℓ is introduced:

$$\ell = a'/a = x'/x\ . \tag{64}$$

Since the problem hinges upon a linear integral equation, the dimensionless parameter relating the experimental concentration to the assumed concentration for curvatures K′ (experimental) and K (numerical solution) is

$$m = C/C' = AC_oK/A'C'_oK' = (AC_o/A'C'_o) \cdot \ell\ . \tag{65}$$

Thus, by writing the general equations for neck migration in the real and numerical system and rearranging, the following result is obtained:

$$1/\ell = (x - x_o)/x' - x'_o) = \frac{\Sigma\ D_v t \cdot \partial C/\partial n}{\Sigma (D_v t)' \cdot \partial C'/\partial n'} = \frac{D_v t}{(D_v t)'} \cdot m \cdot \ell\ . \tag{66}$$

Upon substituting the numerical values of Eq. (63) into Eq. (66), the final conversion equation for determining the experimental $(D_v t)$ value required to sinter to a particular x/a is given by:

$$(D_v t)' = 10^{-13}\ D_v t \cdot \ell^3/A' C'_o\ . \tag{67}$$

This result and pertinent comments are also applicable to the rod-to-plane results which will be presented below.

Conservation of Volume

The total volume of material of two sintering rods should be conserved, so that the total cross-sectional area of two sintering rods should not change in contour plots. One method of checking this is to measure the cross-sectional area planimetrically. This was done for the first three contours of Fig. 28. However, only the material gained by the neck and that lost by the rod body was measured (that is, the areas between the original contours and the generated contours). The apparent material gains for the contours, in order of increasing x/a as shown in Fig. 28, were 21.4, 22.1, and 18.5% of the total material transferred to the neck.

A more refined technique, however, consists of approximating the material gained in the neck root on the ith time step, $g_1(i)$, by summing the positive displacements $\Delta N_j^+(i)$, where the j subscript runs over the neck region:

$$g_1(i) \cong \sum_j \Delta N_j^+(i)\ \Delta s$$

and approximating the material lost from the rod body by summing the displacements on the rod body, $\Delta N_j^-(i)$:

$$g_2(i) \cong \sum_j \Delta N_j^-(i)\ \Delta s\ .$$

Then the percentage of material gained on any time step is simply

$$\text{per cent gain} = 100\% \cdot [g_1(i) - g_2(i)]/g_1(i)\ .$$

This gain was computed for each (k,m) system used to compute $Q(\infty,\infty)$ in "Errors Arising from the Nonclosed Contour and Finite Arc Spacing," page 52. The per cent gain was extrapolated to $\Delta s = 0$ for k approaching infinity. The extrapolated values were 2, 2.5, and 9% at $x/a = 0.05$, 0.10, and 0.30, respectively. The gain in the (4,3) system at $x/a|_o = 0.10$ was 24.5%. This value is in good agreement with the planimetrically measured values. The agreement might be expected, since the planimetric measurements covered a curve of essentially the length of S', which was the contour length used as a basis for the computations.

However, when the solution is corrected (see "Correcting the Solution for the Nonclosed Contour and Reflected Neck," page 58) for the additional contours S_2 and S''', the computed gain for the initial time step (computed over S' and S_2) is 0.157%. The total gain after k time steps is computed as:

$$\text{per cent total gain} = \frac{\sum_{i=0}^{k} g_1(i) - \sum_{i=0}^{k} g_2(i)}{\sum_{l=0}^{k} g_1(i)} \times 100\%\ .$$

Typical values were −0.17, −0.47, −1.05, −0.98, and −0.325% for x/a = 0.103, 0.123, 0.171, 0.228, and 0.315, respectively.

This type of volume conservation check is much more sensitive to small gains or losses of material than planimetric measurement of the entire system. Such small discrepancies provide reassurance that the solutions computed are physically realistic.

The Rod-to-Plane Sintering Problem

The treatment of computed results for the rod-to-plane system so closely parallel those of the rod-to-rod system that it is only necessary to comment on the significant differences between the systems and review the highlights of the numerical treatment and results.

The initial profile is that assumed by Kuczynski, and the geometry is shown in Appendix 1. The initial solutions were based on a region S', defined so that the midpoint of the range of S' is the neck root. A demonstration of the similarity between the systems is provided in Figs. 32 and 33, in which $Q(k,m)$ is plotted versus $(\Delta s)^2$ and $(1/k)$. As in the case of rod-to-rod sintering, the $Q(k,m)$ approaches the limiting value $Q(\infty,\infty)$ as k and m increase. The term $Q(\infty,\infty)$ was only determined for $x/a|_o = 0.10$, where its value is 0.690×10^{-3}. The comparable value of Q, calculated from Eq. (7) is 1×10^{-3}.

The plots of $Q(k,m)$ clearly demonstrate that the restricted length of S' is a greater source of error than the finite Δs for $m \geq 3$, so region S_2 was defined on both the rod and on the plane to be sufficiently long that when $\Phi_I(s)$ is extrapolated on S_2, it decreases to at least 10^{-4} of its maximum computed value on S'. An equation of the form of

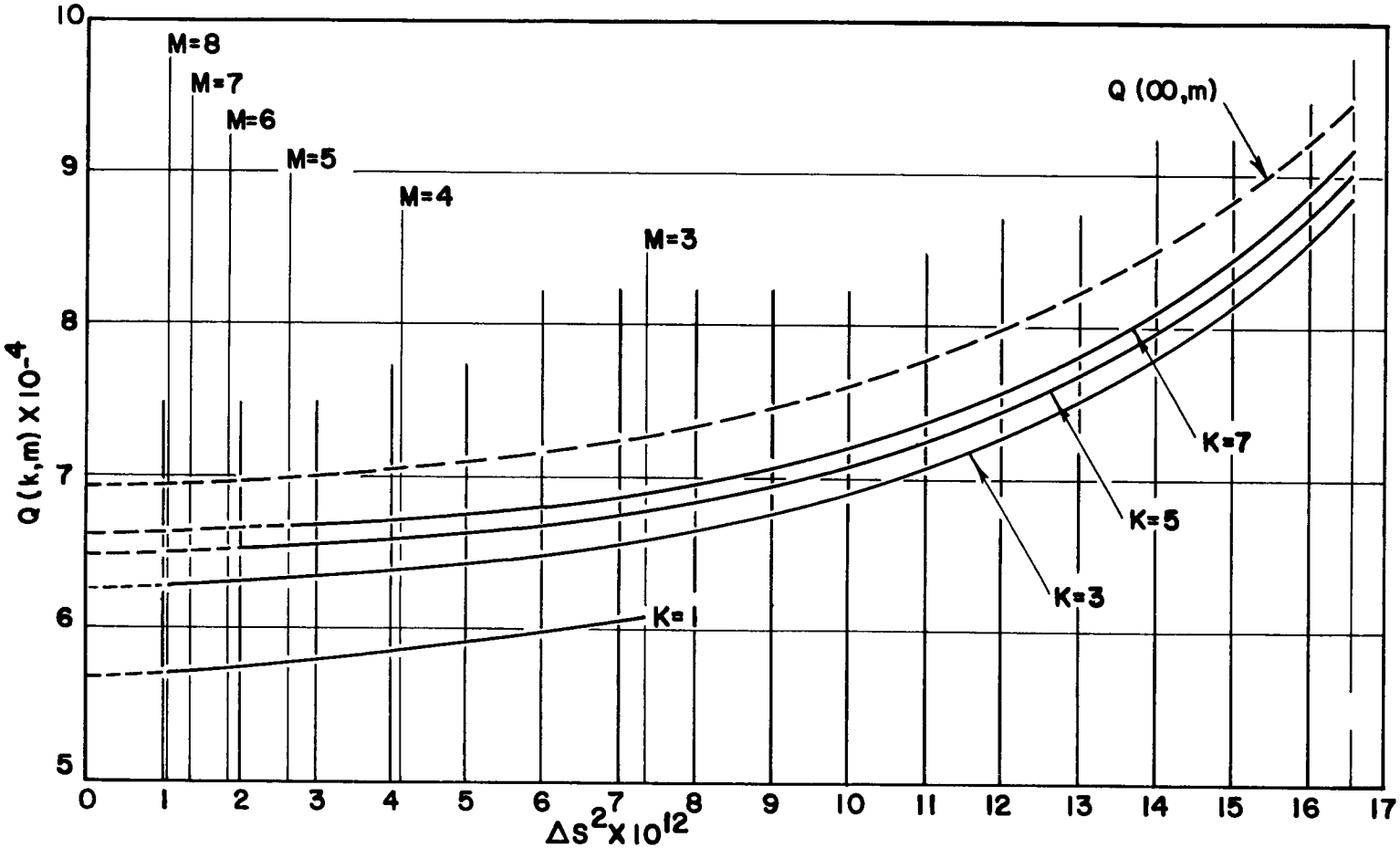

Fig. 32. Plot of Q(k,m) versus $(\Delta s)^2$ for Rod-to-Plane Sintering, $x/a|_o = 0.10$.

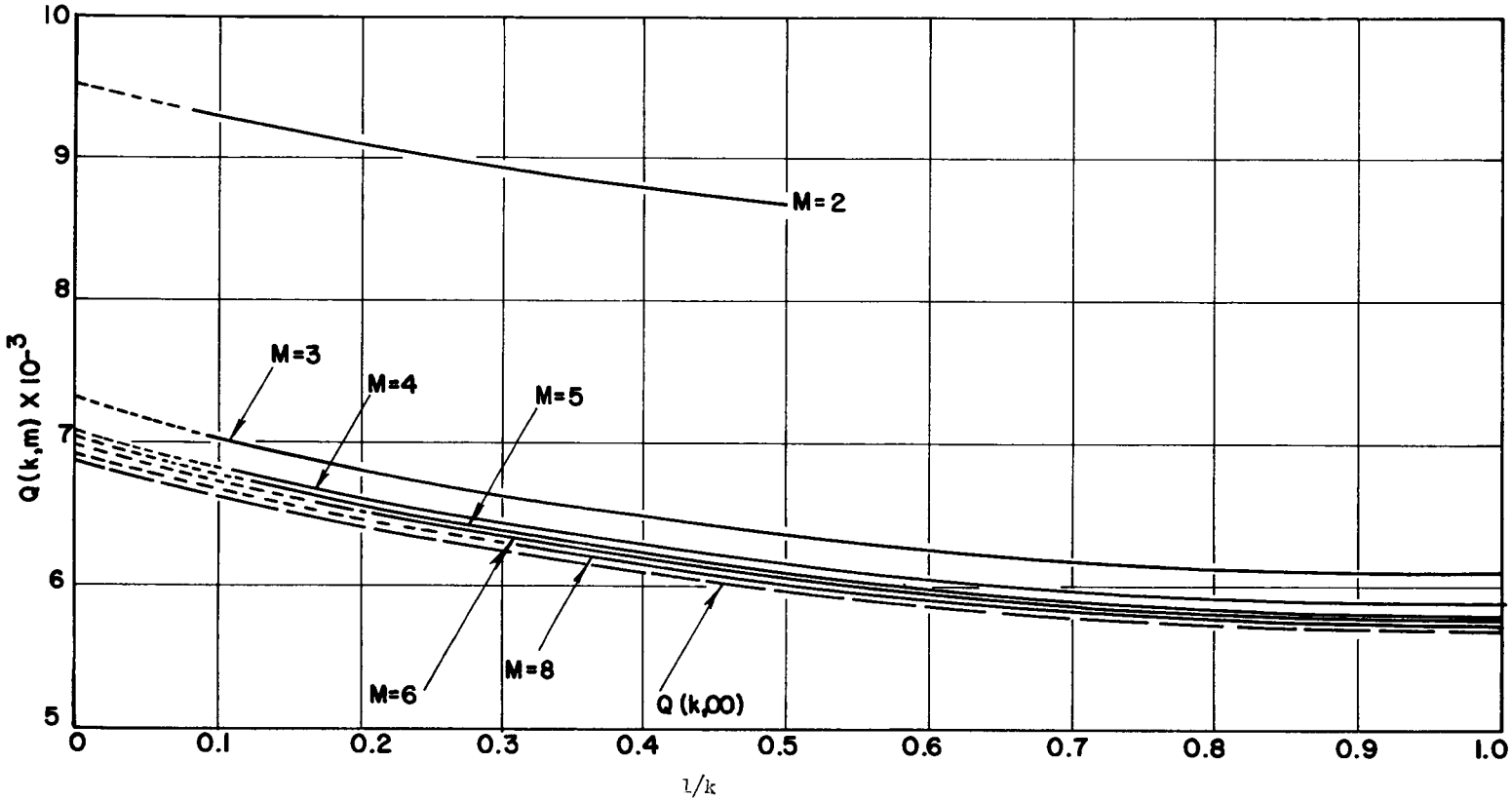

Fig. 33. Plot of Q(k,m) versus 1/k for Rod-to-Plane Sintering, $x/a|_o = 0.10$.

Eq. (56) was used to extrapolate $\phi_I(S_2)$, although different constants were computed for the rod and plane extrapolations, using the first and last three points on S', respectively. In addition, the effect of the reflected neck root was also accounted for, as in the rod-to-rod problem, using symmetry. The solutions for the initial profiles were obtained by matrix inversion, whereas on subsequent time steps equations of the form of Eqs. (57) and (58) were used to compute $\phi_I^{(i)}(S')$ by successive substitution.

The boundary-moving techniques differed from the rod-to-rod techniques only in that the polynomial fits and use of Eq. (61) were initiated at the end of S_2 on the rod rather than at the neck root.

On the basis of an error analysis similar to that used in the rod-to-rod problem, it was decided that the $k = 4$, $m = 3$ system, with an overall error estimated at approximately 17% in computed values of $D_v t$, should comprise the final solution. Figure 34 is the plot of ln (x/a) versus ln $D_v t$, for this system, and Fig. 35 is the set of 1/n values computed from Eq. (62). The dimensionless parameter discussion of "Dimensionless Parameters and Treatment of Experimental Data," page 77, is valid for this problem; in fact, the same parameter values given in Eq. (63) were used in the solution. Typical profiles are shown in Fig. 36.

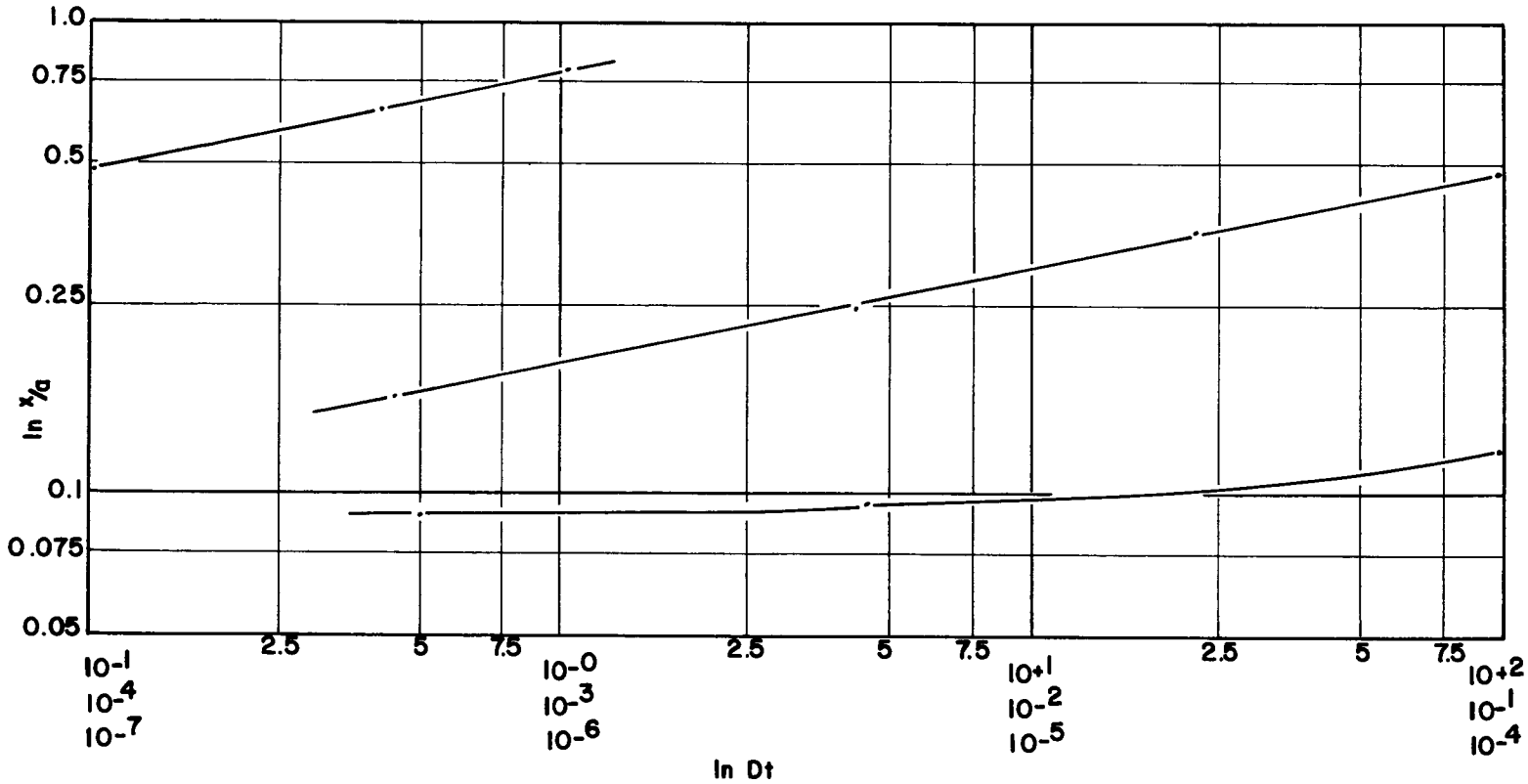

Fig. 34. Log-Log Plot of x/a versus $D_v t$ for Rod-to-Plane Sintering.

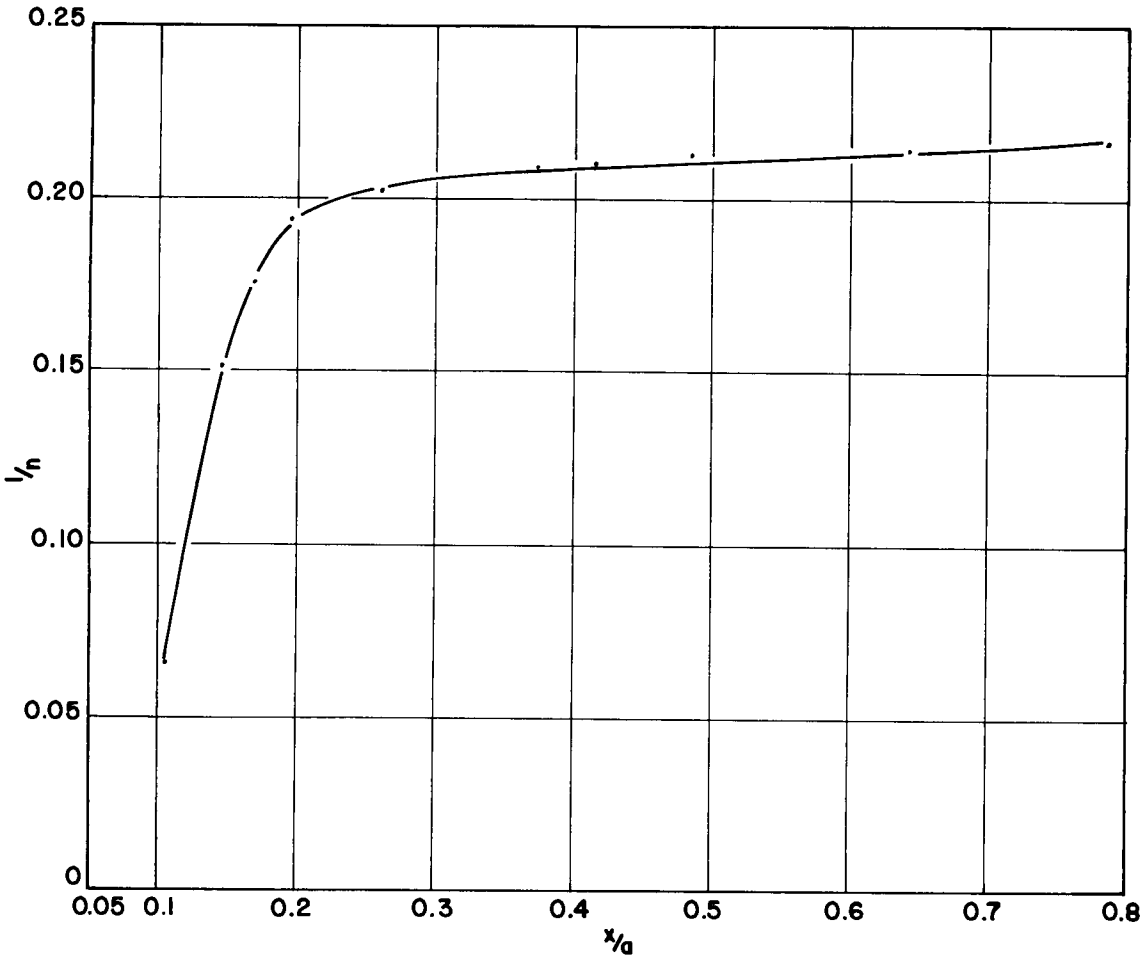

Fig. 35. Plot of 1/n versus x/a for Rod-to-Plane Sintering.

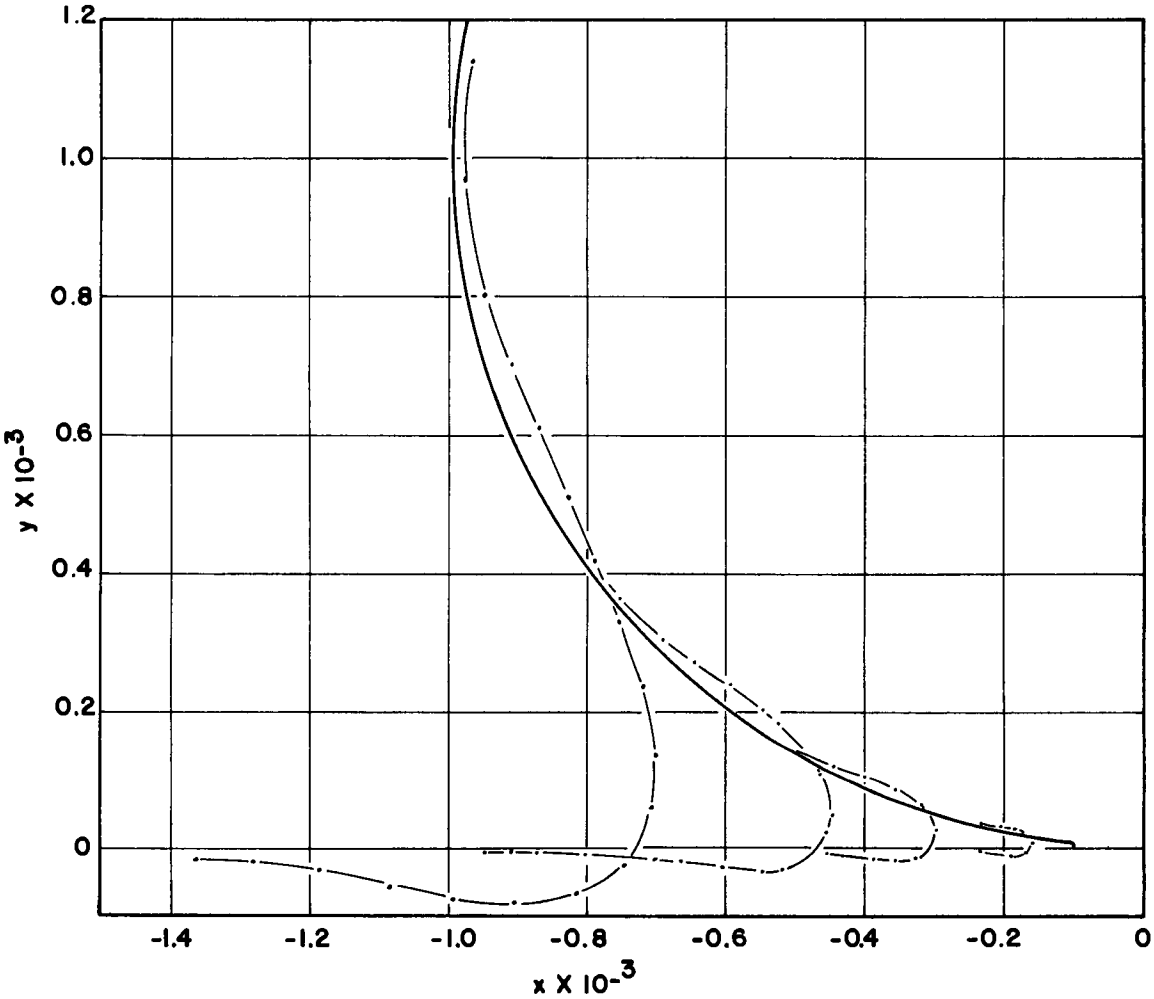

Fig. 36. Profiles Generated During the Sintering of a Rod to a Plane.

DISCUSSION OF RESULTS

The numerical results of this work fall into two categories: (1) interface migration during sintering for the geometrical constraints described by Kuczynski; and (2) interface migration during sintering by a volume diffusion mechanism with no geometrical constraints placed on the shapes developed. The former results were developed primarily to show a need for the latter results. Since the systems without geometrical constraints are more accurate descriptions of experimental sintering conditions, there is little need to discuss the results from the geometrically constrained systems.

Numerical Methods and Errors

It is felt that the test cases described on pages 40 through 47 (the ellipse and planar source problems) demonstrate the validity of the linear integral equation [Eq. (26)] for both closed and nonclosed contours. The numerical results for the ellipse test case demonstrate that the numerical solutions converge accurately to the known analytic solution in the limit of small δ for the ellipse. The agreement between the numerical and analytical results for an initial shape of Kuczynski geometry provides assurance that these results are reasonable.

The error in the final solutions for the rod-to-rod and rod-to-plane sintering problems is reasonably well known. The $D_v t$ parameters for rod-to-rod and rod-to-plane sintering have nearly constant known errors for all x/a, being approximately 15 and 17% too large, respectively. For the sake of consistency, all further calculations will be based on the reported

results for the (4,3) cases without correcting for this known error. These errors lie at least within the range of the experimental scatter in diffusion and sintering data.

Comparison with Earlier Analyses

In contrast to the gross discrepancies between the relationships predicted by Kuczynski and the numerical results of Nichols, it is found that Kuczynski's analyses of the volume-diffusion sintering problems are quite similar to the numerical results reported here. In fact, the (4,3) system rod-to-rod results may be represented to within ±8% of $D_v t$ for $0.2 \leq x/a \leq 0.7$ by

$$\frac{x^5}{a^2} \cong 5.8 \frac{\gamma \Omega C_v^\circ}{kT} D_v t \ . \tag{68}$$

The rod-to-plane results may be represented over the same range by

$$\frac{x^5}{a^2} \cong 2.2 \frac{\gamma \Omega C_v^\circ}{kT} D_v t \ . \tag{69}$$

It is not surprising that the numerical results can be represented in this manner, since computed values of $d \ln(x/a) d \ln t$ for the rod-to-rod and rod-to-plane cases yield values of approximately 1/5, as shown in Figs. 31 and 35, respectively.

Furthermore, Alexander and Baluffi (9) have observed that the neck root regions, which they described as triangular cusps, "...became rather bulbous due to smoothing effects with a radius about twice that predicted analytically." This enlargement of the neck radius is predicted by the

numerical results for the rod-to-rod sintering case. The ratio of ρ, the neck radius of curvature predicted by Kuczynski, to $\Delta s/(\theta_{n'+1} - \theta_{n'-1})$, the approximate radius of curvature at the neck root in the numerical solution, varies from 2.8 at $x/a = 0.10$ to 1.7 at $x/a = 0.40$. As will be demonstrated below, the rod-to-rod solutions can not be applied to layers of wire above $x/a \cong 0.25$. However, the difference between Kuczynski's results and these results may not be ascribed to enlargement of the neck radius (and hence an alteration of the driving force). Based on the Kuczynski geometry, Q_k exceeds the values of $Q(\infty,\infty)$, as described on pages 52 through 58, by factors ranging from 1.2 ($x/a = 0.05$) to 1.6 ($x/a = 0.3$). Thus, a significant amount of the difference between these analyses must result from inaccuracy in Kuczynski's estimate of the concentration gradient dC/dn.

Calculations of Diffusion Coefficients from Experimental Data

Nichols has demonstrated that for $x/a < 0.4$, there is little difference between the rates of sintering of lines of spheres and two isolated spheres by surface diffusion. Furthermore, for $x/a < 0.25$, less than 20% of the material contributed to the neck root in rod-to-rod sintering comes from beyond the 60° sector of the original rod in which the neck was located. Within this range it is felt that the rod-to-rod sintering results are applicable to the three-wire compacts sintered by Brett and Seigle (14) and to the wire-wound bobbins of Alexander and Baluffi (9). The rod-to-plane sintering results are felt to be applicable to single layers of wire-wound bobbins up to $x/a \sim 0.35$, since interference from necks not accounted for in the numerical solution should be smaller than in the case of hexagonal arrays of wires.

As an example of the numerical computations, the volume-diffusion coefficient for nickel will be computed for the 0.0254-cm-diam wires sintered by Brett and Seigle at 1300°C. The values γ = 1500 ergs/cm (36) and $\Omega = 1.095 \times 10^{-23}$ cm^3/atom (calculated from densities and atomic weights in reference 34) were used in these calculations. Thus, the parameter A′ in Eq. (67) is given by:

$$A' = 0.756 \times 10^{-7} \text{ cm} .$$

The dimensionless parameter, ℓ, is computed from the defining of Eq. (64) for $a' = 1.27 \times 10^{-2}$ cm as:

$$\ell = 1.27 \times 10^{-2} \text{ cm}/10^{-3} \text{ cm} = 1.27 \times 10^{1} .$$

The time t′ to grow a neck from x/a = 0.1 to x/a = 0.25 is 370 hr, whereas from Fig. 30, it may be seen that $Dt = 1.9 \times 10^{-3}$ cm^2. Substituting these values in Eq. (67) and solving for D′, the bulk diffusion coefficient for nickel at 1573°K,

$$D' = \frac{10^{-13} \text{ cm} \cdot 1.9 \times 10^{-3} \text{ cm}^2 \cdot (12.7)^3}{0.756 \times 10^{-7} \text{ cm } 25.2 \times 10^{5} \text{ sec}} = 0.62 \times 10^{-11} \text{ cm}^2/\text{sec} .$$

Recent tracer diffusion experimental results may also be used to calculate the bulk diffusivity of nickel at 1573°K as

$$D_{Ni}^{1573°K} = 1.9 \exp\left(\frac{-68{,}000 \text{ cal/mole}}{1.987 \text{ cal/mole °K} \cdot 1573°K}\right) = 0.714 \times 10^{-11} \text{ cm}^2/\text{sec} .$$

Considering the uncertainty in diffusion and neck growth data, this represents excellent agreement. It is thus possible that, for these relatively large diameter nickel wires, volume diffusion contributes substantially to the sintering process for $0.1 < x/a$.

However, such good agreement is not obtained for sintering experiments performed with copper and silver wires. Alexander and Baluffi (9) measured the rate of neck growth of 0.0128-cm-diam electrolytic copper wires wound on 1.9-cm-diam copper spools, and obtained data to which the rod-to-rod analysis applies. Alexander and Baluffi calculated an activation energy of 47,000 cal/mole for their experiment. The D_{Cu} was given by the tracer diffusion results (31) as:

$$D_{Cu} = 0.33 \exp(-48{,}200 \text{ cal/mole/RT}) .$$

Alexander et al. (32) performed a rod-to-plane type experiment of the same nature by sintering 0.0127, 0.0251, 0.0381, and 0.508-cm-diam copper wires onto 6.35-cm-diam copper cylinders at 1050 and 1070°C. Kuczynski (17) sintered 0.0127-cm-diam silver wire to a 0.0635-cm-diam silver cylinder at temperatures ranging from 460 to 900°C for various times, and obtained an activation energy of 45,700 cal/mole. The bulk-diffusion coefficient for silver was calculated from the tracer-diffusion results (33) that

$$D_{Ag} = 0.34 \exp(-43{,}500 \text{ cal/mole/RT}) .$$

The calculated results for D′ are tabulated in Table 3, together with other pertinent data and the tracer-diffusion coefficients at the temperature of the sintering experiments. It is apparent that, since the D′

Table 3. Comparison of Calculated D′ with D from Tracer-Diffusion Experiments

System	Temperature (°C)	Time (hr)	x/a	D′ (calculated) (cm^2/sec)	D (tracer) (cm^2/sec)	Material[a]	Surface Tension[a] ($ergs/cm^2$)	Volume[a] ($cm^3/atom$)
								$\times 10^{-23}$
Rod-to-rod	900	25	0.206	2.04×10^{-12}	3.53×10^{-10}	Cu (9)	1670 (9)	1.2 (9)
Rod-to-rod	1075	4	0.264	5.2×10^{-11}	5.02×10^{-9}	Cu (9)	1670 (9)	1.2 (9)
Rod-to-plane	1050	24	0.223	6.13×10^{-10}	4.64×10^{-9}	Cu (33)	1670 (9)	1.2 (9)
Rod-to-plane	900	4	0.313	1.14×10^{-10}	2.7×10^{-9}	Ag (17)	1140 (5)	1.7 (35)
Rod-to-rod	1300	370	0.25	0.41×10^{-11}	0.714×10^{-11}	Ni (14)	1500 (33)	1.09 (35)

[a]Reference given in parentheses.

required to grow a neck of a particular x/a is smaller than the tracer-diffusion coefficient by between one and two orders of magnitude for these experiments, sintering is proceeding more slowly than a volume-diffusion model would predict, as measured by the rate of neck growth. It is interesting to note in this context that 0.05 μ Al_2O_3 particles dispersed in sintering copper wires retard the rate of sintering, whereas Al_2O_3 particles dispersed in nickel wires do not alter the rate of sintering (14). This effect is due to the presence of the second phase, since sintering of copper saturated in oxygen and containing 55 ppm Al sintered faster than copper containing alumina. However, sufficient data were not given for calculating the absolute self-diffusion coefficient of copper from the sintering results.

No clear-cut explanation of the discrepancies in diffusivities measured by tracers and calculated for the sintering of copper and silver wires can be offered at this time. However, on the basis of these results, it is not unreasonable to suspect that some other mechanism, such as an interface reaction, is the rate-limiting step during sintering in some systems.

In order to aid experimenters in determining whether volume diffusion or surface diffusion should dominate in any particular sintering experiment, future work will include a comparison of the relative contributions of volume- and surface diffusion for various physical parameters. It is hoped that the volume diffusion and surface-diffusion numerical techniques may eventually be combined so that the simultaneous operation of both transport mechanisms may be evaluated. Until these future phases of the numerical work have been completed, it does not seem profitable to discuss this matter at great length.

Applicability of Numerical Techniques to Other Problems

Numerous other systems of complex interface geometry in which the interface migration is presumed to be controlled by volume diffusion may be treated using the methods developed here. For application of the present techniques to these systems, it is only necessary that matter be conserved, that $\nabla^2 C = 0$, and that the concentration $C(s)$ be defined just under the boundary surface. Such problems include phase transformations, scratch smoothing, and grain-boundary grooving.

A feasibility study has been made for one phase transformation problem, and some preliminary results are outlined in Appendix 3. The problem discussed is that of an infinitely long crystal of constant cross-section growing from a supersaturated solid solution within the confines of an infinite cylinder on which the concentration of the diffusing species is specified.

It is hoped that this work will stimulate further use of these techniques in treating interface migration problems.

SUMMARY AND CONCLUSIONS

Numerical results for the rate of neck growth during the sintering of rods and spheres to themselves and to planes by volume and surface diffusion have been obtained by relaxing the mathematical restriction that $x/a \ll 1$ used by Kuczynski, but retaining his geometrical constraints. Under these conditions it is found that $d \ln(x/a)/d \ln(t)$ is not constant for $x/a < 0.3$ as the earlier analyses predicted.

Use of the Cauchy integral equation and the Cauchy-Riemann differential equations permits definition of the gradient of a harmonic function bounding a two-dimensional region on which the function is defined. The values of the function on the curve are specified as boundary conditions. Numerical techniques are developed for treating a curve of arbitrary shape.

The numerical methods are applied to trial cases for which the solutions are known, and then are used to solve for the rate of neck growth and morphologies developed during rod-to-rod and rod-to-plane sintering by a volume-diffusion mechanism. Although some variation in d ln(x/a)/d ln(t) is found over the range of x/a investigated in the solutions, it is found that the results may be represented accurately for the case of rod-to-rod sintering by:

$$\frac{x^5}{a^2} = 5.8 \frac{\gamma \Omega C_v^\circ}{kT} D_v t \ .$$

For the rod-to-plane sintering case the results may be represented by:

$$\frac{x^5}{a^2} = 2.2 \frac{\gamma \Omega C_v^\circ}{kT} D_v t \ .$$

Application of these results to available data indicates that neck growth in the sintering of copper and silver wire proceeds from one to two orders of magnitude too slowly. However, the volume-diffusion coefficient for nickel calculated from sintering data is in excellent agreement with that obtained by tracer-diffusion techniques. This suggests that neither surface- nor volume diffusion is the rate-limiting step during sintering in some systems.

REFERENCES

REFERENCES

1. M. Salkind, F. Lenel, and G. Ansell, Trans Met. Soc. AIME 233, 39 (1965).
2. F. Sauerwald, Z. anorg. u. allegem. Chem. 122, 277 (1922).
3. R. C. Smith, J. Chem. Soc. 119, 1683 (1921).
4. M. Yu. Bal'shin, Vestnik Metalloprom. 16(18), 82 (1936).
5. C. Herring, "Surface Tension as a Motivation for Sintering," p. 143 in Symposium on Physics of Powder Metallurgy, Bayside, New York, 1949, ed. by W. E. Kingston, McGraw-Hill, New York (1951).
6. T. L. Wilson and P. G. Shewmon, Trans. Met Soc. AIME 236, 48 (1966).
7. J. Frenkel, J. Phys. 9, 385 (1945).
8. G. C. Kuczynski, J. Appl. Phys. 20, 1160 (1949).
9. B. H. Alexander and R. W. Baluffi, Acta Met. 5, 666 (1957).
10. J. Early, F. Lenel, and G. Ansell, Trans. Met. Soc. AIME 230, 1641 (1964).
11. J. Weertman, J. Appl. Phys. 26, 1213 (1955).
12. J. Weertman, J. Appl. Phys. 28, 362 (1957).
13. G. Ansell and J. Weertman, Trans. Met. Soc. AIME 215, 838 (1959).
14. J. Brett and L. Seigle, Acta Met. 14, 575–582 (1966).
15. G. C. Kuczynski, Trans. Am. Inst. Mining, Met. Petrol. Eng. 185, 169 (1949).
16. F. Nichols, Thesis, Carnegie-Mellon University (1965).
17. G. C. Kuczynski, J. Appl. Phys. 21, 632 (1950).
18. W. D. Kingery and M. Berg, J. Appl. Phys. 26, 1205 (1950).
19. L. Lapidus, Digital Computation for Chemical Engineers, McGraw-Hill, New York (1962).

20. W. W. Mullins and R. F. Sekerka, J. Appl. Phys. 34, 323 (1963).

21. W. W. Mullins and R. F. Sekerka, J. Appl. Phys. 35, 444 (1964).

22. I. S. Sokolnikoff and R. M. Redheffer, pp. 559–560 in Mathematics of Physics and Modern Engineering, McGraw-Hill, New York (1953).

23. S. G. Mikhlin, Linear Integral Equations, Hindustan Publishing Corporation, Dehli, India (1960).

24. Wilfred Kaplan, Advanced Calculus, Addison-Wesley, Reading, Mass. (1952).

25. W. V. Lovitt, Linear Integral Equations, Dover, New York (1950).

26. S. G. Mikhlin, Integral Equations, Pergamon Press, New York (1957).

27. L. Fox and E. T. Goodwin, Phil. Trans. Proc. Roy. Soc. 245, 501 (1953).

28. L. V. Kantorovich and V. I. Krylov, Approximate Methods of Higher Analysis, p. 97, Interscience, New York (1958).

29. F. Nichols, Thesis, Carnegie-Mellon University (1965).

30. W. W. Mullins, "Morphologies Governed by Capillarity," p. 53 in Metal Surfaces, American Society for Metals, Metals Park, Ohio (1962).

31. K. Monma, H. Suto, and H. Oikawa, J. Japan Inst. Metals (Sendia) 28, 188 (1964).

32. B. H. Alexander, G. C. Kuczynski, and M. H. Dawson, The Physics of Powder Metallurgy, Chap. 21, ed. by W. E. Kingston, McGraw-Hill, New York (1951).

33. A. V. Savitski, Fiz Metal i Metalloved 16, 886 (1963).

34. Handbook of Chemistry and Physics, 39 ed., Chemical Rubber Publishing Company, Cleveland, Ohio (1957–1958).

35. G. A. Geach, Progr. Metal Phys. 4, 174 (1953).

36. H. E. McCoy, Jr., private communication.

APPENDICES

APPENDIX 1

NUMERICAL SOLUTION OF SINTERING PROBLEMS USING KUCZYNSKI-TYPE GEOMETRICAL RELATIONS

In this appendix, the solutions to a number of sintering problems are set up using the type of geometrical approximations suggested by Kuczynski (that is, the neck profile is a fillet of radius, ρ, tangentially joined to bodies of circular or planar projection in the cases of rod-to-plane and sphere-to-plane sintering, respectively). The body radius, a, is assumed to remain constant during the sintering process. The neck-body junction is located such that dy/dx is continuous over the entire profile, although d^2y/dx^2 is discontinuous at the junction. In contrast with Kuczynski's analysis, however, no mathematical approximations are made which would require $x \ll a$.

By defining $U = x/a$ and $\rho' = \rho/a$, it is found that the mathematics of the cases of (1) rod-to-rod, (2) rod-to-plane, (3) sphere-to-sphere, and (4) sphere-to-plane sintering by either volume diffusion or surface diffusion may be formulated as equations of the general form

$$dV/dt = K \cdot f(U) \qquad \text{(A-1)}$$

where K and f(U) are different for each of the eight cases. The terms of Eq. (A-1) for each of the eight cases are defined in this appendix, but the solutions are discussed in the text of this work.

Three subscript letters are added to K and f(U) for the different cases, with the first two subscripts indicating the morphology of the sintering bodies (r for rod, p for plane, and s for sphere) and the final

subscript s for surface diffusion and v for volume diffusion. Thus, K_{rpv} refers to rod-to-plane sintering by volume diffusion.

The geometrical terms which are common to rod-to-rod and sphere-to-sphere sintering may be deduced by examining Fig. 1-1. The common terms are:

$$U = x/a \ , \tag{A-2}$$

$$\rho' = \rho/a \ , \tag{A-3}$$

$$\theta = \arctan\left(\rho' + U\right) \ , \tag{A-4}$$

$$\sin\theta = \left(\frac{\rho + x}{\rho + a}\right) = \left(\frac{\rho' + U}{\rho' + 1}\right) \ , \tag{A-5}$$

$$\cos\theta = \left(\frac{a}{\rho + a}\right) = \left(\frac{1}{\rho' + 1}\right) \ . \tag{A-6}$$

The geometrical terms common to rod-to-plane and sphere-to-plane sintering are deduced from Fig. 1-2. By applying the Pythagorean theorem, and retaining the definition, U = x/a, the following relationships are obtained:

$$\rho' = \rho/a = 2 - U - 2\sqrt{1 - U} \ , \tag{A-7}$$

$$\phi = \arctan\left(\frac{U + \rho'}{1 - \rho'}\right) \ , \tag{A-8}$$

The common trigonometric terms for rod-to-plane and sphere-to-plane sintering are:

$$\sin\phi = \frac{U + \rho'}{1 + \rho'} \ , \tag{A-9}$$

$$\cos\phi = \frac{1 - \rho'}{1 + \rho'} \ . \tag{A-10}$$

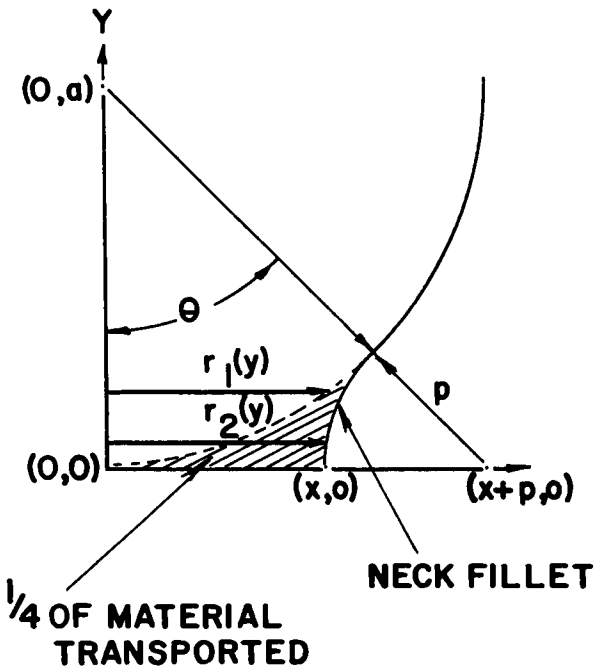

Fig. 1-1. Geometry Common to Rod-to-Rod And Sphere-to-Sphere Sintering.

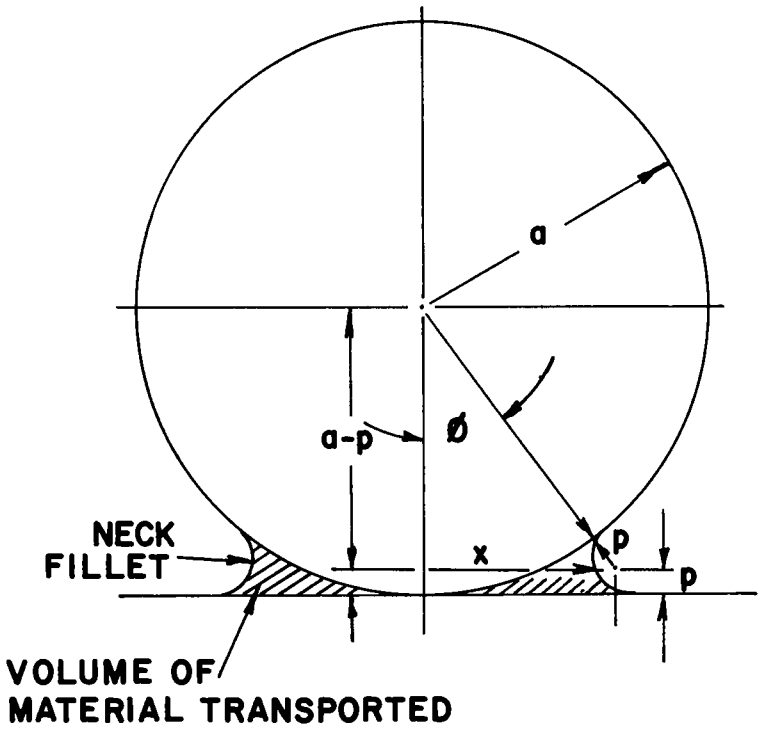

Fig. 1-2. Geometry Common to Rod-to-Plane and Sphere-to-Plane Sintering.

The preceding discussion has defined the geometrical relationships involved in the eight sintering cases. For each case, a dV/dt term, a transport area (for volume diffusion) or length (for surface diffusion) and driving force remain to be defined. This is shown in some detail for the rod-to-rod cases, and outlined briefly for all others.

The volume of material which must be transported to grow a neck radius, x, in rod-to-rod sintering is

$$V = 4 \int_{o}^{\rho\cos\theta} \int_{r_1(y)}^{r_2(y)} 1 \cdot dr \cdot dy = 2a^2 \left[(U + \rho') - \theta - (\rho')^2 \left(\frac{\pi}{2} - \theta \right) \right] . \quad \text{(A-11)}$$

The rate of change of V is given by

$$dV/dt = 2a^2 \left\{ 1 + [(\rho')^2 - 1] \frac{d\theta}{dU} + \left[1 - 2\rho' \left(\frac{\pi}{2} - \theta \right) \right] \frac{d\rho'}{dU} \right\} \frac{dU}{dt}$$

$$= 2a^2 \, C_1(U) \frac{dU}{dt} \quad \text{(A-12)}$$

where the equations of (A-12) define $C_1(U)$ as the term in braces as a function of U, only.

For rod-to-rod sintering by volume diffusion, the area over which material diffuses is given by:

$$A = 4a \cdot \rho' \, (\pi/2 - \theta) = 4aC_2(U) \; . \quad \text{(A-13)}$$

The definitions $B = D_s \gamma \, \Omega \upsilon / kT$ and $E = \gamma \, \Omega C_o / kT$ will be used. The driving force is assumed to be $\Delta C/\rho$, where

$$\frac{\Delta C}{\rho} = \frac{E}{\rho' a^2} \left(\frac{1}{\rho'} + 1 \right) = - C_3(U) \; . \quad \text{(A-14)}$$

A flux balance for the system yields

$$\frac{dV}{dt} = D_v \frac{\Delta C}{\rho} \cdot A \tag{A-15}$$

and substituting Eqs. (A-12), (A-13), and (A-14) into Eq. (A-15), the result is obtained that:

$$dU/dt\Big|_{rrv} = \frac{2ED_v C_2(U) \cdot C_3(U)}{a^2 C_1(U)} \ . \tag{A-16}$$

For rod-to-rod sintering by surface diffusion, flux occurs over four lines of unit length at the body-neck junction, a total diffusion length of

$$L = 4 \ . \tag{A-17}$$

The surface flux is given by

$$J_s = B \cdot \frac{\partial K}{\partial s} = -\frac{B}{a^2 \rho'}\left(\frac{1}{\rho'} + 1\right) = -\frac{B}{a^2} \cdot C_3(U) \ . \tag{A-18}$$

Thus, a material balance on the system yields:

$$\frac{dV}{dt} = J_s L \tag{A-19}$$

or, substituting Eq. (A-12) for dV/dt, Eq. (A-17) for L and Eq. (A-18) for J_s,

$$dU/dt\Big|_{rrs} = \frac{B}{a^4} \cdot \frac{2C_3(U)}{C_1(U)} \ . \tag{A-20}$$

The following equations were obtained for the various sintering cases mentioned earlier in a manner analogous to that used to obtain the rod-to-rod equations.

Sphere-to-Sphere:

$$V_{ss} = 2 \int_{o}^{\rho\cos\theta} \int_{r_1(y)}^{r_2(y)} \int_{o}^{2\pi} d\psi \cdot r dr \cdot dy \ , \tag{A-21}$$

$$dV_{ss}/dt = 2\pi a^3 \cdot C_5(U) \cdot dU/dt \ , \tag{A-22}$$

$$A_{ss} = 4\pi \int_{o}^{\rho\cos\theta} r_2(y) dy = 4\pi a^2 C_4(U) \ , \tag{A-23}$$

$$\Delta C/\rho = \frac{E}{\rho' a^2} \cdot (2 + 1/\rho' - 1/U) = \frac{E}{a^2} C_6(U) \ , \tag{A-24}$$

$$L = 4\pi a U \ , \tag{A-25}$$

$$J_s = BC_6(U)/a^2 \ , \tag{A-26}$$

$$dU/dt\big|_{ssv} = \frac{ED_v}{a^3} \cdot \frac{2C_4(U) \cdot C_6(U)}{C_5(U)} \ , \tag{A-27}$$

$$dU/dt\big|_{sss} = -\frac{B}{a^4} \frac{2U \cdot C_6(U)}{C_5(U)} \ . \tag{A-28}$$

Rod-to-Plane:

$$V_{rp} = 2 \int_{0}^{\rho\cos\theta+\rho} \int_{r_1(y)}^{r_3(y)} dr \cdot dy \ , \tag{A-29}$$

$$dV_{rp}/dt = a^2 C_7(u)\ du/dt\ , \tag{A-30}$$

$$\Delta C/\rho = -\frac{E}{\rho' a^2}\left(\frac{1}{2} + \frac{1}{\rho'}\right) = -\frac{E}{a^2} C_9(U)\ , \tag{A-31}$$

$$A_{rp} = 2a\rho'(\pi - \phi) = a \cdot C_8(U)\ , \tag{A-32}$$

$$L = 4\ , \tag{A-33}$$

$$J_s = -\frac{B}{a^2}\frac{2C_9(U)}{(\pi - \phi)}\ , \tag{A-34}$$

$$dU/dt\big|_{rpv} = \frac{ED_v}{a^3}\frac{C_8(U)\ C_9(U)}{C_7(U)}\ , \tag{A-35}$$

$$dU/dt\big|_{rps} = \frac{B}{a^4}\frac{8C_9(U)}{(\pi - \phi)C_7(U)}\ , \tag{A-36}$$

<u>Sphere-to-Plane</u>:

$$V_{sp} = \int_0^{\rho(1+\cos\phi)} \int_{r_1(y)}^{r_2(y)} \int_0^{2\pi} d\phi\ r\ dr\ dy\ , \tag{A-37}$$

$$dV_{sp}/dt = \pi a^3 C_{10}(U) du/dt\ , \tag{A-38}$$

$$A_{sp} = 2\pi \int_0^{\rho(1+\cos\phi)} r_3(y)\ dy = 2\pi a^2 C_{11}(U)\ , \tag{A-39}$$

$$\Delta C/\rho = -\frac{E}{a^2\rho'}(1 + 1/\rho' - 1/U) = -\frac{E}{a^2} C_{12}(U) \tag{A-40}$$

$$L = 2\pi a U \ , \tag{A-41}$$

$$J_s = - BC_{12}(U)/a^2 \ , \tag{A-42}$$

$$dU/dt\big|_{spv} = \frac{2D_v E}{a^3} \frac{C_{11}(U)\ C_{12}(U)}{C_{10}(U)} \ , \tag{A-43}$$

$$dU/dt\big|_{sps} = \frac{2B}{a^4} \frac{UC_{12}(U)}{C_{10}(U)} \ . \tag{A-44}$$

APPENDIX 2

QUADRATURE WEIGHTING FACTORS

In the text, the use of weighting factors in quadrature formulae was indicated without any specific detail on how they should be obtained. Equations (31), (32), (35), and (36) of the text make specific reference to these weighting factors.

The factors arise from approximating a contour integral as:

$$\int_a^b f(s)\, ds \cong \sum_{k=0}^{n} A_k f(s_k)\Delta s + e \; . \qquad \text{(B-1)}$$

Separate consideration will be given to closed and nonclosed contours, for both the contour integrals on the right side of Eq. (26) in the text.

Closed Contour

Consider the general closed contour of the type shown in Fig. 2-1. Points P_o, P_1, ...P_n (n = even integer) are spaced at equal increments of arc length, Δs, on the contour, where P_o and P_n coincide.

Nonsingular Contour Integral

The integrand of the second term of Eq. (26) consists of the kernel $\cos(r\upsilon)/|r|$ and the integrand function $C_I(s)$, neither of which is singular. Thus, a simple Simpson quadrature formula may be used to approximate the integral at any point P_i. The formulations below make use of the definitions of K'_s and K'_c in Eqs. (33) and (34). The Simpson quadrature for any point P_i is written:

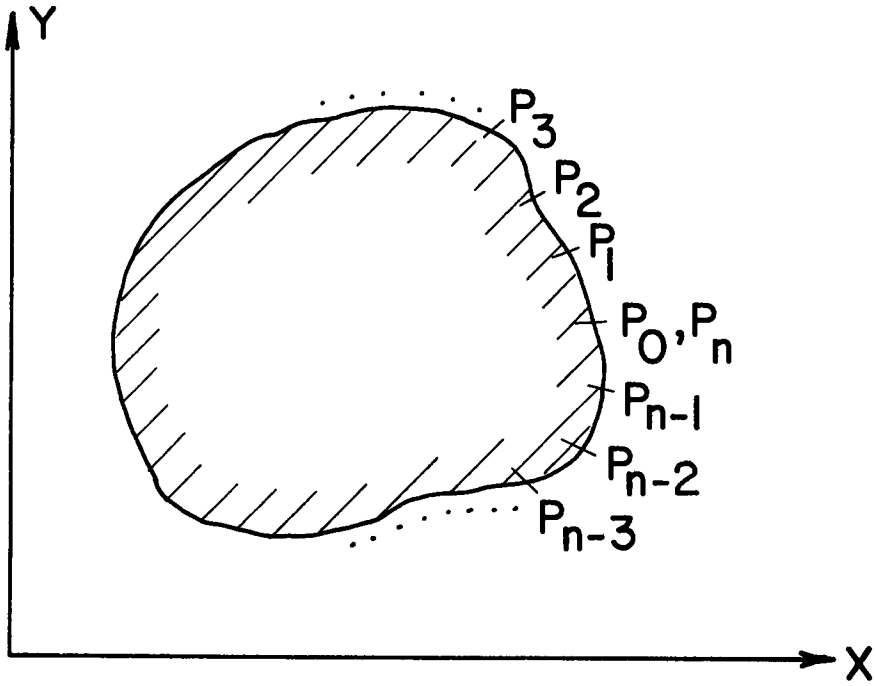

Fig. 2-1. General Closed Contour

$$\oint \frac{C_I(s)\sin(r\upsilon)}{|r|}\,ds \cong \frac{\Delta s}{3}\,[C_I(i+1)\,K_c(i,i+1) + 4C_I(i+2)\,K_c(i,\,i+2)$$

$$+\,2C_I(i+3)\,K_c(i,i+3) + 4C_I(i+4)\,K_c(i,i+4) + \ldots\ldots$$

$$+\,4C_I(i-2)\,K_c(i,i-2) + 2C_I(i-1)\,K_c(i,i-1)$$

$$+\,4C_I(i)\,K_c(i,i) + C_I(i+1)\,K_c(i,i+1)]\,. \qquad \text{(B-2)}$$

Nonclosed Contours

The general treatment of nonclosed contours resembles that of closed contours in most respects. It differs in that the so-called "four-point" Simpson quadrature formula is introduced, and in that the end points require careful consideration.

Consider the nonclosed contour shown in Fig. 2-2, which is composed of a region S' over which a preliminary solution is determined by matrix inversion, and a region S_2 over which an approximate solution is assumed (which is the case in both rod-to-rod and rod-to-plane sintering). The reflected neck S'' will be considered separately.

Nonsingular Nonclosed Contour Integral

The weighting factors may be defined for any point P_i on S' by integrating from P_u to P_m; the result is:

$$A(i,j) = \Delta s/3, \quad j = u, \quad j = m$$

$$A(i,j) = 2\Delta s/3, \quad j = \text{odd integer}$$

$$A(i,j) = 4\Delta s/3, \quad j = \text{even integer}\,.$$

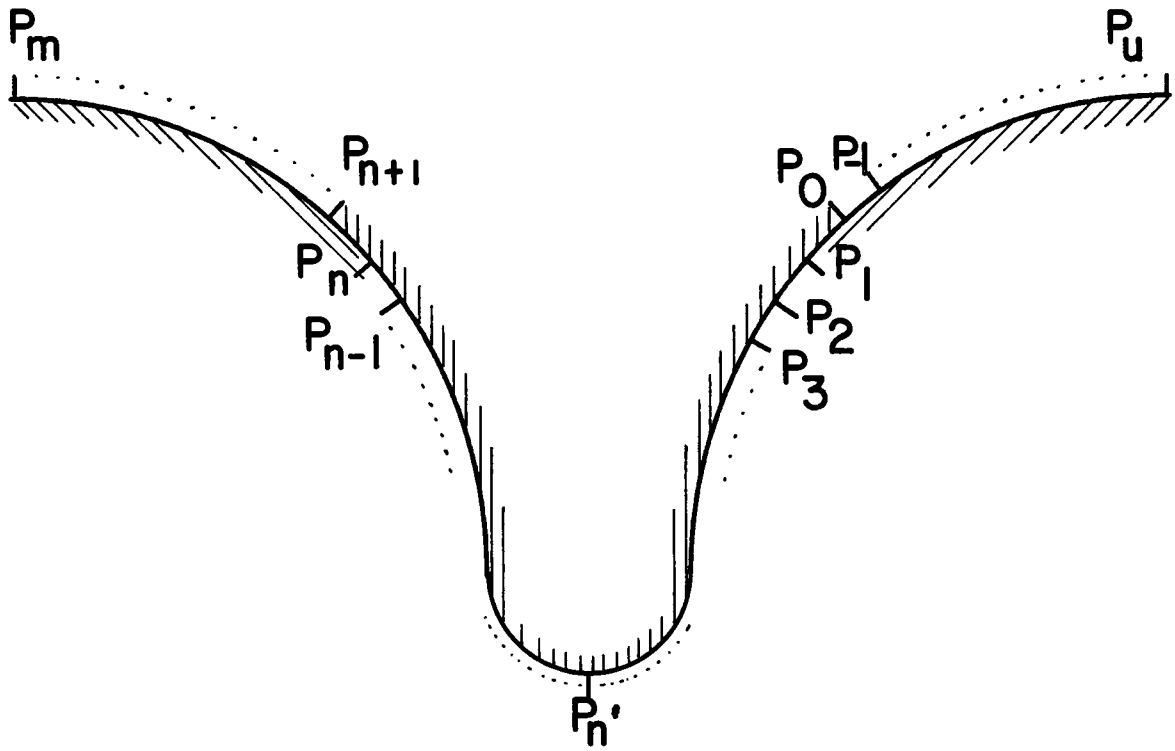

Fig. 2-2. Nonclosed Contour for Rod-to-Rod Sintering.

Singular Nonclosed Contour Integral

The limits of the Simpson singular integral for even i naturally match the limits of the Simpson nonsingular integral above, when the Cauchy principal value of the contour integral is used from P_{i-1} to P_{i+1}.

However, for odd i, the Simpson singular integrals limits do not match those of the nonsingular integrals unless an odd-interval quadrature is used. A trapezoidal integration from P_{i-1} to P_{i-2} fulfills this requirement, as does the use of a three-interval Simpson quadrature, such as:

$$\int_{P_o}^{P_3} f(s)\, ds = 3\Delta s[f(0) + 3f(1) + 3f(2) + f(3)] \ . \qquad \text{(B-6)}$$

Thus, if the A(i,j) matrix [Eq. (36)] is written for a closed contour, it is defined by:

$$A(i,j) = 2\Delta s/3, \quad i,j \text{ mixed (even-odd or odd-even integers)} ,$$

$$A(i,j) = 4\Delta s/3, \quad i,j \text{ unmixed (even-even or odd-odd integers)} . \qquad \text{(B-3)}$$

Two points are worthy of comment. First, the cyclic boundary condition that P_o and P_n are identical is used to compute the integral from P_{n-1} to (P_o or P_n)to P_1. Second, the limits over which the terms of Eq. (26) are integrated are chosen to be identical; for example, the value of the second term in Eq. (26) at the ith point is obtained by integrating from P_{i-1} to P_{i+1}, and the value of the first integral is obtained likewise. If the ranges do not conform in this sense, the final solution for $\Phi_I(s)$ has been found experimentally to be in error.

Singular Closed Contour Integral

The integrand of the first term of Eq. (26) consists of the kernel $\sin(r\upsilon)/|r|$ and the integrand function $C_R(s)$, where the kernel is singular as $|r| \to 0$. A Simpson quadrature formula may be used to approximate the integral for point P_i over the intervals beginning at P_{i+1} and ending at P_{i-1}. Equation (30) is used to approximate the Cauchy principal value of the integral from P_{i-1} to P_{i+1}. The $A(i,j)$ matrix [Eq. (36)] for a closed contour is thus:

$$A(i,j) = 2\Delta s/3, \quad i,j \text{ mixed}, \quad j \neq i+1, \quad j = i-1$$

$$A(i,j) = 4\Delta s/3, \begin{cases} i,j \text{ mixed}, & j = i+1, \quad j = i-1 \\ i,j \text{ unmixed}, & i \neq j \,. \end{cases}$$

$$A(i,j) = 0, \quad i = j \tag{B-4}$$

Note that cyclic boundary conditions apply when $i + 1 = n$ or when $i - 1 = -1$. The latter was selected because of its higher accuracy. Applying the three interval Simpson quadrature from P_{i+1} to P_{i+4} and from P_{i-1} to P_{i-4}, and using the usual Simpson quadrature formula elsewhere (except for the Cauchy principal value approximation from P_{i-1} to P_{i+1}), it is found that:

$$A(i,j) = 2\Delta s/3, \quad \text{all } i, \quad \text{odd } j$$

$$A(i,j) = 4\Delta s/3, \quad \text{all } i, \quad \text{even } j$$

where the following exceptions are noted:

$$A(i,j) = \Delta s/3, \quad j = u,m$$

$$A(i,j) = 0, \quad i = j$$

$$A(i,j) = 4\Delta s/3, \quad \text{even } i, \quad j = i + 1,\ i - 1$$

$$A(i,j) = 11\Delta s/8, \quad \text{odd } i, \quad j = i + 1,\ i - 1$$

$$A(i,j) = 9\Delta s/8, \quad \text{odd } i, \quad j = i + 2,\ i - 2,\ i + 3,\ i - 3$$

$$A(i,j) = 17\Delta s/16, \quad \text{odd } i, \quad j = i + 4,\ i - 1\ . \qquad \text{(B-7)}$$

The Reflected Neck

If P_{1r} and P_{nr} denote the reflections of P_1 and P_n, the end points of S', then a simple Simpson quadrature yields:

$$A(i,j) = A(i,j) = \Delta s/3, \quad \text{all } i, \quad j = 1r,\ nr$$

$$A(i,j) = A(i,j) = 4\Delta s/3, \quad \text{all } i, \quad \text{even } j$$

$$A(i,j) = A(i,j) = 2\Delta s/3, \quad \text{all } i, \quad \text{even } j \neq 1r,\ 1n\ . \qquad \text{(B-8)}$$

APPENDIX 3

TWO-DIMENSIONAL CRYSTAL GROWTH

Introduction and Circle Test Case

The text of this work deals primarily with the solutions for two-dimensional sintering problems. A slightly different class of problems may be treated with the mathematical and numerical techniques developed here. In these problems the growth of a body is controlled by volume diffusion external to the body. In particular, in this discussion the growth of an infinitely long cylindrical rod whose axis coincides with the axis of an infinitely long right circular boundary is considered. No attempt will be made to observe the growth of rods of any cross section other than circular cross sections.

Figure 3-1 is a schematic of the cylinder boundary S_4, the rod boundary S_1, and the shaded internal region T within which diffusion occurs. Within T, it is assumed that $\nabla^2 C = 0$. If the cylinder and rod cross sections are both circular, and the diffusing species concentration is fixed at C_1 on S_1 and at C_4 on S_4, then within T the concentration of the diffusing species is given by

$$C'(z) = C_1 + \frac{(C_4 - C_1)}{\ln (R/\rho)} . \qquad \text{(C-1)}$$

This may readily be demonstrated by showing that $\nabla^2 C'(z) = 0$. Separating $C'(z)$ into its real and imaginary parts, $C_R(z)$ and $C_I(z)$, (since $z = re^{i\theta}$) illustrates that the imaginary part of $C(z)$ is multiple-valued in θ and increases by $2\pi(C_4 - C_1)/\ln (R/\rho)$ for each 2π increment in θ:

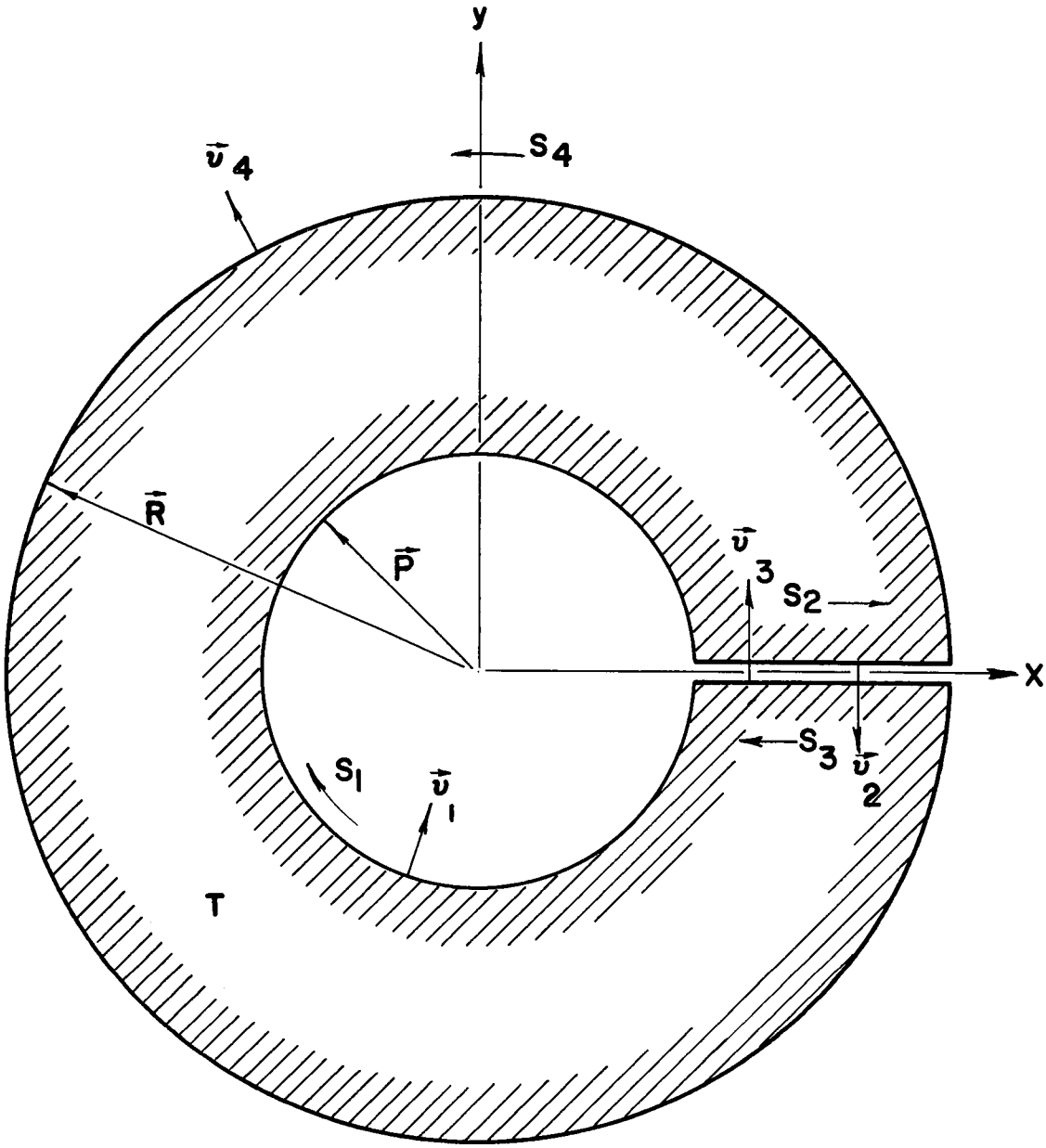

Fig. 3-1. Two-Dimensional Crystal Growth System.

$$C_I(z) = (C_4 - C_1)\theta/\ln(R/\rho) .$$

For the integral Eq. (26) of the text to apply, a simple closed region T is obtained by introducing a cut along $\theta = 0$, where S_2 is the cut surface from $|\vec{r}| = |\vec{\rho}|$ to $|\vec{r}| = |\vec{R}|$, and S_3 is the cut surface in the opposite direction. The integral equation is then written for the four segments of the total contour, and the notation is introduced that:

$$C_i(t) = \frac{1}{\pi}\int_{S_i} \frac{C_R(s)\sin(r\upsilon)_{ts}}{|\vec{r}_{ts}|}\,ds - \frac{1}{\pi}\int_{S_i} \frac{C_I(s)\cos(r\upsilon)_{ts}}{|\vec{r}_{ts}|}\,ds . \qquad \text{(C-3)}$$

where

$$C_I(t) = I_1(t) + I_2(t) + I_3(t) + I_4(t) . \qquad \text{(C-4)}$$

The following assumptions are made to evaluate the I_i for physically reasonable conditions:

1. $C_I(s)$ is multiple-valued, but $C_R(s)$ is not multiple-valued.
2. The maximum radius vector to a point on S_1, ρ_{max}, is much smaller than R.
3. S_1 is a simple curve, but not necessarily circular in shape.
4. $C_I(s_2)$ and $C_I(s_3)$ are constants.

This latter condition is true if the cut is made along a plane of mirror symmetry of S_1, since $\partial C_R/\partial n = 0$ along such a cut, requiring that $\partial C_I/\partial s = 0$ along the cut surfaces S_2 and S_3. Under these conditions it may be shown that:

$$\lim_{\rho_{max}/R} [I_2(t) + I_3(t)] = \frac{C_I(S_3) - C_I(S_2)}{2} (1 - \theta/\pi) \ . \qquad \text{(C-5)}$$

It may further be shown that if $C_I(S_4) = C_3\theta$ and $C_R(S_4)$ = constant, then

$$I_4(t) \cong 2\pi[1 - 2(\rho/R)^2]C_3 \qquad \text{(C-6)}$$

for $\rho \ll R$.

As a specific test case, it may be shown that if S_1 is a circle and $C_I(s) = C_3\theta$, that

$$I_1(t) = -\pi C_3 \ . \qquad \text{(C-7)}$$

By substituting Eqs. (C-5), (C-6), and (C-7) into Eq. (C-4), it may be shown that

$$\lim_{\rho_{max}/R \to 0} \Phi_I(t) = \lim_{\rho_{max}/R \to 0} \sum_{i=1}^{t} I_i(t) = C_3\theta \ . \qquad \text{(C-8)}$$

This result is in agreement with Eq. (C-2), and demonstrates by internal consistency the validity of Eqs. (C-5) and (C-6).

Method of Numerical Solution for Noncircular S_1

Consider now the problem of an infinitely long rod growing within an infinitely long matrix of cylindrical boundary, where the matrix is supersaturated in the diffusing species, and the cylinder wall is nearly infinite in radial extent compared to the rod dimension. The rod is permitted any boundary contour which has at least one plane of mirror symmetry coincident with the cylinder axis. The supersaturation is obtained by

prescribing the concentration of the diffusing species to be C_4 on S_4, and defining C_1 at each point on S_1 by the Gibbs-Thompson equation. Then at any point t,

$$C_3(t) = \frac{C_4 - C_1(t)}{\ln (R/\rho)} \tag{C-9}$$

is a measure of the supersaturation at point t.

Now, if the integral Eq. (26) be written for the entire contour, $I_2(t) + I_3(t)$ may be evaluated by Eq. (C-5), and Eq. (C-6) may be used to evaluate $I_4(t)$ for fixed C_4, R, ρ, θ, and $(\gamma\Omega C_o/kT)$. The evaluation of $I_4(t)$ may be performed in the usual manner. Points P_i are located so as to divide S_1 into n arc segments of equal length. A set of integral equations is then generated by writing the integral equation for each of the P_i. The set of integral equations is then replaced by a system of linear equations by means of quadrature formulae identical to those used in the ellipse decay case (Appendix 2), except that care must be taken to avoid integration across the cut. The sum of the integral over S_1 of the $C_R(s) \sin (r\upsilon)/|\vec{r}|$, $I_2(t) + I_3(t)$, and $I_4(t)$ are treated as an inhomogeneous term, and matrix inversion may be used to solve for $\vec{\Phi}_I$.

It is possible to study the effects of anisotropy of surface tension, γ, in this numerical scheme, since if γ is anisotropic, the Gibbs-Thompson becomes (31) for dilute solutions:

$$C_R(s) = C_o + C_a\Omega(\gamma_o + \gamma_o'')K/(kt) \ . \tag{C-10}$$

The term γ'' may be found at any point by introducing centered differences to approximate the equation

$$\gamma'' = \frac{\partial}{\partial s}\left(\frac{\partial \gamma}{\partial s}\frac{\partial s}{\partial \theta}\right)\frac{\partial s}{\partial \theta}$$

provided that $\gamma(\theta)$ does not have a cusp, or discontinuous curvature.

Trial Applications of the Methods Developed

The techniques described in the preceding section were applied to the growth of rods of circular cross section for the cases of isotropic and anisotropic surface tension. The results of these applications are described briefly below.

The circle of isotropic surface tension was solved for n equals 8, 16, 24, 32, 40, and 48. Solutions were obtained for these systems with $C_3(t) = 0$, and the calculated $\vec{\phi}_I(i)$ were constant to at least six significant places for each system.

Solutions were also obtained for $C_3(t) = 10^4$, and the values of $\vec{\phi}_I(i)$ for all systems agreed with Eq. (10) to at least six significant places (as many as were printed out by the computer). These two tests indicate the validity of the mathematical treatments of $(I_2 + I_3)$ and I_4.

In addition, the boundary of a circular rod of isotropic surface tension was allowed to migrate 30 time steps, where the boundary displacement was $10^{-3}|\vec{\rho}|$ per time step. Nichols' techniques for boundary migration and point relocation are well-suited to handling contours of slowly changing curvature, and were used for this work. The values of $\vec{\phi}_I(t)$ agreed with $C_3(t)$ to six significant figures after 30 time steps, and the velocities of all points agreed to at least four significant figures on each time step.

The velocities of the anisotropic rod of circular cross section were computed for the case

$$\gamma = \gamma_o + \gamma_1 \cos 2\theta \ .$$

It was found that the velocities of the points were proportional to cos 2θ to at least three significant places for $n = 8$ and to at least four significant places for $n > 16$.

Although it has not been possible to utilize this approach to study the behavior of two-dimensional crystals of various shapes as yet, it is felt that a number of interesting studies on the stability of interfaces and growth morphologies may be performed using these techniques.

INTERNAL DISTRIBUTION

1–3. Central Research Library
4–5. ORNL – Y-12 Technical Library
Document Reference Section
6–25. Laboratory Records
26. Laboratory Records, ORNL R.C.
27. ORNL Patent Office
28. E. E. Bloom
29. G. E. Boyd
30. J. E. Cunningham
31. W. W. Davis
32. C. W. Dollins
33. D. I. Dunthorn (K-25)
34. J. H Frye, Jr.
35. D. G. Gates
36. J. L. Gregg
37. D. G. Harmon
38. R. W. Hendricks
39–43. M. R. Hill
44. C. R. Kennedy
45–59. R. T. King
60. G. R. Love
61. H. G. MacPherson
62. H. E. McCoy
63. C. J. McHargue
64. C. S. Morgan, Jr.
65. R. L. Stephenson
66. D. A. Sundberg
67. R. W. Swindeman
68. J. R. Weir, Jr.
69. F. R. Winslow
70. J. W. Woods
71. C. S. Yust

EXTERNAL DISTRIBUTION

72. D. F. Cope, RDT, SSR, AEC, Oak Ridge Operations
73. W. J. Larkin, AEC, Oak Ridge Operations
74. P. J. Levine, Westinghouse Advanced Reactors Division, Waltz Mill Site, Box 158, Madison, Pa. 15663
75. W. W. Mullins, Carnegie-Mellon, Pittsburgh, Pa.
76. A. Nichols, Fuel Element Development Dept., Westinghouse Electric Corp., Bettis Atomic Power Laboratory, P. O. Box 79, West Miflin, Pa. 15122
77. W. E. Ray, Westinghouse Advanced Reactors Division, Waltz Mill Site, Box 158, Madison, Pa. 15663
78. F. C. Schwenk, AEC, Washington
79. P. G. Shewmon, Argonne National Laboratory
80. J. M. Simmons, AEC, Washington
81. E. E. Stansbury, the University of Tennessee
82. D. K. Stevens, AEC, Washington
83. Rohit Trevedi, Ames Laboratory, Iowa State University, Ames, Iowa
84. G. W. Wensch, AEC, Washington
85. G. A. Whitlow, Westinghouse Advanced Reactors Division, Waltz Mill Site, Box 158, Madison, Pa. 15663
86. Laboratory and University Division, AEC, Oak Ridge Operations
87–101. Division of Technical Information Extension